Reidar Brekken

Ultrasound-based Estimation of Strain in Abdominal Aortic Aneurysm

Thesis for the degree of Philosophiae Doctor

Trondheim, December 2012

Norwegian University of Science and Technology
Faculty of Medicine
Department of Circulation and Medical Imaging

NTNU – Trondheim
Norwegian University of
Science and Technology

NTNU
Norwegian University of Science and Technology

Thesis for the degree of Philosophiae Doctor

Faculty of Medicine
Department of Circulation and Medical Imaging

ISBN 978-82-471-4069-7 (printed ver.)
ISBN 978-82-471-4070-3 (electronic ver.)
ISSN 1503-8181

Doctoral theses at NTNU, 2012:369

Printed by NTNU-trykk

Sammendrag: Ultralydmåling av veggtøyning i abdominalt aortaaneurisme
Abdominalt aortaaneurisme (AAA) er en sykdomstilstand som innebærer at det oppstår en utposning på hovedpulsåren (aorta) gjennom magen. AAA er anslått å ramme 1.3-8.9% av menn og 1.0-2.2% av kvinner over 60 år. Risikofaktorer inkluderer røyking, høyt blodtrykk, høyt kolesterol og familieforekomst av AAA. Sykdommen er som oftest asymptomatisk og oppdages tilfeldig i forbindelse med undersøkelse for andre lidelser. AAA medfører fare for at blodåren kan sprekke (ruptur), noe som medfører høy dødelighet. Forebyggende behandling kan gjøres ved å forsterke blodåren med en protese, enten med åpen kirurgi eller endovaskulær behandling, hvor man fører protesen inn fra lysken. Behandling er forbundet med en viss risiko, og anbefales derfor først når sannsynligheten for ruptur anslås å være tilstrekkelig høy. Nåværende kriterium for å anbefale behandling er at diameteren av aneurismet overstiger 50-55 mm eller øker raskt. Noen aneurismer sprekker imidlertid før de når denne størrelsen, mens andre kan være intakte til langt over 55 mm, og man ønsker derfor tilleggsinformasjon som kan gi en bedre individuell vurdering av tilstanden til aneurismet.

Tema for avhandlingen har vært bruk av ultralyd for å bidra til forbedret håndtering av AAA. Ultralyd er en relativt billig, enkel og ufarlig avbildingsmodalitet. Mulige bruksområder inkluderer deteksjon og monitorering av aneurisme, veiledning og deteksjon av lekkasje i forbindelse med endovaskulær behandling, målsøkende kontrastmidler for diagnostikk og lokal medikamentell behandling, samt estimering av tøyning i åreveggen, som har vært hovedfokus for avhandlingen.

Aorta utvider og trekker seg sammen ettersom blodet pulserer fra hjertet og gjennom åren. Aneurisme medfører endret bevegelse som kan være relatert til videre vekst og ruptur. Denne endringen kan potensielt avdekkes ved å analysere dynamikk i ultralydbilder. Ved å utvikle en metode for å estimere tøyning i flere segment av veggen, viste vi at tøyningen er inhomogen og gir tilleggsinformasjon sammenlignet med måling av diameter. Metoden ble videre anvendt for å måle tøyning i åreveggen før og etter endovaskulær behandling, og viste som forventet redusert tøyning etter behandling. Metoden er basert på to-dimensjonale (2D) ultralyd bilder. Ettersom veggtøyningen er inhomogen, vil det være nødvendig å undersøke flere snitt. Vi utviklet en metode for å kombinere 2D ultralyd med 3D bilder, noe som gir en samlet visualisering av data fra flere snitt, og gjør at vi lettere kan kombinere vår metode med metoder for veggspenningsanalyse basert på 3D bilder. Vi har også utviklet et rammeverk som kan benyttes for å evaluere metoder for estimering av tøyning.

Metodikken utviklet i denne avhandlingen har spennende potensiale i forhold til å forutsi utvikling av AAA. Større studier for å undersøke klinisk signifikans av metoden anbefales for på sikt å kunne tilby forbedret seleksjon av pasienter.

Kandidat:	Reidar Brekken
Institutt:	Sirkulasjon og bildediagnostikk, NTNU
Veileder:	Prof. Toril A Nagelhus Hernes
Biveileder:	Prof. Hans Olav Myhre
Finansieringskilder:	Samarbeidsorganet mellom Helse Midt-Norge RHF og NTNU, Nasjonalt kompetansesenter for ultralyd og bildeveiledet terapi.

Ovennevnte avhandling er funnet verdig til å forsvares offentlig for graden Philosophiae Doctor (PhD) i medisinsk teknologi. Disputas finner sted i Auditoriet, MTFS, 18. desember 2012, kl. 12.15.

Abstract

Abdominal aortic aneurysm (AAA) is a vascular disease resulting in a permanent local dilatation of the abdominal aorta. Different studies estimate the prevalence of AAA to 1.3-8.9% of men and 1.0-2.2% of women over 60 years of age. Risk factors include smoking, hypertension, high serum cholesterol, diabetes, and family history. The weakening of the wall and altered wall stress associated with aneurysm formation and progression may eventually lead to aneurysm rupture, which causes haemorrhage and severe blood loss and is associated with very high mortality. AAA is responsible for 1.3% of deaths among men aged 65-85 in developed countries. Elective repair of asymptomatic AAA is recommended when the risk of rupture is estimated to exceed the risk associated with repair. Currently, best clinical practice is to recommend repair when the maximum diameter of the aneurysm exceeds 50-55 mm or increases rapidly. This is a population-based criterion, meaning that in average, an aneurysm with diameter exceeding this criterion is more likely to rupture than to experience complications with repair. Individually, however, some aneurysms rupture before 50 mm, while several aneurysms larger than 55 mm are still intact. More patient-specific information about the state of the individual aneurysm is therefore warranted.

In this PhD thesis I have developed and investigated concepts and methods for ultrasound based strain estimation in AAA. The physiological motivation is that progression of aneurysm is associated with altered wall tissue composition, which leads to altered elastic properties, and altered wall stress (geometry and flow conditions). The underlying hypothesis is that it may be possible to detect and quantify this alteration from dynamic ultrasound images, and through that predict further progression.

We have developed a method for estimation of cyclic circumferential strain from 2D ultrasound. The method relies on the user to define the wall in an ultrasound image, and then automatically tracks a number of points in the wall over the cardiac cycle based on correlation between frames. The relative change in distance between neighboring points are used as a measure for strain estimation. Inhomogeneous strain values were found along the circumference of the aneurysms, suggesting that additional information could be obtained compared to using diameter alone. The method was further used for investigating strain in aneurysms before and after endovascular aortic repair (EVAR) in ten patients. Since insertion of a stentgraft reduces the load imposed on the wall, a successful EVAR should result in reduced strain. The results showed a clear reduction, which means that the expected reduction was indeed detectable using our method. The study included a limited patient material, and it remains to investigate if the strain values can be used for predicting clinical outcome after EVAR.

Because only a limited part of the aneurysm can be imaged in each cross-sectional view, we demonstrated a method for visualizing the circumferential strain from several image planes together in a 3D model using navigation technology. The 3D model may enhance

interpretation of results by relating circumferential strain from several parts of the aneurysm to a 3D geometry. This is also an important step towards integration with wall stress simulations for adding more patient specific information.

Abdominal images may have relatively low signal to noise ratios, which will negatively influence the performance of the correlation based tracking method. Before larger clinical trials are initiated, it is therefore important to investigate the quality of the strain estimates obtained by the method. We developed a simulation model, for simulation of wall motion due to a time-varying blood pressure, and for simulation of ultrasound images including speckle, direction dependent reflection and absorption. The simulation model is an important part of future evaluation and tuning of the strain method.

Further refinement includes implementation of the processing method on an ultrasound scanner for real-time data analysis, which would benefit workflow and make it easier to find the most relevant image planes during investigation. Also, strain estimation from real-time 3D ultrasound is interesting for evaluating several strain components. Finally, clinical trials must be implemented for further investigating potential correlation between strain and clinically relevant parameters, including formation, growth and rupture of AAA.

Preface

This thesis has been submitted in partial fulfillment of the requirements for the degree Philosophiae Doctor (PhD) in medical technology at the Faculty of Medicine of the Norwegian University of Science and Technology (NTNU). The work was funded by The Liaison Committee between the Central Norway Regional Health Authority and the Norwegian University of Science and Technology, SINTEF Department of Medical Technology and the National Center of Competence for Ultrasound and Image-guided Therapy. Supervisors have been Professor Toril A. Nagelhus Hernes at the Department of Circulation and Medical Imaging at NTNU and the Department of Medical Technology at SINTEF, and Professor Hans Olav Myhre at the Department of Circulation and Medical Imaging NTNU and St. Olav's University Hospital.

I wish to thank my supervisors for always being willing to help, and for providing important motivation and guidance during the work with this PhD thesis. I would also like to thank all my other co-authors for contributing importantly to the work: Torbjørn Dahl, Jon Bang, Asbjørn Ødegård, Jenny Aasland, Jon Harald Kaspersen, Geir Arne Tangen, Sebastién Muller and Sjur Gjerald, as well as other colleagues and collaborators at SINTEF, NTNU and St. Olav's University Hospital for creating an inspiring working environment and for generously sharing material, knowledge, time and ideas.

Finally, I would like to thank my family for support and motivation, and especially Evy and our children for always being there to remind me that even though some things are important, other things are even more important.

Trondheim, September 2012

Reidar Brekken

Contents

List of Publications

The thesis includes the following four publications:

I. Brekken R, Bang J, Ødegård A, Aasland J, Hernes TAN, Myhre HO. Strain estimation in abdominal aortic aneurysms from 2D ultrasound. Ultrasound Med Biol 2006;32(1):33-42.

II. Brekken R, Dahl T, Hernes TAN, Myhre HO. Reduced strain in abdominal aortic aneurysms after endovascular repair. J Endovasc Ther 2008;15:453:461.

III. Brekken R, Kaspersen JH, Tangen GA, Dahl T, Hernes TAN, Myhre HO. 3D visualization of strain in abdominal aortic aneurysms based on navigated ultrasound imaging. In Armando Manduca, Xiaoping P. Hu (Eds): SPIE Medical Imaging 2007: Physiology, Function, and Structure from Medical Images. Proceedings Vol. 6511-52.

IV. Brekken R, Muller S, Gjerald SU, Hernes TAN. Simulation model for assessing quality of ultrasound strain estimation in abdominal aortic aneurysm. Ultrasound Med Biol 2012;38(5):889–896.

In addition, the work or part of the work has been published in a book chapter and presented at three scientific conferences:

- Brekken R, Dahl T, Hernes TAN. Ultrasound in abdominal aortic aneurysm. In Prof. dr. R.T. Grundmann (Ed.): Diagnosis, screening and treatment of abdominal, thoracoabdominal and thoracic aortic aneurysms. InTech, Croatia, 2011. ISBN 978-953-307-466-5.

- Brekken R, Hernes TAN, Myhre HO. Ultrasound strain estimation in abdominal aortic aneurysm. Invited speech, 6th World Congress of Biomechanics, Singapore, 01-06 August 2010.

- Brekken R, Dahl T, Hernes TAN, Myhre HO. Ultralydmåling av strain i abdominal aorta aneurisme. Kirurgisk Høstmøte, Oslo, 22-26 Oktober 2007.

- Brekken R, Kaspersen J, Tangen G, Dahl T, Hernes TAN, Myhre HO. 3D visualization of strain in abdominal aortic aneurysms based on navigated ultrasound imaging. SPIE Medical Imaging, San Diego, 17-22 February 2007.

Background

Abdominal aortic aneurysm

Abdominal aortic aneurysm (AAA) is a vascular disease resulting in a permanent local dilatation of the abdominal aorta. Normal diameter of the abdominal aorta varies from 15-24 mm, depending on e.g. age, sex, bodyweight and blood pressure (Bengtsson et al., 1996; Johnston et al., 1991; Liddington & Heather 1992). AAA is defined as a widened aorta which diameter is exceeding 30 mm, or 1.5 times the normal diameter (Johnston et al., 1991; McGregor et al., 1975). AAAs can have different morphologies with respect to e.g. size, elongation, bulging and tortuosity, and can be fusiform or saccular. Aortic aneurysms may form in more proximal parts of the aorta, but the abdominal aorta is the most common location. Aortic aneurysms occurring in any part of the infra-diaphragmatic aorta may be termed as abdominal aortic aneurysm, but the most common definition restricts to the infra-renal aorta, including aneurysms involving the renal ostia or the iliac arteries (Fig 1). (Sakalihasan et al., 2005).

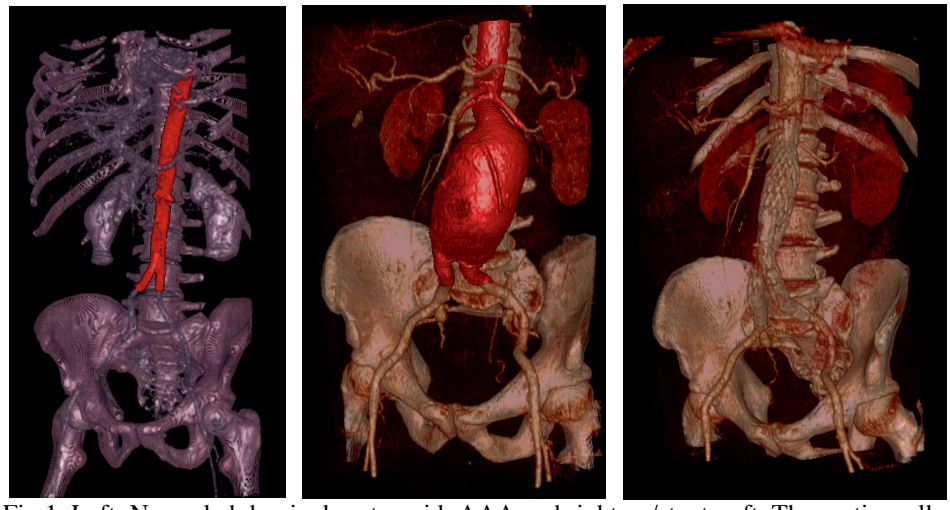

Fig 1. Left: Normal abdominal aorta, mid: AAA and right: w/stentgraft. The aortic wall is segmented from CT using the open-source software ITK snap (www.itksnap.org), and visualized using CustusX (SINTEF, Trondheim, Norway).

After formation, the aneurysm may grow and eventually progress to rupture, which causes haemorrhage and severe blood loss. Rupture is associated with very high overall mortality (65%-85%) (Kniemeyer et al., 2000; Thompson, 2003). In some cases an aneurysm may lead to back and abdominal pain or a palpable pulsating mass in the abdomen, but AAA is most often asymptomatic until rupture, and only coincidentally

detected during examination for other diseases or through ultrasound-based screening programs. AAA can be treated either with open surgery or endovascular aneurysm repair (EVAR). In addition to acute repair of ruptured or otherwise symptomatic aneurysms, elective repair of asymptomatic AAA is recommended when the risk of rupture is estimated to exceed the risk associated with elective repair (1.1-7.0% 30-day mortality). The prevalence of AAA is estimated to 1.3-8.9% of men and 1.0-2.2% of women over 60 years of age. Risk factors include cigarette smoking, hypertension, high serum cholesterol, diabetes, and family history. AAA is responsible for 1.3% of deaths among men aged 65-85 in developed countries (Sakalihasan et al., 2005).

Pathophysiology

The aortic wall consists of three layers. Intima is closest to the lumen, and is a thin layer composed of endothelial cells. Media consists of elastin and collagen (extracellular matrix), and smooth muscle cells (SMC), whereas the adventitia mainly consists of collagen fibres. The aortic tissue is fed both directly through the inner layer and by supplying blood vessels (vasa vasorum).

The function of the aorta is to distribute blood flow from the pulsating heart to smaller vessels that supply blood to the tissue. As the blood flow pulsates through the aorta, the mechanical properties of the aortic wall allow the tissue to pulsate. Elastin contributes especially to the elasticity of the aorta, whereas collagen is stiffer and strengthens the aortic wall. Due to the combined mechanical properties, the pulsating blood flow into the aorta is transformed to a more even blood flow to continuously supply blood to the organs and tissues throughout the body.

To maintain its function over time, mechanoreceptors in the endothelial cells respond to mechanical stimuli on the vessel wall by sending chemical signals, activating pathways within the cells that control the expression of genes and proteins to alter the microstructure of the artery (Chien, 2007). In some cases, abnormal shear stress stimuli or disturbed pathways may cause a pathologic remodelling of the tissue. The aetiology of AAA is complex, and affected by genetic, mechanical and life-style related risk factors (e.g. smoking and high cholesterol). Most AAAs are associated with atherosclerosis. “The main pathophysiological mechanisms in development and progression of AAA are inflammation, proteolysis and apoptosis” (Zankl et al., 2007).

The abdominal aorta is more susceptible to aneurysms compared with other parts of the aorta. This may partly be caused by local hemodynamics, e.g. turbulence distal to the renal artery inlets, and pressure augmentation due to reflection of pressure waves from distal bifurcations. Also, the abdominal aorta is stiffer than more proximal parts of the aorta, and contains less elastin and less medial vasa vasorum than the more proximal aorta (Zatina et al., 1984). The connective tissue may therefore be more susceptible to ischemic injury.

Morphological changes including growth and wall thickening are characteristics of the aneurysmal aorta. Intraluminal thrombus (ILT) is often found in the aneurysm sac, caused by endothelial injury (e.g. atheroma) or by abnormal blood flow (e.g.

turbulence). According to Yushimura et al. (2011) and references therein, the size and growth rate of the ILT is associated with AAA growth rate and rupture risk. Also, "the AAA wall covered by the ILT has been shown to be thinner and exhibit an increased number of inflammatory cells, a lower density of smooth muscle cells, and severely degraded extracellular matrix, especially elastin, compared to the thrombus-free wall. The AAA wall underlying a thick ILT was also shown to have less tensile strength compared to the wall covered with a thin ILT". They further commented that although ILT may not necessarily be an active source of proteases, it is possible that ILT plays an active role in AAA, for example by producing inflammatory mediators. Neo-vascularization is also found in relation to AAA (Herron et al., 1991; Holmes et al., 1995; Thompson et al., 1996). Choke et al. (2006) found that rupture of AAA was associated with increased medial neovascularization. In addition, aneurysm tissue is stiffer than normal aortic tissue.

The association between evolution of aneurysms and alteration of the elastic properties of the vessel wall is caused by biological processes affecting elastin and collagen (and SMC), which are the main load bearing constituents in the aortic wall. Matrix-metalloproteinase (MMP) activity and apoptosis causes loss of elastin, higher collagen turnover and loss of smooth muscle cells (Freestone et al., 1995). The different elastic properties of elastin and collagen, explains why AAA tissue is stiffer than normal, age-matched abdominal aortic tissue.

It has been suggested that aneurysm growth is associated with loss or degradation of elastin, and that the content of collagen increases, which is believed to be a compensatory response to increase the strength of the tissue. A study by He and Roach (1994) reported that normal aorta contained 22.7% elastin, 22.6% SMC and 54.8% collagen, versus 2.4%, 2.2% and 96.5% for AAA. If further progress results in loss of collagen (or fail to synthesize properly cross-linked collagen), the wall becomes weakened, potentially leading to the point where wall tissue fails to withstand the load imposed by the blood pressure, and the aneurysm ruptures (Petersen et al., 2002). Due to loss of collagen, the weakened wall will be more extensible. Consistent with this, it has been shown that aneurysm tissue is stiffer than normal tissue, but that softer aneurysm tissue is more prone to rupture than stiff aneurysm tissue (Di Martino et al., 2006).

Clinical management

Due to cost and risk associated with elective aneurysm repair, patient selection is important in clinical management of AAA. Specifically, the risk of rupture should be balanced against the expected risk/benefit associated with repair to determine appropriate time for intervention. Population based studies have suggested that therapy should be recommended for eligible patients with aneurysm diameter exceeding 50-55 mm or increasing rapidly (more than 3-6 mm/year) (Brewster et al., 2003). Smaller aneurysms are kept under surveillance, usually with CT or ultrasound imaging. Risk factor modification, e.g. cessation of smoking, treatment of hypertension and pharmaceutical inhibition of inflammation and protease, could reduce growth in these aneurysms (Baxter et al., 2008; Chaikof et al., 2009; Moll et al., 2011).

The validity of aneurysm size as prognostic marker of rupture may however be questioned. Specifically, rupture does occur in smaller aneurysm, while on the other hand, several aneurysms with diameter larger than 55 mm are still intact. Brewster et al. (2003) summarized findings from several studies, and estimated annual rupture risk versus size to vary as illustrated in Fig 2. Darling et al. (1977) reported an autopsy study comprising 459 unoperated AAAs of which 112 had ruptured. Out of 265 aneurysms with diameter less or equal to 50 mm, 34 ruptured, whereas out of 194 aneurysms with diameter larger than 50 mm, 116 were unruptured. I.e. 7.4% ruptured at diameter less than 50 mm, whereas 25.3% was intact despite a diameter exceeding 50 mm. Additional indicators are therefore warranted to predict rupture at an individual level.

Aneurysm formation and progression may both weaken the wall due to biological changes, and alter the stress condition due to altered flow and geometry. Considering that rupture is caused by the wall strength failing to withstand the stress caused by the blood pulse, more accurate estimation of rupture risk depends on estimation of wall stress and strength at a patient specific level.

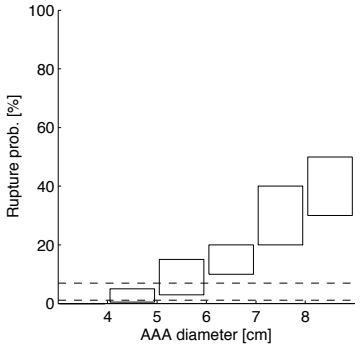

Fig 2. Graph illustrating annual rupture risk versus diameter. (Based on Brewster et al., 2003). The dashed lines indicate risk (30-day mortality) associated with repair (1.1-7%).

Biomechanics of abdominal aortic aneurysm

Mechanics

Mechanics is the study of forces and how forces interact with objects. Statics relates to systems in mechanical equilibrium (in rest or constant motion), whereas dynamics is the study of forces causing changed motion. Mathematical modelling of forces and motion helps describing, understanding and predicting mechanical processes.

In continuum mechanics, objects are described and analysed based on macroscopic properties (average over volume elements containing many cells, molecules or atoms). Material properties are described by constitutive model equations.

Deformation is a mechanical process describing change in size or shape. Elastic deformation means that the deformation is reversible, whereas plastic deformation is irreversible. A material usually deforms elastically below a certain limit (yield), and plastically above. Further deformation may lead to fracture.

Local deformations in a material can be quantified as *strain*. Longitudinal, shear and volumetric strain are the primary strain concepts. Longitudinal strain (or normal strain) is defined as the change in length of a line element relative to the length of the line element. Shear strain is the change in angle between two line elements, and the volumetric strain is change in volume relative to the original volume. Longitudinal strain can be expressed by considering an incremental change of length resulting in an incremental strain

$$d\varepsilon = \frac{dl}{l}$$

The strain resulting from a line being stretched from length L_0 to length L is found by integration:

$$\varepsilon = \ln\left(\frac{L}{L_0}\right) \approx \frac{L}{L_0} - 1 = \frac{L - L_0}{L_0} = \frac{\Delta L}{L_0}$$

The exact result is called natural (or logarithmic) strain, while the approximation, which is valid for low strain, is called engineering (or linear) strain.

A more general approach is to express strain as a tensor (Irgens, 2005, p134-141). The Green strain tensor E can be expressed in terms of the deformation gradient F as

$$E = \frac{1}{2}(F^T F - I)$$

The deformation gradient F gives the relation between a line-element dr_0 (with length ds_0) in the original configuration and dr (length ds) in the deformed configuration

$$d\boldsymbol{r} = F \cdot d\boldsymbol{r}_0 \Leftrightarrow F = \frac{d\boldsymbol{r}}{d\boldsymbol{r}_0} = grad(\boldsymbol{r})$$

$$\left(\frac{ds}{ds_0}\right)^2 = \boldsymbol{e}(F^T F)\boldsymbol{e} = 1 + 2\boldsymbol{e}E\boldsymbol{e}$$

The longitudinal strain in direction **e** can thus be expressed in terms of Green strain tensor E as

$$\varepsilon = \sqrt{1 + 2\boldsymbol{e}E\boldsymbol{e}} - 1$$

It can also be shown that shear strain γ between two originally orthogonal line-elements along **e** and **ê**, and volumetric strain ε_v can be expressed as

$$\sin\gamma = \frac{2\hat{\boldsymbol{e}}E\boldsymbol{e}}{\sqrt{(1 + 2\hat{\boldsymbol{e}}E\hat{\boldsymbol{e}})(1 + 2\boldsymbol{e}E\boldsymbol{e})}}$$

$$\varepsilon_v = \sqrt{\det(I + 2E)} - 1$$

When small strain values can be assumed, the Green strain tensor can be approximated to (using cylindrical coordinates)

$$E = \begin{bmatrix} \varepsilon_r & \gamma_{r\theta}/2 & \gamma_{rz}/2 \\ \gamma_{\theta r}/2 & \varepsilon_\theta & \gamma_{\theta z}/2 \\ \gamma_{zr}/2 & \gamma_{z\theta}/2 & \varepsilon_z \end{bmatrix}$$

ε denotes normal strains, γ shear strains. When a material is deformed, internal stresses occurs. Stress can also be expressed as a tensor. With normal stress σ and shear stress τ, the tensor can be written (in cylindrical coordinates) as

$$T = \begin{bmatrix} \sigma_r & \tau_{r\theta} & \tau_{rz} \\ \tau_{\theta r} & \sigma_\theta & \tau_{\theta z} \\ \tau_{zr} & \tau_{z\theta} & \sigma_z \end{bmatrix}$$

Strain is related to stress through material properties modelled by a constitutive equation (T=T(E)), and typically characterized by stress-strain diagrams determined by applying a load to a specimen of the material, and measure the resulting elongation or compression. A stiff material will resist deformation more than a softer material. Material properties can be isotropic or anisotropic and homogeneous or inhomogeneous. Elastic materials can be linear or non-linear and purely elastic or viscoelastic. For viscoelastic materials, the strain-stress response is time dependent (T=T(E,dE/dt)). High viscosity delays the response. Hysteresis, creep and stress relaxation are consequences of viscoelasticity.

Biomechanics

In biomechanics, mechanics is used for analysing biological systems, which are complex in terms of geometry and material properties (inhomogeneous, anisotropic, non-linear, viscoelastic. Fung, 2004). Properties are also time-varying due to the fact that biomechanics deals with living tissues and auto-regulating systems. Through mechanotransduction, biological materials respond to altered mechanical environment, making biomechanical stress/strain decisive in healthy as well as pathological remodeling. Biological systems can be described on various levels ranging from cells and molecules to tissues, organs and systems of organs. For some purposes (growth, development of pathology), the continuum mechanics approach may be supplemented with multi-scale modeling, taking into account mechanisms in lower levels.

Significant insight can be obtained from biomechanical models. Only a few simple models can be solved analytically, but increased computational power facilitates numerical computer simulations (finite-element models (FEM), e.g. for solid-state stress estimation, flow simulation (computational fluid dynamics, CFD) and fluid-structure-interactions (FSI)). These simulations should be combined with experimental measurements for parameter estimation and verification.

AAA biomechanics

Progression of AAA is associated with altered elastic properties of the aorta, and changed geometries and flow conditions, which changes the wall stresses and strains, as well as wall strength. Altered mechanical stimuli further triggers remodeling of the aortic wall. Biomechanical analysis can provide important insight into formation, growth and rupture of aneurysms. Although prediction of formation and growth by including remodeling, mechano-transduction and signaling pathways has been described (Sheidaei et al., 2011; Volokh & Vorp al., 2008; Watton et al., 2004), most research has focused on predicting rupture.

It has been shown that blood vessels exhibit a nonlinear viscoelastic relation between stress and strain (Fung, 2004; Imura et al., 1990). This property has been linked to the microscopic structure of the tissue, specifically the contents of elastin, collagen and smooth muscle cells (Apter et al., 1966). Mechanical properties of AAA have been investigated by in-vitro tensile testing, showing that aneurysm tissue is stiffer than normal tissue, and that the mechanical properties are inhomogeneous over the wall length and circumference. (di Martino et al., 2006; He and Roach, 1994; Ragahavan et al., 1996; Sumner et al., 1970; Thubrikar et al., 2001; Vande Geest et al., 2006a). He and Roach (1994) found that elastin and SMC was reduced by 91%, and collagen and gel matrix content increased by 77% in AAA compared to normal. Raghavan et al. (1996) showed that the tissue was slightly stiffer, and had a higher ultimate stress, in the circumferential direction compared to the axial direction.

It is generally accepted that rupture occurs when the intramural stress exceeds the wall strength. For certain geometries there are clear relations between diameter d and wall stress σ. For example, Laplace equations for a thin-walled cylinder (wall thickness h << d) gives

$$\sigma_\theta = p \cdot \frac{d}{2h} \qquad \sigma_z = p \cdot \frac{d}{4h} \qquad \sigma_r = [-p, 0] \ll \sigma_z < \sigma_\theta$$

where p is the pressure difference between inside and outside the cylinder. However, AAA geometries are complex, with high local wall curvatures and varying ILT and tissue composition. The actual patient-specific geometry can be taken into account combining medical imaging (most often by computed tomography, CT) and numerical simulation of wall stress (finite-element-model, FEM) (Raghavan et al., 2000; di Martino et al., 2001; Wolters et al., 2005). Important results include that stress is heterogenous over the aneurysm, and that maximum stress is not necessarily coincident with maximum diameter. Examples of wall stress calculation are shown in Fig. 3, illustrating inhomogeneous stress over the aneurysm wall, and lower stress values in normal aorta (12 N/cm$^{2)}$ compared to AAA (29-45 N/cm^2) (Raghavan et al., 2000). For reference, failure strength has been reported to be as high as 121 N/cm^2 for nonaneurysmal aorta and 65 N/cm^2 for typical AAA wall (Raghavan et al., 1996; Vorp et al., 1996). Fillinger et al. (2003) reported a clinical study showing that wall stress was a better predictor of rupture compared to diameter. Several studies have shown that presence of ILT reduces and redistributes stress (e.g. di Martino & Vorp, 2003; Georgakarakos et al., 2009; Li et al., 2008; Mower et al., 1997; Wang et al., 2002), but

as discussed previously, ILT is also associated with reduced wall strength. It has also been shown that ILT fissures increase the stress in the underlying wall (Polzer et al., 2011). Attempt on taking into account the strength of the aneurysm tissue based on clinical and image-based parameters has been reported (Vande Geest et al., 2006b).

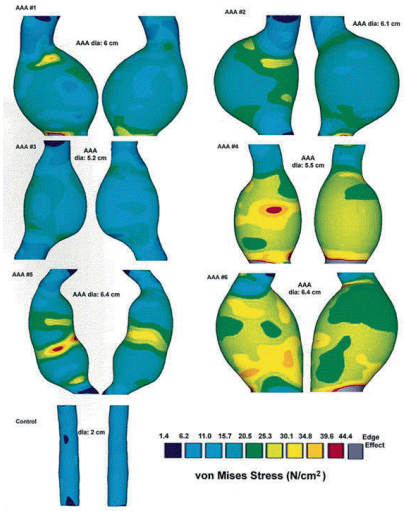

Fig 3. Wall stress under systolic blood pressure in AAA patients and one control. Raghavan et al. (2000) applied the finite-element method to geometries obtained from CT data, and with a nonlinear biomechanical model for AAA wall tissue. In addition to lower stress in the control aorta, large variation in stress is noted over individual aneurysms and between aneurysms with comparable diameters. Posterior and anterior view of all cases. (Reprinted from Raghavan et al. 2000, with permission from Elsevier)

Although wall thickness and material properties are known to vary, these parameters are not available on a patient specific basis. Assumptions about uniform, constant wall-thickness and material properties represent current limitations in wall stress analysis based on CT. By taking advantage of several medical imaging modalities, more patient-specific information can be obtained, thereby providing a more complete image of the state of the aneurysm. Analysis of wall motion in different segments of the aneurysm may reveal information about variations due to thinning, stiffening or weakening of the wall, and thereby contribute to further understanding and prediction of aneurysm progression.

This thesis focuses on ultrasound, which due to being a real-time imaging modality can give both structural and functional (dynamic) information. This may be relevant for directly predicting aneurysm progression, but may also be important in combination with numerical simulations, both for validation purposes and for integrating more patient-specific information into the simulations.

Ultrasound

Ultrasound equipment is portable, relatively inexpensive and does not depend on ionizing radiation. Ultrasound is a real-time imaging modality, and can therefore, in addition to imaging anatomical structures, also be used for investigating blood flow or organ motion, e.g. dynamics of the heart. The ultrasound probe is handheld and manually positioned on the patients' body, which gives an opportunity to interactively investigate the anatomy and potential pathologies. Because ultrasound image quality in some cases is compromised by limited view due to bowel gas or obesity, skills are required both to obtain good images, and to interpret the images.

Medical ultrasound is based on high frequency waves that are transmitted into the body. Structures within the body reflect these waves, and the echoes are analysed for retrieving diagnostic information. Ultrasound refers to frequencies above the audible range, typically in the range 2-20 MHz (megahertz) for medical ultrasound imaging.

Technically, an ultrasound system consists of a scanner generating electrical pulses that are applied to a transducer (probe). The transducer consists of piezoelectric material able to convert between electrical signals and mechanical oscillations. When the transducer is in contact with the skin, these oscillations propagate into the body, comparable to audible sound waves propagating through air. Ultrasound transducers are made up from arrays of elements that are activated with individual time delays to perform beamforming, i.e. focusing and steering of the ultrasound beam. Figure 4 illustates use of electronic delays for beamforming, and transmitted intensity field simulated using Field II (Jensen and Svendsen, 1992).

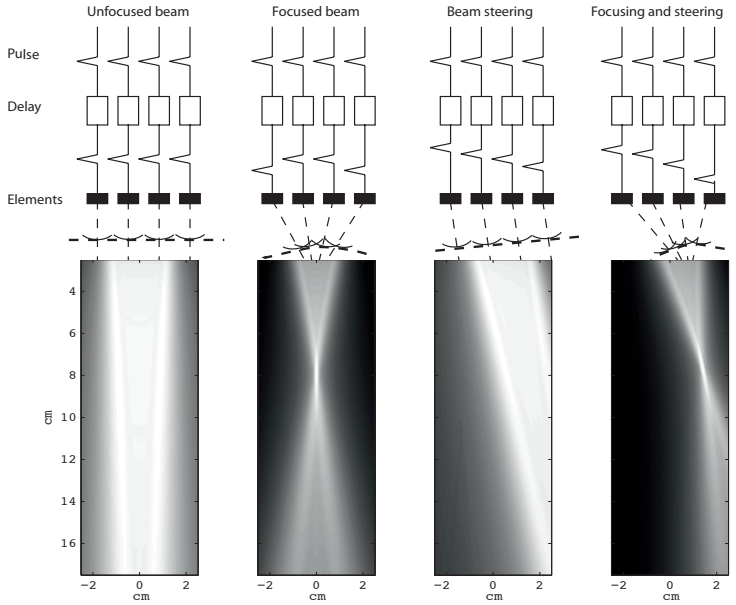

Fig 4. Beamforming. Time delays and corresponding transmitted fields.

Ultrasound propagating into the body is reflected from interfaces between tissues with different acoustical properties, i.e. speed of sound and mass density. Interfaces between soft tissues typically results in reflection of ~1% of the intensity of the ultrasound wave, whereas interfaces between soft tissues and bones reflects ~10-20%. Interfaces between gas and tissue result in almost total reflection, which means that no sound penetrates, thus leaving acoustical shadows behind gas. Penetration is also reduced due to absorption in soft tissue. Bone tissue has higher absorption, resulting in acoustical shadows also behind bones. Sound is not only reflected from interfaces between different tissues, but also scattered from within each tissue due to smaller inhomogeneities. Interference between scattered sound from several inhomogeneities gives rise to speckle pattern. Echogenecity is a term used for describing the reflective properties of different tissues. The relative echogenecity of different structures is described as an-, hypo-, iso- or hyperechoic.

The reflected sound, or echo, is received by the transducer, which converts the acoustical signals back to electrical signals. The received signals are sampled at a time t after transmission of the pulse, and the relation between sample time and depth is given by $t=2d/c$, where c is the speed of sound and d is the depth along the propagation direction. The factor 2 accounts for the two-way distance the pulse propagates forward and back after being reflected. The sampled signals undergo beamforming, post-processing and visualization to retrieve and present diagnostic information (Fig 5).

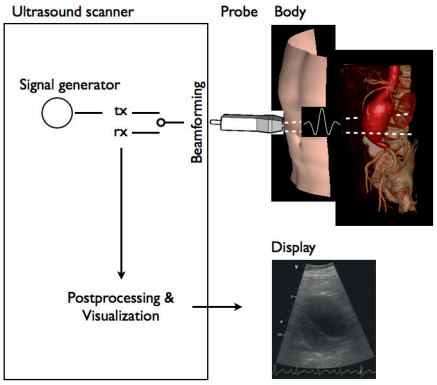

Fig 5. Ultrasound imaging. Signals are transmitted (tx), propagates into the body and are reflected from internal structures. The echoes are received (rx), post-processed and visualized.

The quality of ultrasound systems can be measured in spatial, temporal and contrast resolution. Spatial resolution describes the ability of the ultrasound system to detect and separate nearby structures. The spatial resolution is directionally varying with best resolution along the ultrasound beam (axial), compared with lateral and elevation direction. The spatial resolution of an ultrasound system is characterized by the point-spread-function (PSF). The resolution improves with larger size of the active transducer, smaller depth from the transducer and higher frequency and bandwidth of the transducer. Several techniques are used for obtaining a more homogeneous

resolution also outside of focus; including aperture apodization, dynamic focusing, and multiple transmit foci. PSF in different depths and with different settings has been simulated using Field II (Jensen and Svensen, 1992), as illustrated in Fig 6. Higher frequency gives better resolution, but also increases absorption and obscures imaging of deeper structures. 3.5 MHz is a usual trade-off for imaging the abdominal aorta without too much absorption, while providing a theoretical resolution in the order of 0.5-1 mm in axial and lateral direction, and 2-3 mm in elevation.

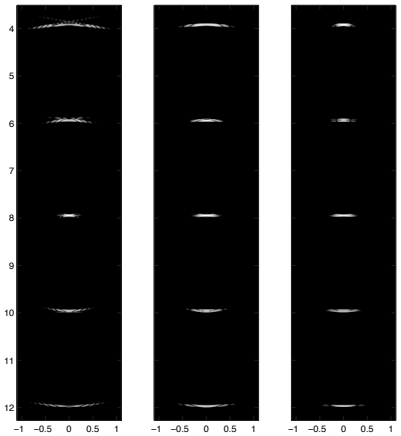

Fig 6. Point-spread-functions in different depths (cm). 3.5 MHz linear array, focus depth 8 cm and aperture 2.8 cm. Compared to the left image, a more homogeneous psf is obtained using apodization (mid), and apodization and dynamic focusing (right).

The temporal resolution is measured in frames per second. Especially for cardiovascular applications, high framerate is necessary to capture dynamics of blood flow and tissue motion. Contrast resolution describes the ability to differentiate between structures with (slightly) different echogenecity. Additional quality measures are sensitivity, which describes the ability to detect low echoes, and dynamic range, which is the ability to simultaneously visualize high and low intensity echoes. Image quality is degraded by noise and absorption, as well as acoustical artefacts from the ultrasound pulse propagation through human tissue with heterogeneous and non-linear acoustic properties. An example of these artefacts is refraction, caused by a change in propagation direction when the ultrasound beam crosses an interface between tissues with different acoustical properties at an oblique angle. Refraction may result in edge shadows or false echoes. Reverberations are multiple reflections between different objects along the propagation direction, causing false echoes and generally degrade the image quality. Aberrations are caused by inhomogeneous speed of sound, which results in degradation of the focusing of the ultrasound system, thus degrading image quality. Substantial efforts are devoted to develop techniques for reducing artefacts. Reverberation artefacts have been reduced by taking advantage of the non-linear propagation of ultrasound, e.g. tissue-harmonic imaging (Caidahl et al., 1998; Desser et al., 1999; Spencer et al., 1998) or SURF imaging (Hansen et al., 2010; Näsholm et al., 2009). (Fig 7). Techniques for aberration correction have been reported (Måsøy et al., 2005; Wang & Li, 2010), and modulated excitation may improve the quality of ultrasound (Misaridis & Jensen, 2005; Sanchez et al., 2009).

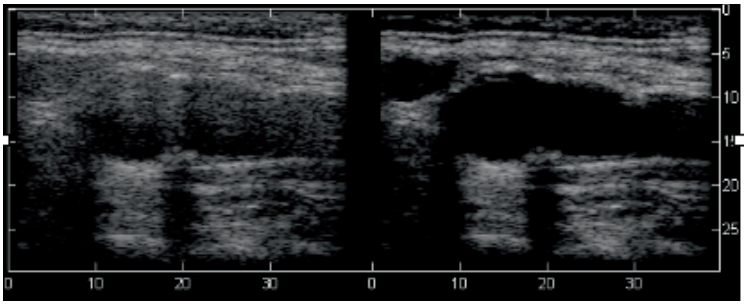

Fig 7. Acoustic noise. Illustrating noise suppression in carotid artery using SURF processing (right) compared to traditional B-mode (left). Courtesy of Rune Hansen (SINTEF/NTNU).

Ultrasound is used in several medical domains, and different ultrasound probes are developed for different applications (Fig 8). Transcutaneous ultrasound imaging is performed using either a linear array probe, typically for imaging superficial structures as the carotid artery; curve-linear array probe (CLA), which is curved to cover a larger sector, typically used for abdominal and obstetric applications; or phased array (PHA) probe, which has a small footprint, but can image a larger sector by steering the ultrasound beam. Phased array probes are typically used in cardiology, where small footprint make it possible to place the probe between the ribs, while obtaining a larger sector to image the heart through the acoustical window. Specialised probes are used for imaging from within the body to come closer to the area of interest, thereby enabling high frequency imaging for high resolution without severe absorption. Further, artefacts caused by bowel gas or propagation through superficial tissues are reduced. One example is the intravascular ultrasound (IVUS) probes that are manoeuvred through blood vessels for investigating cardiovascular diseases.

Structural, functional and even molecular information can be retrieved and presented from ultrasound in a number of ways. In addition to B-mode imaging, this includes estimation of Doppler frequency shift for extraction of velocity information, elastography analysis and contrast-enhanced ultrasound for perfusion imaging. More on these subjects, and specifically in relation to AAA management, can be found in Brekken et al. (2011), appendix. Ultrasound strain estimation is of special interest for this thesis, and will be further described here.

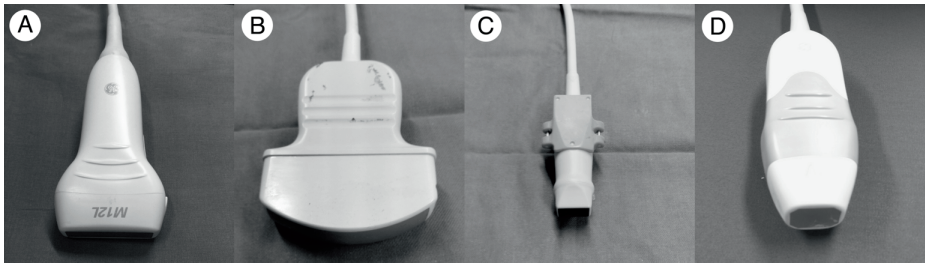

Fig 8. Probes. A-C: Linear, curved linear and phased arrays, respectively. D: 2D matrix array for 3D imaging. Courtesy of Ole Vegard Solberg (SINTEF/NTNU).

Ultrasound strain estimation

Ultrasound strain estimation can be used for obtaining an in-vivo quantitative measure of tissue deformation (Ophir et al., 1991). In cardiology, strain is used for investigating heart function, specifically myocardial contractility (D'Hooge et al., 2000; Sutherland et al., 2004). Strain differentiates between active contraction of the myocardial tissue segment and passive motion caused by contraction of tissue in other segments. Usually, strain imaging refers to imaging of deformation caused by natural motion, e.g. arterial pulsation, in contrast to elastography, which is used when an external force is applied to deform the tissue. Elastography has been used for tissue characterization, e.g. differentiating tumor from normal tissue (Garra, 2007). Strain estimation is relevant for AAA both because strain relates to stress, and because progression of AAA is related to altered mechanical tissue properties changing the elasticity of the wall.

To quantify the deformation based on the ultrasound information, some measure of correlation (e.g. cross-correlation or sum-of-absolute difference) is used to estimate changes from a reference configuration at time t_0 to the current configuration at time t. For tracking of points, the speckle pattern or other features in a neighborhood close to each point (region-of-interest, ROI) is compared to the pattern in a search area around the ROI in the next frame (Fig 9). The motion of the points is used for calculating a deformation field giving the strain. The strain resolution is given by the distance between the points, and is a trade-off between robustness and resolution, since smaller distances between points give larger influence from inaccurate tracking.

Since correlation is used for finding the same point in succeeding frames, the motion of ROIs from frame to frame should ideally be small rigid-body-translation to avoid decorrelation of speckle due to deformation, rotation or large displacements. Therefore, the framerate should be relatively high compared to the motion or velocity. In addition to deformation of the ROI, noise and out-of-plane motion for 2D ultrasound affect tracking negatively. It is therefore beneficial to combine data-driven tracking with some spatial and/or temporal regularization. This could be in form of model based tracking with parameters being optimized to fit the data while constrained to some e.g. biomechanical considerations, physiological constraints or other apriori information.

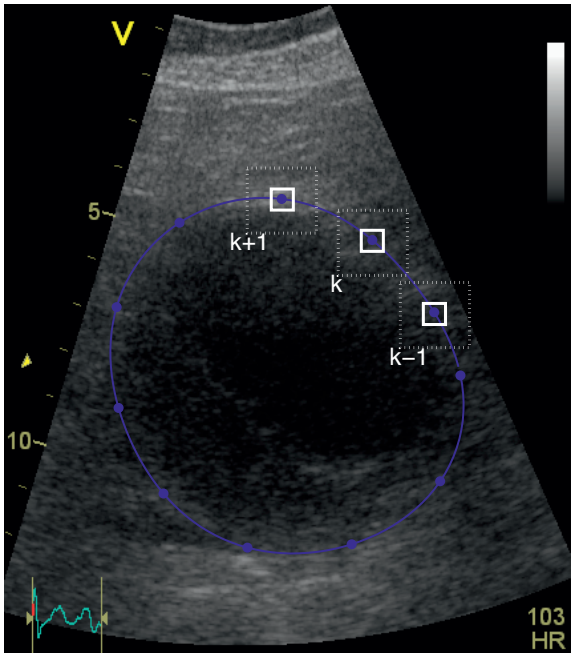

Fig. 9. Tracking. The data inside each ROI (solid square) at time t_n is compared (e.g. by cross-correlation) with data inside search area (dotted square) at time t_{n+1}. More robust tracking can be obtained by making the motion of point k dependent of points k-1 and k+1 through imposing constraints on the shape of the curve.

Aims of study

Ultrasound represents a cost-effective alternative for repeated examinations without increased risk to patients or operators. The subject of this thesis was to investigate use of ultrasound in AAA management, with main focus on developing and investigating concepts and methods for ultrasound based strain estimation in AAA. The physiological motivation is that progression of aneurysm is associated with altered wall tissue composition, which leads to altered elastic properties and altered wall stress. The underlying hypothesis is that it may be possible to detect and quantify this alteration from dynamic ultrasound images, and through that predict further progression and risk of rupture.

Aims:

- Develop a method for ultrasound strain estimation in AAA
- Explore methods for evaluation of strain estimates
- Perform a pilot study for demonstrating clinical use of the method

Summary of papers

Paper I: Strain estimation in AAA from 2D ultrasound

In paper I, we developed a fast, semi-automatic method for estimation of circumferential strain in AAA from sequences of cross-sectional ultrasound B-mode images. A number of points were placed along the circumference of the aneurysm, and tracked over a cardiac cycle. Strain was quantified as the relative change in distance between neighboring points over the cycle. The method was applied to data from 10 AAA patients. We found that local strain values significantly exceeded the circumferential average strain, and that the calculated strain showed no apparent co-variation with diameter over the observed range. This implies that the method gives additional information compared to diameter alone.

Paper II: Reduced strain in AAA after endovascular repair

In paper II, we applied the strain processing method to quantitatively study the difference in mechanical burden on the aneurysm wall before and after EVAR. We showed that strain was inhomogeneous along the circumference, both before and after treatment, and that, despite a significant reduction, cyclic strain was still evident after the stent-graft was placed. For two cases in which endoleak was proven by routine computed tomography, the relative reduction in maximum strain was slightly smaller (35% and 38%, compared to 45%, range 38%–63%) Further studies comprising more patients over time are necessary to investigate the clinical potential for using circumferential strain as an additional indicator of outcome after endovascular repair.

Paper III: 3D visualization of strain in AAA based on navigated ultrasound imaging

An intuitive visualization showing the relation between strain and 3D anatomy may benefit both data acquisition and the interpretation of strain. In paper III, we used navigation technology for combining several 2D ultrasound sectors into a 3D model, augmented with 3D computed tomography (CT) data. To accomplish this, a position frame was mounted to the ultrasound probe, and calibrated to relate the positions in the 2D ultrasound images to 3D spatial coordinates. An optical positioning system was applied to track the position frame. Landmark-based registration was performed to relate CT data to the ultrasound data, and the strain values were mapped onto a model segmented from these CT data. In addition to potentially provide information relevant for assessing the rupture risk of the aneurysm in itself, this model could be used both for comparison with numerical simulations and for integrating measured strain with the

simulations in order to provide a more patient-specific model of the biomechanics of the individual aneurysm.

Paper IV: Simulation model for assessing quality of ultrasound strain estimation in AAA

In paper IV, we developed a simulation model for evaluating methods for ultrasound strain estimation in abdominal aortic aneurysms. Simulated ultrasound features included speckle, absorption and angle dependent reflection, and Gaussian white noise was added to simulate various noise levels. Dynamics was introduced by applying realistic blood pressures to a nonlinear viscoelastic wall model with geometry obtained from a real ultrasound image of an aneurysm. It was concluded that the model simulated realistic circumferential variations in intensity and realistic speckle pattern, and has potential for initial evaluation of strain estimation methods.

Discussion and future work

Clinical impact

While studies indicated increasing prevalence of AAA before the 2000s, more recent data suggest that the prevalence has been declining over the latest years (Sandiford 2011). Still, the increasing age of the population, and increased use of image diagnostics along with potential influence of modern life-style factors is likely to result in a high number of diagnosed aneurysms also in the future. This calls for cost-effective clinical management of AAA.

Being relatively inexpensive, portable and non-ionizing, ultrasound provides an opportunity for cost-effective repeated examinations without increased risk to patient or operator. The investigations are real-time and interactive, making it possible to examine relevant anatomy and potential pathology from different views. Ultrasound is highly suitable for detection of aneurysms and monitoring of aneurysm progression, as well as endoleak detection with contrast-enhanced ultrasound. Further interesting potentials of ultrasound in AAA management include early detection of rupture in emergencies using hand-held ultrasound equipment, and 3D ultrasound for guidance during endovascular repair. Contrast enhanced ultrasound for detection of neo-vascularization, or molecular imaging with targeted micro-bubbles, has potential for early detection, differentiated diagnosis and possible stabilization of aneurysms through local drug-delivery (Brekken et al., 2011, appendix).

The main focus of this PhD study has been to explore ultrasound strain estimation in AAA. By analyzing the dynamics of the wall from ultrasound images with high frame rates (approx. 30-40 images per cardiac cycle), it is possible to retrieve information that may be related to growth or rupture prediction. This information is complementary to structural information such as diameter measurements or CT-based stress analysis. Improved prediction of growth and rupture enables differentiated diagnosis for efficient patient selection, potentially reducing both mortality rates and societal cost by reducing the number of unnecessary examinations and interventions. Although screening of subgroups with increased AAA susceptibility has been shown to reduce AAA mortality (Cosford & Leng, 2007; Ferket et al., 2011; Takagi et al., 2010), improved prediction would also benefit efficiency and ethical aspects of screening programs.

The motivation for investigation of aneurysm progression by ultrasound strain estimation is that formation and progression of aneurysms are associated with altered stress and mechanical wall properties. Biological processes affecting elastin, collagen and SMC result in altered elastic properties. This alteration could possibly be examined using ultrasound for analyzing the pulsatile wall motion. Specifically, aneurysm formation and growth is associated with stiffening of the aortic tissue, which causes

lower strain values. If further progress results in loss of collagen or fail to synthesize collagen, the wall will be weakened and the aneurysm may rupture. Loss of collagen could make the tissue more extensible, which potentially could be observed through higher strain values compared to size-matched aneurysms that are less prone to rupture.

Imura et al. (1986) used ultrasound for studying elastic behavior of the aorta. Ultrasound was used for tracking the diameter pulsation over the cardiac cycle, and elasticity was quantified by the pressure-strain elastic modulus, $E_p=\Delta p/(\Delta D/D)$, where Δp and ΔD are the differences between systolic and diastolic pressure and diameter, respectively, while D is mean diameter. In addition to pressure-strain elastic modulus, due to non-linearity between strain and stress, stiffness (β) have also been quantified as $\beta=\ln(\Delta p)/(\Delta D/D)$. Several authors have used similar techniques to study the elastic behavior of AAA. It has been shown that the aorta is stiffer in men than age-matched women, that stiffness increases with age, and that aneurysm tissue is significantly stiffer compared with normal aorta (Länne et al., 1992; Sonesson et al., 1993). Wilson et al. (1998) also found that aneurysm tissue was stiffer than normal tissue, while less stiff aneurysms tended to be more prone to rupture. They later showed that large aneurysms were stiffer than smaller, but with large variations for equally sized aneurysms (Wilson et al., 1999), and that increased distensibility over time (compared to baseline) indicated significantly reduced time to rupture (Wilson et al., 2003). Long et al. (2005) reported a trend toward increased distensibility with increased AAA diameter. On the other hand, Sonesson et al. (1999) found no significant difference in wall mechanics in those AAAs that subsequently ruptured compared with electively operated AAAs in a study comprising 285 patients.

While the mechanical properties are known to vary heterogeneously over the aneurysm wall (Thubrikar et al., 2001), the dynamic change in diameter over the cardiac cycle gives a measure of the average elasticity over the cross-section of the aneurysm wall. Using ultrasound for estimation of segmental strain gives a local assessment of tissue properties, which could potentially give information relevant to infer the state and predict further progression of the aneurysm and thereby improve selection of patients for AAA treatment.

Ultrasound strain processing in AAA

We have investigated concepts and methods for estimating strain from 2D cross-sectional ultrasound images. Preliminary results indicate that the implemented methods reveal heterogeneous local wall strain and may have additional information compared to diameter measurements. However, there are limitations still to be overcome, including method refinement and verification, and further investigations on correlation with clinically relevant parameters.

The strain estimation algorithm presented in Paper I is based on tracking of a number of points along the aneurysm circumference. A set of points are semi-automatically chosen, and these points are then tracked normal to the wall using temporal correlation of ROIs in the neighborhood of each point, in combination with dynamic programming

to impose spatial smoothness and avoid large geometrical changes compared to the initial configuration. A curve is then obtained by spline interpolation between the points for each time frame, resulting in a moving curve following the pulsation of the aortic wall. A second set of (equidistant) points is then (automatically) chosen and tracked along this curve, and strain is estimated as the relative distance between each neighboring point. The tracking method could possibly be improved by taking more information into account. First, instead of using data only in the neighborhood of each point, data along the entire circumference should be used in order to optimize the moving curve, e.g. by optimizing control points of the spline curve or by using a Fourier parameterization of the curve (e.g. Ravon et al., 2001). We implemented an example of a Fourier parameterization with the curve described in polar coordinates (r,θ):

$$r_k = r(\theta_k) = \sum_{n=-M}^{M} c_n \cdot e^{in\theta_k}$$

$$x_k(t) = x_c(t) + \left(\sum_{n=-M}^{M} c_n(t) \cdot e^{in\theta_k} \right) \cdot \cos(\theta_k)$$

$$y_k(t) = y_c(t) + \left(\sum_{n=-M}^{M} c_n(t) \cdot e^{in\theta_k} \right) \cdot \sin(\theta_k)$$

As illustrated in Fig 10, the wall can be represented with few parameters (M=3) and parameter optimization can be a robust approach to tracking. Secondly, it may be necessary to allow points tracked along this curve to be slightly off the curve to compensate for possible inaccuracies in the tracking of the curve. In addition to the B-mode based tracking approach, it is also possible that Doppler information could be used for improving tracking results (Heimdal et al., 1998, McDicken et al., 1992; Sutherland et al., 1994). Also, temporal regularization could be imposed in addition to spatial constraints by a model-based tracking approach. (Orderud et al., 2008). Last, a fully automatic method would improve repeatability by avoiding variation due to manual initial indication of the wall.

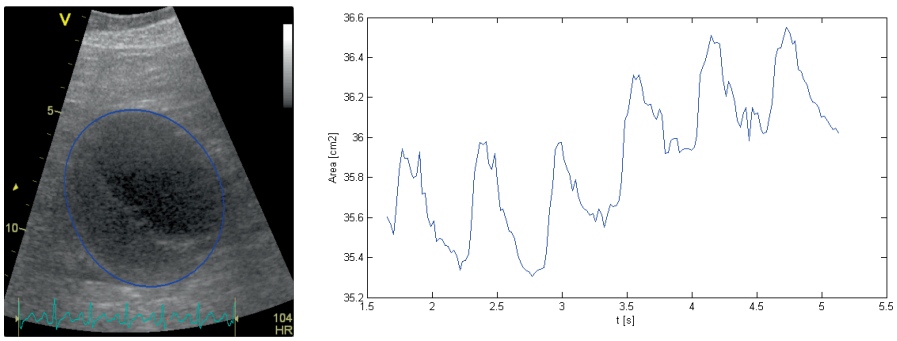

Fig 10. Left: Ultrasound image of AAA with a Fourier parameterized curve adapted to the wall. Right: The area of the aneurysm tracked over six consecutive cardiac cycles.

A further improvement would be achieved by implementing the strain processing method on an ultrasound scanner for online, (close to) real-time evaluation and data acquisition. This would not only improve logistics in larger patient studies, but also make it easier to evaluate strain in several cross-sections and with different angles to find planes with maximum and minimum strain values. Since repeated consecutive measurements may differ slightly in position and orientation, online real-time processing could also reduce variability because several views could be investigated. Use of navigation technology for combining several cross-sections, as described in Paper III, could be useful for visualizing the combined results from different cross-sections. In addition, recent advances in 3D ultrasound imaging technology could provide a possibility for real-time 3D strain estimation, which has been investigated for cardiology (Crosby et al., 2008; Elen et al., 2008; Orderud et al., 2008), and is interesting for future research also on AAA dynamics. Advances in ultrasound technology are further expected to reduce noise, which will benefit strain estimation, since tracking accuracy, and therefore accuracy of strain estimation, is negatively influenced by noise.

It is worth noting that when estimating strain caused by cardiac or arterial pulsation, ultrasound only gives a cyclic strain relative to diastole, not absolute strain, since it is not possible to measure how much the tissue is deformed in diastole relative to a non-pressurized configuration (i.e. diastolic strain is unknown).

To estimate the elastic properties of the tissue, it is important to consider wall stress in addition to strain. Patient specific simulation could be combined with ultrasound strain to obtain a more complete picture for predicting further aneurysm progression. The method described in Paper III is an important step towards combining ultrasound strain with FEM analysis based on 3D CT data. This combined information may improve assessment of growth and rupture potential compared to each modality alone.

Clinical validation

Before initiation of larger clinical studies, as much as possible should be known about the quality of the strain estimation. As a starting point, the method could be evaluated using simulated data, e.g. as suggested in Paper IV. The benefit of simulation is particularly that all parameters are known with absolute certainty, while compromising realism may be a disadvantage. Simulation should therefore be used in combination with other testing, e.g. including laboratory models. In addition, reproducibility should be studied. Reproducibility is necessary in order to investigate possible correlation with clinical parameters, to assure that the estimates are consistent over time and between different operators and patients.

After initial method verification, the most important in the end is clinical studies to investigate if strain can be correlated with clinically significant parameters. In Paper II we showed that the method could be used to measure an expected reduction in strain after EVAR. Further studies with more patients and longer follow-up after EVAR could be performed to study a possible relation between strain and endoleak or endotension.

This could give more insight into the potential relation between strain and shrinkage, stability and growth of aneurysms.

Studies investigating potential relation between strain and rupture are difficult since intervention will usually be recommended for aneurysms kept under surveillance if the diameter exceeds 50-55 mm. Possibilities for studying rupture include a few ruptures of small aneurysms, and investigations of patients with larger aneurysms refusing or unfit for repair. Inclusion of ruptured aneurysms could be increased through multicenter studies. A simpler study would be to investigate if strain could be used to predict growth of small aneurysms, since patients could then be included prospectively and followed over a longer time-period without intervention to see if strain is different in aneurysms that are stable or slow or fast growing.

Further insight may be obtained by studying strain in relation to more secondary measures, e.g. including both normal subjects and aneurysm patients to investigate strain versus age, gender, presence and size of aneurysms and amount of thrombus. Further studies could be initiated to investigate correlation between strain and known risk factors. This could include investigating if risk-factor modification (e.g. smoking cessation, blood pressure regularization, medication, exercise and diet) gives an associated modification of strain. It would also be interesting to study if strain is different between fusiform and saccular aneurysms, especially if strain is different in growing parts of the aneurysm compared to non-growing parts. Yet a possible study could be to investigate if the suggested method could be used to relate in-vivo strain to the extent of biological constituents (e.g. elastin, collagen, SMC or vasa vasorum), either by harvesting tissue samples from patients during open surgery, or from animal studies. E.g. Favreau et al. (2012) showed that stiffening of the aorta after angiotensin II injection in mice could be observed as reduced strain measured by murine ultrasound. Finally, ultrasound strain measurements could be compared to other diagnostic alternatives, including e.g. numerical wall stress analyses (Fillinger et al., 2003).

Conclusion

Ultrasound is useful in several aspects of assisting clinical management of AAA. The main focus of this thesis has been to investigate ultrasound strain estimation in AAA, with a future goal to provide better prediction of growth and rupture, and thereby assist in patient selection. Compared to earlier approaches measuring the dynamic changes in diameter over the cardiac cycle, a strain estimation method with spatial resolution was developed in this thesis, thereby providing more detailed information. It was observed that strain varied along the circumference of the aneurysm wall, and that strain provided information that was additional to size. The strain processing method managed to differentiate strain before from after insertion of stent-graft, despite varying image quality among patients.

We further developed a method for combining 2D strain analysis with anatomical information from CT. This illustrated how structural and functional imaging from different imaging modalities could be combined to increase the amount of available information. Further work may include integration of ultrasound strain measurements with numerical wall stress simulation.

Correlation based tracking is susceptible to noise and out-of-plane motion. Considering the varying quality of abdominal ultrasound imaging, it is necessary to evaluate how well the strain estimation method performs. For this purpose we developed a simulation model for simulating both dynamic behavior and ultrasound images of AAA. The model will be useful for future method refinement and verification. Future technology that improves noise-suppression in ultrasound images can further improve the accuracy and resolution of strain estimation methods.

In summary, methods and concepts with promising potential have been developed and illustrated. Future refinement of methods may include online, real-time processing and 3D ultrasound for 3D strain analysis. Clinical studies, comprising more patients followed over longer time, are necessary to investigate if strain could differentiate between aneurysms with different prognosis.

References

Apter JT, Rabinowitz M and Cummings DH. (1966). Correlation of visco-elastic properties of large arteries with microscopic structure. *Circ. Res.* Vol.19, No.1, (Jul), pp. 104-121.

Baxter BT, Terrin MC, Dalman RL. (2008). Medical management of small abdominal aortic aneurysms. *Circulation*. Vol.117, No.14, (Apr), pp. 1883-1889.

Bengtsson H, Sonesson B, Bergqvist D. (1996). Incidence and prevalence of abdominal aortic aneurysms, estimated by necropsy studies and population screening by ultrasound. *Ann N Y Acad Sci*. Vol.800, No., (Nov), pp. 1–24.

Brekken R, Dahl T, Hernes TAN. (2011). Ultrasound in abdominal aortic aneurysm. In Prof. dr. R.T. Grundmann (Ed.): Diagnosis, screening and treatment of abdominal, thoracoabdominal and thoracic aortic aneurysms. InTech, Croatia.

Brewster DC, Cronenwett JL, Hallett JW Jr, Johnston KW, Krupski WC & Matsumura JS. (2003). Guidelines for the treatment of abdominal aortic aneurysms. Report of a subcommittee of the Joint Council of the American Association for Vascular Surgery and Society for Vascular Surgery. *J Vasc Surg*. Vol.37, No.5 (May), pp. 1106-1117.

Caidahl K, Kazzam E, Lidberg J, Neumann Andersen G, Nordanstig J, Rantapää Dahlqvist S, Waldenström A, Wikh R. (1998). New concept in echocardiography: harmonic imaging of tissue without use of contrast agent. *Lancet*. Vol.352, No.9136, (Oct), pp. 1264-1270.

Chaikof EL, Brewster DC, Dalman RL, Makaroun MS, Illig KA, Sicard GA, Timaran CH, Upchurch GR Jr, Veith FJ. (2009). The care of patients with an abdominal aortic aneurysm: the Society for Vascular Surgery practice guidelines. *J Vasc Surg*. Vol.50, No.4S, (Oct), pp. S2-S49.

Chien S. (2007). Mechanotransduction and endothelial cell homeostasis: the wisdom of the cell. *Am J Physiol Heart Circ Physiol*. Vol.292, No.3, (Mar), pp. H1209-1224.

Choke E, Thompson MM, Dawson J, Wilson WR, Sayed S, Loftus IM, Cockerill GW. (2006). Abdominal aortic aneurysm rupture is associated with increased medial neovascularization and overexpression of proangiogenic cytokines. *Arterioscler Thromb Vasc Biol*. Vol.26, No.9, (Sep), pp. 2077-2082.

Cosford PA, Leng GC. (2007). Screening for abdominal aortic aneurysm. *Cochrane Database Syst Rev*. Vol.18, No.2, (Apr), CD002945.

Crosby J, Amundsen BH, Hergum T, Remme EW, Langeland S, Torp H. (2009). 3-D speckle tracking for assessment of regional left ventricular function. *Ultrasound Med Biol*. Vol.35, No.3, (Mar), pp. 458-471.

D'hooge J, Heimdal A, Jamal F, Kukulski T, Bijnens B, Rademakers F, Hatle L, Suetens P, Sutherland GR. (2000). Regional strain and strain rate measurements by cardiac ultrasound: principles, implementation and limitations. *Eur J Echocardiogr*. Vol.1, No.3, (Sep), pp. 154-170.

Darling RC, Messina CR, Brewster DC, Ottinger LW. (1977). Autopsy study of unoperated abdominal aortic aneurysms. The case for early resection. *Circulation*. Vol.56, No.3 Suppl, (Sep), pp. II161-164.

Desser TS, Jeffrey RB Jr, Lane MJ, Ralls PW. (1999). Tissue harmonic imaging: utility in abdominal and pelvic sonography. *J Clin Ultrasound*. Vol.27, No.3, (Mar-Apr), pp. 135-142.

Di Martino ES, Bohra A, Vande Geest JP, Gupta N, Makaroun MS,Vorp DA. (2006). Biomechanical properties of ruptured versus electively repaired abdominal aortic aneurysm wall tissue. *J Vasc Surg*. Vol.43, No.3, (Mar), pp. 570-576.

Di Martino ES, Guadagni G, Fumero A, Ballerini G, Spirito R, Biglioli P, Redaelli A. (2001). Fluid-structure interaction within realistic three-dimensional models of the aneurysmatic aorta as a guidance to assess the risk of rupture of the aneurysm. *Med Eng Phys*. Vol.23, No.9, (Nov), pp. 647-655.

Di Martino ES, Vorp DA. (2003). Effect of variation in intraluminal thrombus constitutive properties on abdominal aortic aneurysm wall stress. *Ann Biomed Eng*. Vol.31, No.7, (Jul-Aug), pp. 804-809.

Elen A, Choi HF, Loeckx D, Gao H, Claus P, Suetens P, Maes F, D'hooge J. (2008). Three-dimensional cardiac strain estimation using spatio-temporal elastic registration of ultrasound images: a feasibility study. *IEEE Trans Med Imaging*. Vol.27, No.11, (Nov), pp. 1580-91.

Favreau JT, Nguyen BT, Gao I, Yu P, Tao M, Schneiderman J, Gaudette GR, Ozaki CK. (2012). Murine ultrasound imaging for circumferential strain analyses in the angiotensin II abdominal aortic aneurysm model. *J Vasc Surg*. Apr 13. Epub ahead of print.

Ferket BS, Grootenboer N, Colkesen EB, Visser JJ, van Sambeek MR, Spronk S, Steyerberg EW, Hunink MG. (2011). Systematic review of guidelines on abdominal aortic aneurysm screening. *J Vasc Surg*. Epub: Feb 14.

Fillinger MF, Marra SP, Raghavan ML, Kennedy FE. (2003). Prediction of rupture risk in abdominal aortic aneurysm during observation: wall stress versus diameter. *J Vasc Surg*. Vol.37, No.4, (Apr), pp. 724-732.

Freestone T, Turner RJ, Coady A, Higman DJ, Greenhalgh RM, Powell JT. (1995). Inflammation and matrix metalloproteinases in the enlarging abdominal aortic aneurysm. *Arterioscler Thromb Vasc Biol*. Vol.15, No.8, (Aug), pp. 1145-1151.

Fung, YC. (2004). *Biomechanics – Mechanical properties of living tissues*. 2nd Edition. Chapter 8: Mechanical properties and active remodeling of blood Vessels. Springer Verlag. New York, US.

Garra BS. (2007). Imaging and estimation of tissue elasticity by ultrasound. *Ultrasound Q*. Vol.23, No.4, (Dec), pp. 255-268.

Georgakarakos E, Ioannou CV, Volanis S, Papaharilaou Y, Ekaterinaris J, Katsamouris AN. (2009). The influence of intraluminal thrombus on abdominal aortic aneurysm wall stress. *Int Angiol*. Vol.28, No.4, (Aug), pp. 325-333.

Hansen R, Måsoy SE, Johansen TF, Angelsen BA. (2010). Utilizing dual frequency band transmit pulse complexes in medical ultrasound imaging. *J Acoust Soc Am*. Vol.127, No.1, (Jan), pp. 579-587.

He CM, Roach MR. (1994). The composition and mechanical properties of abdominal aortic aneurysms. *J Vasc Surg*. Vol.20, No.1, (Jul), pp. 6-13.

Heimdal A, Støylen A, Torp H, Skjaerpe T. (1998). Real-time strain rate imaging of the left ventricle by ultrasound. *J Am Soc Echocardiogr*. Vol.11, No.11, (Nov), pp. 1013-1019.

Herron GS, Unemori E, Wong M, Rapp JH, Hibbs MH, Stoney RJ. (1991). Connective tissue proteinases and inhibitors in abdominal aortic aneurysms. Involvement of the vasa vasorum in the pathogenesis of aortic aneurysms. *Arterioscler Thromb Vasc Biol*. Vol.11, No.6, (Nov-Dec), pp. 1667-1677.

Holmes DR, Liao S, Parks WC, Thompson RW. (1995). Medial neovascularization in abdominal aortic aneurysms: a histopathologic marker of aneurysmal degeneration with pathophysiologic implications. *J Vasc Surg*. Vol.21, No.5, (May), pp. 761-771.

Imura T, Yamamoto K, Kanamori K, Mikami T, Yasuda H. (1986). Non-invasive ultrasonic measurement of the elastic properties of the human abdominal aorta. *Cardiovasc Res*. Vol.20, No.3, (Mar), pp. 208-214.

Imura T, Yamamoto K, Satoh T, Kanamori K, Mikami T, Yasuda H. (1990). In vivo viscoelastic behavior in the human aorta. *Circ Res*. Vol.66, No.5, (May), pp. 1413-1419.

Irgens F. (2005). *Continuum mechanics*. Vol 1. Lecture compendium. NTNU, Trondheim, Norway.

Jensen JA, Svendsen NB. (1992). Calculation of pressure fields from arbitrarily shaped, apodized, and excited ultrasound transducers. *IEEE Trans Ultrason Ferroelectr Freq Control*. Vol.39, No.2, pp. 262-267.

Johnston KW, Rutherford RB, Tilson MD, Shah DM, Hollier L, Stanley JC. (1991). Suggested standards for reporting on arterial aneurysms. Subcommittee on Reporting Standards for Arterial Aneurysms, Ad Hoc Committee on Reporting Standards, Society for Vascular Surgery and North American Chapter, International Society for Cardiovascular Surgery. *J Vasc Surg*. Vol.13, No.3, (Mar), pp. 452-458.

Kniemeyer HW, Kessler T, Reber PU, Ris HB, Hakki H, Widmer MK. (2000). Treatment of ruptured abdominal aortic aneurysm, a permanent challenge or a waste of resources? Prediction of outcome using a multi-organ-dysfunction score. *Eur J Vasc Endovasc Surg*. Vol.19, No.2, (Feb), pp. 190–196.

Länne T, Sonesson B, Bergqvist D, Bengtsson H, Gustafsson D. (1992). Diameter and compliance in the male human abdominal aorta: influence of age and aortic aneurysm. *Eur J Vasc Surg*. Vol.6, No.2, (Mar), pp. 178-184.

Li ZY, U-King-Im J, Tang TY, Soh E, See TC, Gillard JH. (2008). Impact of calcification and intraluminal thrombus on the computed wall stresses of abdominal aortic aneurysm. *J Vasc Surg*. Vol.47, No.5, (May), pp. 928-935.

Liddington MI, Heather BP. (1992). The relationship between aortic diameter and body habitus. *Eur J Vasc Surg*. Vol.6, No.1, (Jan), pp. 89–92.

Long A, Rouet L, Bissery A, Rossignol P, Mouradian D, Sapoval M. (2005). Compliance of abdominal aortic aneurysms evaluated by tissue Doppler imaging: correlation with aneurysm size. *J Vasc Surg*. Vol.42, No.1, (Jul), pp. 18-26.

Måsøy SE, Varslot T, Angelsen B. (2005). Iteration of transmit-beam aberration correction in medical ultrasound imaging. *J Acoust Soc Am*. Vol.117, No.1, (Jan), pp. 450-461.

McDicken WM, Sutherland GR, Moran CM, Gordon LN. (1992). Colour doppler velocity imaging of the myocardium. *Ultrasound Med Biol*. Vol.18, No.6-7, pp. 651–654.

McGregor JC, Pollock JG, Anton HC. (1975). The value of ultrasonography in the diagnosis of abdominal aortic aneurysm. *Scott Med J*. Vol.20, pp. 133–37.

Misaridis T, Jensen JA. (2005). Use of modulated excitation signals in medical ultrasound. Part I: Basic concepts and expected benefits. *IEEE Trans Ultrason Ferroelectr Freq Control*. Vol.52, No.2, (Feb), pp. 177-191.

Moll FL, Powell JT, Fraedrich G, Verzini F, Haulon S, Waltham M, van Herwaarden JA, Holt PJ, van Keulen JW, Rantner B, Schlösser FJ, Setacci F, Ricco JB. (2011). Management of abdominal aortic aneurysms clinical practice guidelines of the European society for vascular surgery. *Eur J Vasc Endovasc Surg*. Vol.41, No.S1, (Jan), pp. S1-S58.

Mower WR, Quiñones WJ, Gambhir SS. (1997). Effect of intraluminal thrombus on abdominal aortic aneurysm wall stress. *J Vasc Surg*. Vol.26, No.4, (Oct), pp. 602-608.

Näsholm SP, Hansen R, Måsøy SE, Johansen TF, Angelsen BA. (2009). Transmit beams adapted to reverberation noise suppression using dual-frequency SURF imaging. *IEEE Trans Ultrason Ferroelectr Freq Control*. Vol.56, No.10, (Oct), pp. 2124-2133.

Ophir J, Céspedes I, Ponnekanti H, Yazdi Y, Li X. (1991). Elastography: a quantitative method for imaging the elasticity of biological tissues. *Ultrason Imaging*. Vol.13, No.2, (Apr), pp. 111-134.

Orderud F, Kiss G, Langeland S, Remme EW, Torp HG, Rabben SI. (2008). Combining edge detection with speckle-tracking for cardiac strain assessment in 3D echocardiography. Ultrasonics Symposium. IEEE IUS 2008, pp. 1959-1962.

Petersen E, Wagberg F, Angquist KA. (2002). Proteolysis of the abdominal aortic aneurysm wall and the association with rupture. *Eur J Vasc Endovasc Surg*. Vol.23, No.2, (Feb), pp. 153-157.

Polzer S, Gasser TC, Swedenborg J, Bursa J. (2011). The impact of intraluminal thrombus failure on the mechanical stress in the wall of abdominal aortic aneurysms. Eur J Vasc Endovasc Surg. Vol.41, No.4, (Apr), pp. 467-473. ILT.

Raghavan ML, Vorp DA, Federle MP, Makaroun MS, Webster MW. (2000). Wall stress distribution on three-dimensionally reconstructed models of human abdominal aortic aneurysm. *J Vasc Surg.* Vol.31, No.4, (Apr), pp. 760 – 769.

Raghavan ML, Webster MW, Vorp DA. (1996). Ex vivo biomechanical behavior of abdominal aortic aneurysm: assessment using a new mathematical model. *Ann Biomed Eng*. Vol.24, No.5, (Sep-Oct), pp. 573-582.

Ravhon R, D. Adam D, Zelmanovitch L. (2001). Validation of Ultrasonic Image Boundary Recognition in Abdominal Aortic Aneurysm. *IEEE Trans Med Imag*. Vol.20, No.8, (Aug), pp. 751-763.

Sakalihasan N, Limet R, Defawe OD. (2005). Abdominal aortic aneurysm. *Lancet*. Vol.365, No.9470, (Apr 30-May 6), pp. 1577-1589.

Sanchez JR, Pocci D, Oelze ML. (2009). A novel coded excitation scheme to improve spatial and contrast resolution of quantitative ultrasound imaging. *IEEE Trans Ultrason Ferroelectr Freq Control*. Vol.56, No.10, (Oct), pp. 2111-2123.

Sandiford P, Mosquera D, Bramley D. (2011). Trends in incidence and mortality from abdominal aortic aneurysm in New Zealand. British Journal of Surgery. Vol. 98, No. 5, (May), pp. 645-651.

Sheidaei A, Hunley SC, Zeinali-Davarani S, Raguin LG, Baek S. (2011). Simulation of abdominal aortic aneurysm growth with updating hemodynamic loads using a realistic geometry. *Med Eng Phys*. Vol.33, No.1, (Jan), pp. 80-88.

Sonesson B, Hansen F, Stale H, Länne T. (1993). Compliance and diameter in the human abdominal aorta--the influence of age and sex. *Eur J Vasc Surg*. Vol.7, No.6, (Nov), pp. 690-697.

Sonesson B, Sandgren T, Länne T. (1999). Abdominal aortic aneurysm wall mechanics and their relation to risk of rupture. *Eur J Vasc Endovasc Surg*. Vol.18, No.6, (Dec), pp. 487-493.

Spencer KT, Bednarz J, Rafter PG, Korcarz C, Lang RM. (1998). Use of harmonic imaging without echocardiographic contrast to improve two-dimensional image quality. *Am J Cardiol*. Vol.82, No.6, (Sep), pp. 794-799.

Sumner DS, Hokanson DE, Strandness DE Jr. (1970). Stress-strain characteristics and collagen-elastin content of abdominal aortic aneurysms. *Surg Gynecol Obstet*. Vol.130, No.3, (Mar), pp. 459-466.

Sutherland GR, Stewart MJ, Groundstroem WE, Moran CM, Fleming A, Guell-Peris FJ, Riemersma RA, Fenn LN, Fox KAA, McDicken WN. (1994). Color doppler myocardial imaging: a new technique for the assessment of myocardial function. *J Am Soc Echocardio*. Vol.7, No.5, (Sept-Oct), pp. 441–458.

Sutherland GR, Di Salvo G, Claus P, D'hooge J, Bijnens B. (2004). Strain and strain rate imaging: a new clinical approach to quantifying regional myocardial function. *J Am Soc Echocardiogr*. Vol.17, No.7, (Jul), pp. 788-802.

Takagi H, Goto SN, Matsui M, Manabe H, Umemoto T. (2010). A further meta-analysis of population-based screening for abdominal aortic aneurysm. *J Vasc Surg*. Vol.52, No.4, (Oct), pp. 1103-1108.

Thompson MM, Jones L, Nasim A, Sayers RD, Bell PR. (1996). Angiogenesis in abdominal aortic aneurysms. *Eur J Vasc Endovasc Surg*. Vol.11, No.4, (May), pp. 464-469.

Thompson MM. Controlling the expansion of abdominal aortic aneurysms. (2003). *Br J Surg*. Vol. 90, No.8, (Aug), pp. 897–898.

Thubrikar MJ, Labrosse M, Robicsek F, Al-Soudi J, Fowler B. (2001). Mechanical properties of abdominal aortic aneurysm wall. *J Med Eng Technol*. Vol.25, No. 4, (Jul-Aug), pp. 133-142.

Vande Geest JP, Di Martino ES, Bohra A, Makaroun MS, Vorp DA. (2006b). A biomechanics-based rupture potential index for abdominal aortic aneurysm risk assessment: demonstrative application. *Ann N Y Acad Sci*. Vol.1085, (Nov), pp. 11-21.

Vande Geest JP, Sacks MS, Vorp DA. (2006a). The effects of aneurysm on the biaxial mechanical behavior of human abdominal aorta. *J Biomech*. Vol.39, No. 7, (), pp. 1324-1334.

Volokh KY, Vorp DA. (2008). A model of growth and rupture of abdominal aortic aneurysm. *J Biomech*. Vol.41, No.5, (), pp. 1015-1021.

Vorp DA, Raghavan ML, Muluk SC, Makaroun MS, Steed DL, Shapiro R, Webster MW. (1996). Wall strength and stiffness of aneurysmal and nonaneurysmal abdominal aorta. *Ann N Y Acad Sci*. Vol.800, (Nov), pp. 274–277.

Wang DH, Makaroun MS, Webster MW, Vorp DA. (2002). Effect of intraluminal thrombus on wall stress in patient-specific models of abdominal aortic aneurysm. *J Vasc Surg*. Vol.36, No.3, (Sep), pp. 598-604.

Wang SL, Li PC. (2010). Aperture-domain processing and its applications in ultrasound imaging: a review. *Proc Inst Mech Eng H*. Vol.224, No.2, (), pp. 143-154.

Watton PN, Hill NA, Heil M. (2004). A mathematical model for the growth of the abdominal aortic aneurysm. *Biomech Model Mechanobiol*. Vol.3, No.2, (Nov), pp. 98–113.

Wilson K, Bradbury A, Whyman M, Hoskins P, Lee A, Fowkes G, McCollum P, Ruckley CV. (1998). Relationship between abdominal aortic aneurysm wall compliance and clinical outcome: a preliminary analysis. *Eur J Vasc Endovasc Surg*. Vol.15, No.6, (Jun), pp. 472-477.

Wilson K, Whyman M, Hoskins P, Lee AJ, Bradbury AW, Fowkes FG, Ruckley CV. (1999). The relationship between abdominal aortic aneurysm wall compliance, maximum diameter and growth rate. *Cardiovasc Surg*. Vol.7, No.2, (Mar), pp. 208-213.

Wilson KA, Lee AJ, Lee AJ, Hoskins PR, Fowkes FG, Ruckley CV, Bradbury AW. (2003). The relationship between aortic wall distensibility and rupture of infrarenal abdominal aortic aneurysm. *J Vasc Surg*. Vol.37, No.1, (Jan), pp. 112-117.

Wolters BJ, Rutten MC, Schurink GW, Kose U, de Hart J, van de Vosse FN. (2005). A patient-specific computational model of fluid-structure interaction in abdominal aortic aneurysms. *Med Eng Phys*. Vol.27, No.10, (Dec), pp. 871-883.

Yoshimura K, Ikeda Y, Aoki H. (2011). Innocent bystander? Intraluminal thrombus in abdominal aortic aneurysm. *Atherosclerosis*. Vol.218, No.2, (Oct), pp. 285-286.

Zankl AR, Schumacher H, Krumsdorf U, Katus HA, Jahn L, Tiefenbacher CP. (2007). Pathology, natural history and treatment of abdominal aortic aneurysms. *Clin Res Cardiol*. Vol.96, No.3, (Mar), pp-140-151.

Zatina MA, Zarins CK, Gewertz BL, Glagov S. (1984). Role of medial lamellar architecture in the pathogenesis of aortic aneurysms. *J Vasc Surg*. Vol.1, No.3, (May), pp. 442-448.

Paper I

Ultrasound in Med. & Biol., Vol. 32, No. 1, pp. 33–42, 2006

0301-5629/06/$–see front matter

ELSEVIER

doi:10.1016/j.ultrasmedbio.2005.09.007

● *Original Contribution*

STRAIN ESTIMATION IN ABDOMINAL AORTIC ANEURYSMS FROM 2-D ULTRASOUND

REIDAR BREKKEN,* JON BANG,* ASBJØRN ØDEGÅRD,† JENNY AASLAND,† TORIL A. N. HERNES,*‡ and HANS OLAV MYHRE†

*SINTEF Health Research, Trondheim, Norway; †St. Olav's Hospital, University Hospital of Trondheim, Trondheim, Norway; and ‡Norwegian University of Science and Technology, Trondheim, Norway

(*Received* 9 *June* 2005, *revised* 9 *September* 2005, *in final form* 14 *September* 2005)

Abstract—The rupture risk of abdominal aortic aneurysms (AAAs) is routinely inferred from the maximum diameter of the AAA. However, clinical experience indicates that this criterion has poor accuracy and that noninvasive assessment of the elastic properties of the vessel might give better correspondence with the rupture risk. We have developed a method for analysis of circumferential strain in AAAs from sequences of cross-sectional ultrasound B-mode images. The algorithm is fast, semiautomatic and well-suited for real-time applications. The method was developed and evaluated using data from 10 AAA patients. The preliminary results demonstrate that the method is sufficiently accurate and robust for clinically acquired data. An important finding is that local strain values may exceed the circumferential average strain significantly. Furthermore, the calculated strain shows no apparent covariation with the diagnosed diameter. This implies that the method may give new and essential information on the clinical condition of the AAA. (E-mail: reidar.brekken@sintef.no) © **2006 World Federation for Ultrasound in Medicine & Biology.**

Key Words: **Ultrasound, Strain, Abdominal aortic aneurysm, Elastography, Rupture risk.**

INTRODUCTION

Abdominal aortic aneurysm (AAA) represents a serious risk to the patient because of the high mortality rate associated with rupture. About half of the patients having an AAA rupture never reach the hospital and less than half of the patients undergoing an emergent repair survive, giving a total mortality rate in the range of 80% to 90%. In the USA, more than 15,000 deaths occur annually as a result of ruptured AAAs. Of the diagnosed AAAs 20% are detected when ruptured, some are detected after the patient has experienced abdominal pain and as many as 75% are asymptomatic and found during examination for other diseases (Hsiang et al. 2001; Kazmers et al. 2001; Wilmink and Quick 1998).

When an unruptured AAA is detected, it could be scheduled either for surveillance or for elective repair by open surgery or by endovascular treatment. The surgical mortality (< 30 days) for elective repair is about 2 to 6% (UKSATP 2002), and the clinician must evaluate the risk for rupture vs. the risk associated with elective repair. The patient's age and general health condition are weighed against the state of the AAA, which means that an accurate measure of the risk associated with the AAA is needed. Present practice is that surgery is recommended when maximum AAA diameter exceeds 55 mm and is expanding (Brewster et al. 2003). Aneurysms with a diameter in the range of 30 mm to 54 mm are kept under surveillance until they exceed 55 mm, show a rapid expansion or become symptomatic. It has been suggested that a diameter of less than 55 mm should be chosen for intervention in women (UKSATP 1998).

Because of the potentially rapid increase in AAA diameter, patients kept under surveillance undergo frequent observations. But, despite this, rupture does occur. Older patients with an AAA diameter larger than 55 mm, who are kept under surveillance because of high risk for surgery, show a rupture rate of more than 50% (Lederle et al. 2002). Even with a diameter less than 55 mm, there is still a 2% rupture rate in some subgroups (Brown and Powell 1999; Nicholls et al. 1998).

Because AAA diameter may be a weak indicator for rupture risk, wall stress has been suggested as a more accurate measure. Stress analysis could be performed by segmenting the aorta from a computed tomography (CT)

Address correspondence to: Reidar Brekken, SINTEF Health Research, Medical Technology, Trondheim NO-7465 Norway. E-mail: reidar.brekken@sintef.no

scan to obtain the 3-D geometry of the AAA, and then apply the finite element method (FEM) for estimating stress in the aortic wall (Raghavan et al. 2000; Vorp et al. 1998). It has been shown that wall stress is highly correlated to rupture risk. Stress is not only an acute event before rupture, but actually differentiates patients under surveillance better than diameter size (Fillinger et al. 2003).

Strain is a measure quantifying elongation and compression of a material and relates to stress during deformation. Because the aortic wall is deformed by the passing blood pulses, stress could be obtained from strain measurements through knowledge of material parameters and deformation conditions (Cheng et al. 2002; Raghavan and Vorp 2000). Circumferential cyclic strain of an aneurysm in the thoracic aorta has been quantified by using cine phase contrast magnetic resonance imaging (MRI) (Draney et al. 2002).

Unlike the thoracic aorta, the abdominal aorta is available for noninvasive ultrasound (US), which is an easier, faster and less expensive imaging modality. Strain estimation based on US measurements has been developed for cardiology, using tissue Doppler imaging (TDI) to extract the tissue velocities (D'hooge et al. 2000; Fleming et al. 1994; Heimdal et al. 1998; Urheim et al. 2000) and also on B-mode image sequences by using 2-D speckle tracking (Leitman et al. 2004). Strain from US examination has also been demonstrated for tissue characterization in other organs (*e.g.*, brain tumors, Selbekk et al. 2005; lesions in the breast, Garra et al. 1997; Hall et al. 2003; and the prostate gland, Souchon et al. 2003).

Aortic compliance (pressure-strain elastic modulus and stiffness) has been suggested as a measure for evaluating AAA rupture risk using US (Imura et al.1986; Long et al. 2004; Wilson et al. 2003). These studies indicate that aortic compliance provides actual information about the probability of AAA rupture and that aortic compliance is not correlated to maximal diameter. The idea is to estimate the change of diameter because of the passing blood pulse by tracking the anterior and posterior wall in a longitudinal view through the cardiac cycle. The changing diameter is then used to achieve a measure of strain. This approach provides information about the dilation of the aorta as a function of time and space along a segment of the aorta.

Our hypothesis is that imaging the spatial variations in strain along the circumference of the aorta would provide additional information about the probability of AAA rupture. The aim of the present study was, therefore, to develop and demonstrate a method for estimation of strain along the circumference of the AAA from cross-sectional 2-D US data.

METHODS AND MATERIALS

Processing

Strain quantifies the relative compression and elongation of the tissue. If the aortic wall is divided into N segments, the linear Lagrangian strain (ε) in each segment is defined as:

$$\varepsilon(t)_i = \frac{L(t)_i - L_{0,i}}{L_{0,i}},\ L_{0,i} = L(0)_i, i = 1 \ldots \mathrm{N} \qquad (1)$$

where $L(t)_i$ is the distance between the two endpoints of segment i and t is the time instance corresponding to each frame through the cardiac cycle. L is a time varying quantity because of the expansion and contraction imposed by the blood pulse passing through the aorta. The reference time ($t = 0$) is defined as a time instance between two passing blood pulses. To measure $L(t)$, it is necessary to track the position of the endpoints of each segment through the cardiac cycle. Tracking of points in the 2-D B-mode image sequence is here performed in two steps:

- The vessel wall is identified manually in the first frame and a curve representing the wall is automatically updated throughout the cardiac cycle,
- A number of points, defining the endpoints of each segment, are tracked along the updated curve representing the vessel wall.

Step 1. The aortic wall is initially identified manually by an operator placing a number of points (typically < 10) along the AAA circumference. The wall is then represented by a cubic spline interpolation (de Boor 2001) between these points, and the points should be chosen so that the resulting curve lies fully inside the aortic wall (Fig. 1). For each of the initial points, the intensity profile normal to the spline curve is extracted from the US data; thus, giving a pattern characterizing the intensity in these parts of the aortic wall. By using correlation (sum of absolute difference, SAD) the best match to this pattern in the next frame is searched for in the direction normal to the aortic wall. Because of varying image quality, the robustness of the method is enhanced by requiring that the curve in each frame is smooth and does no differ too much from the curve in the preceding frame. This results in an optimization problem that is solved by using a dynamic programming method (Amini et al. 1990) giving the position of each initial point as tracked from one frame to the next in a direction normal to the spline curve.

The result of this processing step is a sequence of spline-interpolated curves lying in the aortic wall. The curves are drawn on top of the underlying US data, allowing for visual inspection of how well the curve sequence follow the radial pulsation of the aortic wall.

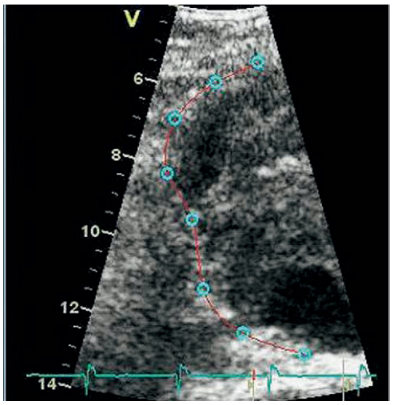

Fig. 1. 2-D US image showing part of AAA cross-section with manually placed initial points (blue) and resulting spline interpolation (red) along the vessel wall. High intensities inside the vessel wall are thrombus and lumen is the darker area in lower right.

Step 2. To perform tracking along the tangential direction, the circumferential spline from step 1 is divided into 1000 equidistant points for each frame. At each of these points, the image brightness is found by linear interpolation of the four nearest data points. As illustrated in Fig. 2, these brightness values are displayed as one vertical line for each frame; thus, obtaining an M-mode image visualizing the image intensity under the curve throughout the cardiac cycle. This means that the tangential motion of points in the aortic wall can be found by tracking the vertical displacement of the intensity patterns found in the M-mode. These intensity patterns are tracked by applying a Gaussian gradient filter, differentiating the M-mode image in the vertical direction. Curves in the gradient image correspond to borders between dark and bright segments in the M-mode and, by tracking these curves, the tangential motion is extracted. In the first frame, some points (typically 15) with high gradient values are automatically chosen from different curves to be tracked. To enhance robustness, the curves are first tracked forward from first frame to the last frame and then backward from last to first. The trace is then found by combining the results from the forward and backward tracking. Further robustness enhancement is achieved by taking the mean value of some neighboring traces. The number of traces are reduced to 10 and made equidistant by a linear transform to obtain equal spatial resolution of the strain along the wall. A similar approach for measuring displacement in the myocardium has been suggested by Brodin et al. (1998). The method, called curved anatomical M-mode, differs from the approach suggested here because the tracking is performed using TDI.

Recognizing that the vertical axis in the M-mode represents indices into the 1000-point spline curve in the aortic wall, this curve can be indexed to give the updated positions of the points in the original B-mode image sequence. The results of combining the two processing steps are ten points traced in 2-D during one cardiac cycle (Fig. 3). To evaluate the tracking process, the points for each frame are drawn onto the 2-D image sequence. This sequence is then played as a movie for visual inspection of the tracking results. The tracking is said to be successful if the motion of the points is consistent with the motion of the intensity pattern of the US image.

By calculating the distance L between each neighboring point in each frame, strain can be calculated from eqn (1). Because strain is calculated for each segment between two neighboring points, a spatial resolution is

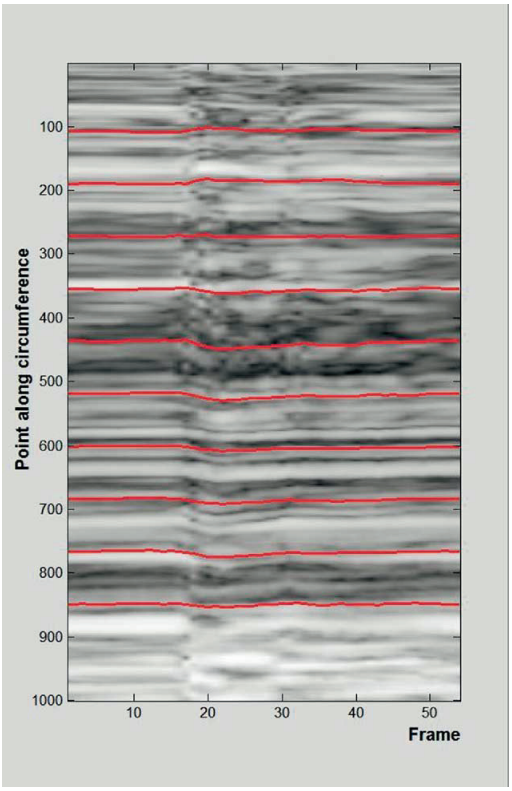

Fig. 2. M-mode image of the circumference of the aortic wall. The spline curve from Fig. 1 forms the leftmost vertical line, followed by the updated splines from the subsequent frames. The red lines show the tracking results from step 2.

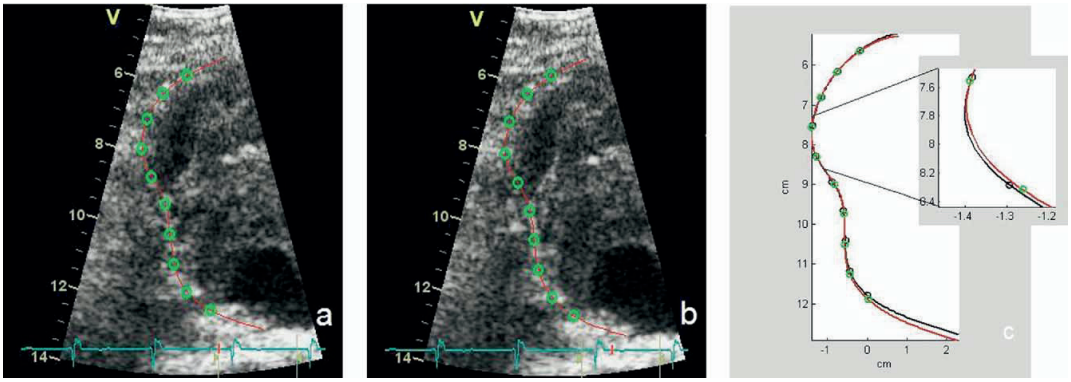

Fig. 3. Curve representation of the aortic wall in (a) the initial frame and (b) the frame corresponding to maximum dilation. The red curve is tracked based on the initial points shown in Fig. 1. These initial points differ from the green points, which represent the final result after tracking 10 points along the red curve. The strain is calculated over the segments defined by these points. (c) The curve and points from (a) are plotted in black, together with those from (b).

obtained along the circumference of the AAA given by the number of points tracked.

The strain results are visualized both as a color-coded overlay on the 2-D US data, and as a color M-mode (Figs. 4–7). The first case shows the strain values obtained along the circumference in a chosen frame. In the second case, the strain values from the first frame are color-coded and drawn as the first column in the M-mode. The relations between the M-mode and AAA anatomy are obtained by recognizing that the upper part of the column represents the upper wall segment. By repeating this for all frames, we are able to present the strain values obtained along the circumference throughout the entire cardiac cycle in one view. When drawing the ECG trace together with the M-mode, it is possible to relate the strain image to the cardiac cycle. In both cases, strain values are color-coded from red representing $+10\%$ to blue representing -10%. In the first case, the reference value (zero strain) is left transparent, whereas it is parameterized as green in the color M-mode. Also, in the M-mode, the strain values are linearly interpolated in the vertical (spatial) direction to give a more visually appealing image.

To get a quantitative measure of the inhomogeneity of the AAA wall, the average strain and the range of strain values are calculated for each frame. The average over the circumference of the AAA wall is given by:

$$M(t) = \frac{1}{N}\sum_{i=1}^{N} \varepsilon(t)_i \qquad (2)$$

where $\varepsilon(t)$ is the strain as given by eqn (1) and N is the number of segments along the AAA wall. The range is defined as the difference between the maximum and the minimum strain value along the circumference

$$R(t) = \max \varepsilon(t)_i - \min \varepsilon(t)_i,\ i = 1 \ldots \mathrm{N} \qquad (3)$$

In Fig. 8, the maximum of these two functions over the cardiac cycle are plotted against the diameter diagnosed from earlier examinations (Table 1).

The algorithm for strain processing was developed in Matlab (The MathWorks Inc., Natick, MA, USA) using GcMat (GE Vingmed Ultrasound, Horten, Norway and NTNU, Trondheim, Norway) for retrieving and visualizing data and results.

Patients, data acquisition and examination

For developing and demonstrating the method, data were recorded from 10 patients selected consecutively among those scheduled for elective AAA repair at St. Olav's Hospital (Trondheim, Norway) from September to December 2004. During this period, a total of 18 patients were treated. Of these, 1 was excluded because of a missing electrocardiogram (ECG) recording and 7 were not examined because of nonrelated illness, lack of consent or scanning personnel being unavailable at the scheduled examination time. A total of 10 patients gave their informed consent and went through an extra examination for this study the day before the operation. Patient data are summarized in Table 1.

A System FiVe scanner (GE Vingmed Ultrasound, Horten, Norway) was used with a 3.5-MHz curved linear-array probe. The abdominal US application was used, collecting both radiofrequency (RF) and B-mode data with a frame rate higher than 50 frames per s. Data

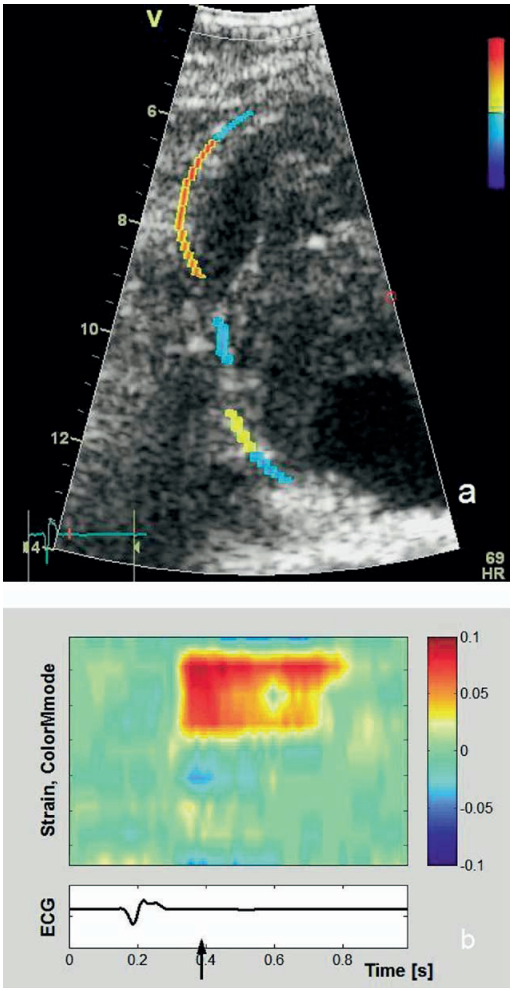

Fig. 4. Patient J, anterior view. (a) 2-D US image with strain color-coded along AAA wall. (b) Strain as color M-mode together with ECG. Arrow on the ECG trace indicates time instance of the 2-D image in (a). For both images, the color scale ranges from −10% (compression, blue) to + 10% (elongation, red). The reference value (zero strain) is left transparent in (a), whereas it is parameterized as green in (b).

were stored for later strain processing on an external personal computer.

Of the examinations, eight were performed by an experienced radiologist, whereas the others were performed by two surgeons with experience in US imaging and interpretation. The patients were lying in supine position. The US probe was placed in an anterior or oblique anterior position, depending on where the best cross-sectional view of the AAA was obtained. Provided the imaging was satisfactory, we did the recording as close to the maximum diameter as possible. The quality of the view depends on avoiding gas in intestines and, at the same time, minimizing the distance to the AAA. The sector depth was adjusted to cover the whole cross-section of the AAA; however, in most recordings the sector width was decreased to increase the frame rate. This was done because high frame rate makes the tracking of points from one frame to the next more robust. In most cases, the lumen, thrombus, vessel wall and surrounding tissue could be identified in the images, because of differences in echolucency. In addition to the US data, an ECG was recorded simultaneously.

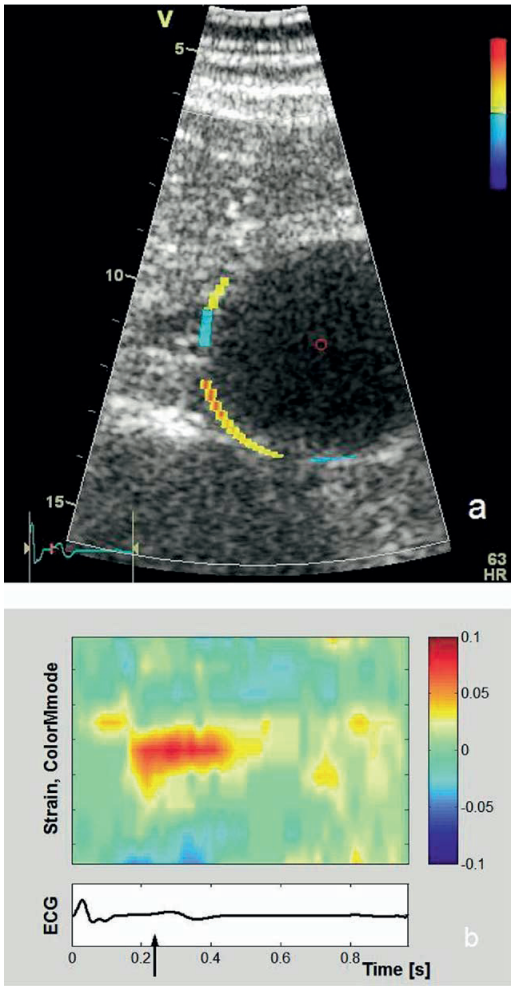

Fig. 5. Patient I, oblique (right) anterior view. Similar to Fig. 4.

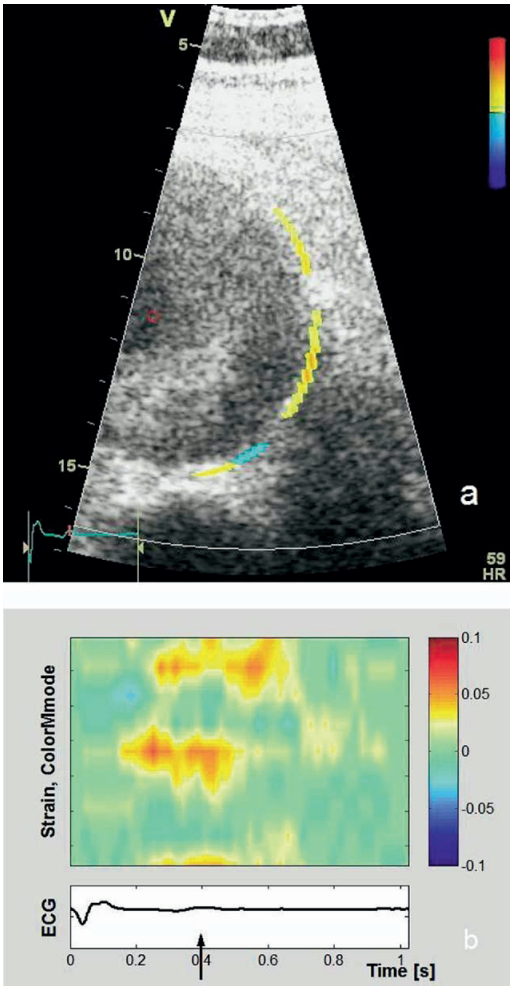

Fig. 6. Patient F, anterior view. Similar to Fig. 4.

RESULTS

For the evaluation of the method, it was applied to data sets from 10 patients. For each data set, 6 to 11 initial points were placed manually. In a few cases, the initial points were edited and reprocessed because the curve from step 1 was not entirely inside the aortic wall. After the initial points were placed, the method was automatic and practically real-time. Based on visual inspection of the tracking results, the method was found to be sufficiently accurate and robust to give reasonable tracking in all 10 data sets.

Figures 4 through 7 demonstrate application of the method to data from four patients. These illustrations confirm that the algorithm is capable of calculating circumferential strain over small segments. This means that the method can detect inhomogeneous strain values along the AAA wall. The figures further indicate that the method finds increased average strain as the blood pulse passes the imaged cross-section.

Figure 8 compares the largest spread in strain values with the largest average strain along the circumference for all 10 patients. The largest average strain is found by maximizing $M(t)$, as given by eqn (2), over the cardiac cycle and the largest spread by maximizing the range $R(t)$ defined by eqn (3). The figure demonstrates that the AAA wall may exhibit large strain inhomogeneities,

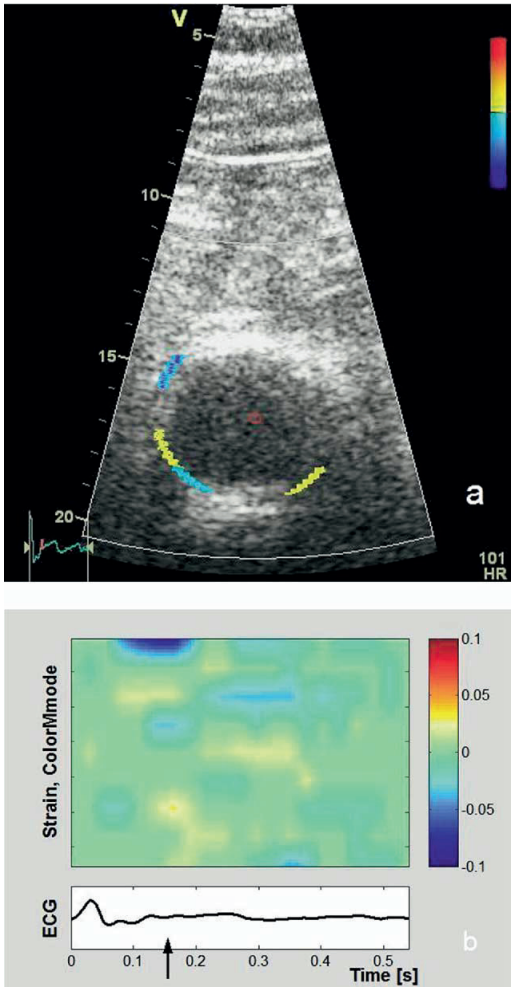

Fig. 7. Patient A, anterior view. Similar to Fig. 4.

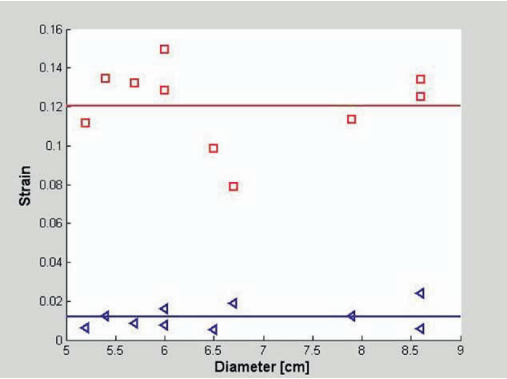

Fig. 8. (□) Maximum strain range and (◁) maximum average strain over the cardiac cycle plotted vs. the diagnosed diameter for the 10 patients (Table 1). The mean values are, respectively, 12% and 1.2%, as indicated by the solid lines.

even when the average strain is low. For the 10 investigated patients, we found no apparent correlation between strain values and diagnosed diameter.

DISCUSSION

Method

The data were collected by standard examination procedures and from a random selection of AAA patients. Thus, the image quality is expected to be representative for patients with this disease.

To estimate strain, the algorithm must be able to track the actual motion of a number of points in the tissue. This motion is generally 3-D but, because of the relatively small motion of the aortic wall, it is reasonable to assume that out-of-plane motion is highly limited and that the motion, therefore, can be extracted from 2-D image sequences. The motion in the US plane, which is perpendicular to the aorta, is typically less than 1 mm per frame. It is physiologically reasonable to expect the motion along the aorta to be even smaller than the motion perpendicular to the aorta. This means that the out-of-plane motion is negligible compared with the width of the US plane, which is typically 1 to 2 mm for the probe used.

Although both B-mode and RF data were recorded during this study, only B-mode data were used. RF data offer a better resolution and increased accuracy along the US beam, but give no advantage over B-mode data in the direction lateral to the US beam. Using only B-mode data seems sufficiently accurate, and including RF data in the 2-D tracking would lead to a more complicated and computationally expensive algorithm.

In this study, a 1-D + 1-D (radial + tangential) approach has been chosen rather than a direct 2-D speckle-tracking method (Leitman et al. 2004). The motivation was to develop a robust method (*i.e.*, the method should perform well on data sets of moderate quality) because US images from abdomen may be distorted because of depth, bowel gas, etc. The 1-D + 1-D tracking method is robust on lower data quality because of the radial tracking (step 1), which uses the more recognizable wall pattern, rather than the speckle pattern, and also imposes curve smoothness criteria *via* the dynamic programming algorithm. On the other hand, this method (step 1) is applied only perpendicular to the aortic wall and tracks only control points, and the curve representation is obtained by cubic spline interpolation. The curve is, therefore, not exactly tied to the tissue, which, in turn, may affect the quality of the M-mode, making it more difficult to track lines in the M-mode accurately (step 2).

The M-mode tracking in step 2 could be replaced by a 2-D speckle tracking in the neighborhood of the curve obtained from step 1. This would compensate for step 1 not being completely accurate, but still exploit the robustness enhancement of step 1. However, it seems that the curve sequence from step 1 is sufficiently accurate to produce an M-mode with consecutive and traceable lines. The requirement of accurate tracking in step 1 was

Table 1. Patient data

Patient	Gender	Age	Hypertension*	Heart disease	Blood pressure	Smoker	AAA diameter (mm)	Diameter acquired from
A	Male	51	Yes	No	125/90	Yes	52	MRI
B	Male	74	No	Yes	120/75	No (former)	60	CT
C	Male	71	No	No	130/65	Yes	86	Angiography
D	Male	76	No	No	–	No (former)	65	CT
E	Male	62	No	No	135/90	No (former)	54	CT
F	Male	84	No	Yes	190/90	No	67	CT
G	Male	73	Yes	No	–	No	57	CT
H	Male	71	Yes	No	150/100	Yes	79	CT
I	Male	78	No	No	160/70	No	60	CT
J	Female	80	Yes	Yes	150/70	–	86	CT

* All patients with hypertension were treated medically.

relaxed because of the relatively small motion and the fact that the tissue inhomogeneities that were used for tracking span over several pixels. The M-mode approach has the advantage of being computationally inexpensive. Because of the backtracking in step 2, the method is not strictly real-time, but the results may be available immediately after recording of one cardiac cycle.

Because of the moderate image quality obtained from noninvasive abdominal US, the robustness of the method is enhanced by averaging some neighbor traces from the M-mode tracking. This reduces the influence of noise and inaccurate tracking, but at the cost of reduced spatial resolution.

Another robustness aspect is the placing of initial points. It appears that changing the initial points affects the result when the data quality is low. Care must, therefore, be taken to place the initial points so that step 1 produces a good result (*i.e.*, the spline must be inside the aortic wall throughout the cycle). The only available quality measure on this type of data is visual inspection of how well the points follow the motion of the underlying B-mode movie. A controlled environment such as a simulation data set or an US-compatible phantom could be used, but there is no guarantee that these data would be realistic enough to give results equivalent to those obtained from real clinical data. When the initial points are appropriately placed, the full 2-D tracking results seem to be reasonable even for image segments of moderate to poor quality. Because the algorithm uses B-mode data, it is reasonable to assume that improved image quality in next-generation US scanners would make the approach even more accurate and robust and, also, enhance the evaluation of the tracking results.

The method is semiautomatic because the initial curve is placed manually. After the initial curve is placed, however, the method is practically real-time. An automatic segmentation method would eliminate, or at least reduce, the need for manual interaction. We have implemented a snake-based segmentation algorithm inspired by Kass et al. (1987) that was shown to be fast and reliable but, because the main focus of this study was elasticity analysis, we chose to use manually-set initial points to eliminate inaccuracies caused by the segmentation algorithm. A deformable model approach for segmenting the AAA wall from thrombus/lumen in 2-D cross-sectional US sequences has also been suggested by Ravhon et al. (2001). Although this approach is computationally expensive, it demonstrates that the method described in our study could ultimately be fully automated, thus shortening examination time and enhancing the inter-/intraobserver reproducibility.

In addition to the circumferential strain, other potentially interesting parameters, such as area, radius and rotation, and their corresponding temporal and spatial variations are immediately available. Strain rate, quantifying the temporal variation in strain, could give additional information about critical phases during the cardiac cycle and may, therefore, also be an interesting clinical parameter.

Clinical applicability

The method is inexpensive, fast and nearly automatic, making it suitable for real-time applications such as screening, surveillance of patients having an untreated AAA and for follow-up after endovascular therapy. For clinical use, the method should be implemented on an US scanner for online processing, providing the possibility to scan over the entire AAA, not just one 2-D cross-section. Also, the method should be further validated with more patients with regard to accuracy, robustness and reproducibility.

To be clinically applicable, the method must give actual information about the probability of AAA rupture. Previous studies have indicated that stress in the AAA wall is directly related to rupture (Fillinger et al. 2003; Raghavan et al. 2000; Vorp et al. 1998). Stress could be derived from strain through knowledge of tissue elasticity parameters and deformation condition and it is, therefore, reasonable to assume that strain measurements provide relevant information about the probability of AAA rupture.

Because of the changing elasticity properties imposed by ageing and evolving of AAAs, the strain values found in healthy young people are most likely not comparable to strain in older people or patients having an AAA. By measuring strain as the relative change in aortic diameter from diastole to systole, strain values for normal subjects have been reported from 8% in young adults down to 3% in subjects above the age of 60 (Imura et al. 1986). It is also known that decreased compliance is more prevalent among men than women and that compliance is less in aneurismal aortas compared with healthy aortas. The numerical strain values should, therefore, be seen in relation to the patients age, gender and *a priori* AAA diagnosis (from measuring diameter). As indicated in Fig. 7, heart rate could also influence the numerical strain values because, with a high heart rate, there might be no time instance where the aortic wall is sufficiently relaxed. Therefore, there might be significant tension in the aortic wall at zero strain. Further research is necessary to evaluate the effect of heart rate, blood pressure and possibly other physiological parameters.

In addition to the numerical strain values, it is also possible that diagnostic information could be drawn from the variations in strain along the circumference (*i.e.*, inhomogeneous strain values indicate that certain segments of the AAA wall have a higher

load than other segments or that some segments are stiffer than others).

The preliminary observations made in this study indicate that there seems to be low average strain along the circumference of the AAA, which was expected because AAA is known to reduce the elasticity of the vessel wall. However, in some segments of the AAA, high strain values are found. These inhomogeneous strain values indicate that certain segments of the AAA have reduced elasticity, resulting in a higher load on other parts of the aortic wall. Because of its potential clinical relevance, the inhomogeneity is quantified by comparing the range of strain values to the average strain (Fig. 8). Based on our data from 10 patients, the parameters show no apparent correlation with the diameter. A total of 10 patients is, however, not sufficient to be conclusive about this, but it is consistent with Wilson et al. (1999), who found aortic compliance not to be correlated with diameter.

To be conclusive about the clinical relevance of circumferential strain, further clinical studies including more patients must be performed. Normal circumferential strain values must be established for healthy people and AAA patients at different ages and it must be evaluated if strain gives additional and more precise information about the probability of AAA rupture.

CONCLUSIONS

A method for calculating strain in AAAs from cross-sectional US B-mode image sequences has been developed. The method depends on a prespecified initial curve but, with that exception, the method is automatic and practically real-time, making it suitable for clinical applications. The method was developed and evaluated using data from 10 AAA patients. By visual inspection of the tracking results, from which strain is derived, the method appears accurate and performs well, even with moderate image quality. An important feature of the method is its ability to calculate circumferential strain over small segments of the AAA wall; thus, revealing possible inhomogeneities. Although the clinical relevance of circumferential strain in AAAs must be evaluated, the method seems promising. As compared with measuring diameter alone, the method provides additional and potentially more significant information on whether or not to recommend elective repair of AAAs.

Acknowledgements—This work was financed by the Norwegian Ministry of Health and Social Affairs through the National Centre of Competence-3D Ultrasound in Surgery and by SINTEF Health Research.

REFERENCES

Amini AA, Weymouth TE, Jain RC. Using dynamic programming for solving variational problems in vision. IEEE Trans Pattern Anal Machine Intell 1990;12:855–876.

Brewster DC, Cronenwett JL, Hallett JW, et al. Guidelines for the treatment of abdominal aortic aneurysms. J Vasc Surg 2003;37: 1106–1117.

Brodin LA, van der Linden J, Olstad B. Echocardiographic functional images based on tissue velocity information. Herz 1998;23:491–498.

Brown LC, Powell JT, for the UK Small Aneurysm Trial Participants. Risk factors for aneurysm rupture in patients kept under ultrasound surveillance. Ann Surg 1999;230:289–296.

Cheng KS, Baker CR, Hamilton G, Hoeks APG, Seifalian AM. Arterial elastic properties and cardiovascular risk/event. Eur J Vasc Endovasc Surg 2002;24:383–397.

de Boor C. A practical guide to splines. New York: Springer Verlag, 2001.

D'hooge J, Heimdal A, Jamal F, et al. Regional strain and strain rate measurements by cardiac ultrasound: Principles, implementation and limitations. Eur J Echocardiogr 2000;1:154–170.

Draney MT, Herfkens RJ, Huges T, et al. Quantification of vessel wall cyclic strain using cine phase contrast magnetic resonance imaging. Ann Biomed Eng 2002;30:1033–1045.

Fillinger MF, Marra SP, Raghavan ML, Kennedy FB. Prediction of rupture risk in abdominal aortic aneurysm during observation: Wall stress versus diameter. J Vasc Surg 2003;37:724–732.

Fleming AD, Xia X, McDicken WN, Sutherland GR, Fenn L. Myocardial velocity gradients detected by Doppler imaging. Br J Radiol 1994;67:679–688.

Garra BS, Cespedes EI, Ophir J, et al. Elastography of breast lesions: Initial results. Radiology 1997;202:79–86.

Hall TJ, Zhu Y, Spalding CS. In vivo real-time freehand palpation imaging. Ultrasound Med Biol 2003;29:427–435.

Heimdal A, Stoylen A, Torp H, Skjaerpe T. Real-time strain rate imaging of the left ventricle by ultrasound. J Am Soc Echocardiogr 1998;11:1013–1019.

Hsiang YN, Turnbull RG, Nicholls SC, et al. Predicting death from ruptured abdominal aortic aneurysms. Am J Surg 2001;181:30–35.

Imura T, Yamamoto K, Kanamori K, Mikami T, Yasuda H. Noninvasive ultrasonic measurement of the elastic properties of the human abdominal aorta. Cardiovasc Res 1986;20:208–214.

Kass M, Witkin A, Terzopoulos D. Snakes: Active contour models. Int J Comp Vision 1987;1:321–331.

Kazmers A, Perkins AJ, Jacobs LA. Aneurysm rupture is independently associated with increased late mortality in those surviving abdominal aortic aneurysm repair. J Surg Res 2001;95:50–53.

Lederle FA, Johnson GR, Wilson SE, et al. Rupture rate of large abdominal aortic aneurysms in patients refusing or unfit for elective repair. JAMA 2002;287:2968–2972.

Leitman M, Lysyansky P, Sidenko S et al. Two-dimensional strain—A novel software for real-time quantitative echocardiographic assessment of myocardial function. J Am Soc Echocardiogr 2004;17: 1021–1029.

Long A, Rouet L, Bissery A. Aortic compliance in healthy subjects: Evaluation of tissue Doppler imaging. Ultrasound Med Biol 2004; 30:753–759.

Nicholls SC, Gardner JB, Meissner MH, Johansen HK. Rupture in small abdominal aortic aneurysms. J Vasc Surg 1998;28:884–888.

Raghavan ML, Vorp D. Toward a biomechanical tool to evaluate rupture potential of abdominal aortic aneurysm: Identification of a finite strain consecutive model and evaluation of its applicability. J Biomech 2000;33:475–482.

Raghavan ML, Vorp D, Federle MP, Makaroun MS, Webster MW. Wall stress distribution on three-dimensionally reconstructed models of human abdominal aortic aneurysm. J Vasc Surg 2000; 31:760–769.

Ravhon R, Adam D, Zelmanovitch L. Validation of ultrasonic image boundary recognition in abdominal aortic aneurysm. IEEE Trans Med Imaging 2001;20:751–763.

Selbekk T, Bang J, Unsgaard G. Strain processing of intraoperative ultrasound images of brain tumours: Initial results. Ultrasound Med Biol 2005;31:45–51.

Souchon R, Rouviere O, Gelet A, et al. Visualization of HIFU lesions using elastography of the human prostate *in vivo*: Preliminary results. Ultrasound Med Biol 2003;29:1007–1015.

UKSATP (The UK Small Aneurysm Trial Participants). Mortality results for randomised controlled trial of early elective surgery or ultrasonographic surveillance of small abdominal aortic aneurysms. Lancet 1998;352:1649–1655.

UKSATP (The UK Small Aneurysm Trial Participants. Long-term outcomes of immediate repair compared with surveillance of small abdominal aortic aneurysms. N Engl J Med 2002;346:1445–1452.

Urheim S, Edvardsen T, Torp H, Angelsen B, Smiseth OA. Myocardial strain by Doppler echocardiography—Validation of a new method to quantify regional myocardial function. Circulation 2000;102:1158–1164.

Vorp D, Raghavan ML, Webster MW. Mechanical wall stress in abdominal aortic aneurysm: Influence of diameter and asymmetry. J Vasc Surg 1998;27:632–639.

Wilmink AB, Quick CR. Epidemiology and potential for prevention of abdominal aortic aneurysm. Br J Surg 1998;85:155–162.

Wilson K, Lee AJ, Hoskins P, et al. The relationship between aortic distensibility and rupture of infrarenal abdominal aortic aneurysm. J Vasc Surg 2003;37:112–117.

Wilson K, Whyman M, Hoskins P, et al. The relationship between abdominal aortic aneurysm wall compliance, maximum diameter and growth rate. Cardiovasc Surg 1999;7:208–213.

Paper II

◆ CLINICAL INVESTIGATION ◆

Reduced Strain in Abdominal Aortic Aneurysms After Endovascular Repair

Reidar Brekken, MSc[1,3]; Torbjørn Dahl, MD[2,3]; Toril A. N. Hernes, PhD[1,3]; and Hans Olav Myhre, MD[2,3]

[1]SINTEF Health Research, Trondheim, Norway. [2]St. Olav's Hospital, The University Hospital of Trondheim, Norway. [3]Norwegian University of Science and Technology, Department of Circulation and Medical Imaging, Trondheim, Norway.

Purpose: To compare in vivo strain in abdominal aortic aneurysms before and after endovascular aneurysm repair (EVAR), thereby obtaining a quantitative measure of changes in mechanical burden on the aneurysm wall.
Method: Transabdominal ultrasound was acquired from 10 patients (9 men; median age 76 years, range 61–83) 1 day before and 2 days after elective EVAR. Strain was estimated as the relative cyclic elongation and contraction of the wall tissue in a number of connected segments along the aneurysm circumference. For each time instance of the cardiac cycle, the maximum and the average strain values along the circumference were recorded. The temporal maximums of these parameters (defined as the maximum strain and the peak average strain, respectively) were compared before and after EVAR.
Results: Both maximum strain and peak average strain were reduced following EVAR by 41% (range 35%–63%) and 68% (range 41%–93%), respectively. Despite the reduction, cyclic strain was still evident after the stent-graft was placed, even when no evidence of endoleak was found. Further, the strain values were inhomogeneous along the circumference, both before and after treatment. In 2 cases, endoleak was proven by routine computed tomography; the relative reduction in maximum strain was slightly less in these cases (35% and 38%) compared to those without endoleak (45%, range 38%–63%). No difference was found in reduction of peak average strain.
Conclusion: Strain is significantly reduced after EVAR, but there may still be a certain level of strain after the treatment. The strain values are inhomogeneous along the circumference both before and after treatment. These results encourage further investigation to evaluate the potential for using circumferential strain as an additional indicator of outcome after endovascular repair.

J Endovasc Ther 2008;15:453–461

Key words: abdominal aortic aneurysm, endovascular aneurysm repair, ultrasound, strain, stent-graft

◆ ◆

Endovascular aneurysm repair (EVAR) is considered successful if the aneurysm sac is fully excluded from the blood circulation, with resulting decrease of aneurysm size over time. Although significant shrinkage has been reported in the absence of endoleak, some aneurysms continue to expand also without evidence of endoleak, a condition referred to

This work was financed by the Norwegian Ministry of Health and Social Affairs through the National Centre for 3D Ultrasound in Surgery and by SINTEF Health Research.

The authors have no commercial, proprietary, or financial interest in any products or companies described in this article.

Address for correspondence and reprints: Reidar Brekken, SINTEF Health Research, Department of Medical Technology, N-7465 Trondheim, Norway; E-mail: *Reidar.Brekken@sintef.no*

as endotension.[1–3] The confidence in using lack of endoleak or endotension as measures of successful treatment has, however, been questioned.[4–8] In order to predict the patient-specific outcome of treatment, additional criteria are therefore warranted.

One suggestion has been to measure the pressurization of the aneurysm sac. Gawenda et al.[9] attempted to measure intrasac pressure during EVAR; the mean and pulsatile pressures were reduced after insertion of a stent-graft, but pulse pressure was still transmitted into the sac even in the absence of endoleak. The authors concluded that measuring intraoperative sac pressure could help to detect endoleak, but not to predict the fate of the aneurysm during follow-up. However, Dias et al.[10] reported that measurements of pressure inside the aneurysm sac during follow-up showed an association between pressurization and expansion of the aneurysm.

A reduction of pulsatile wall motion, defined as the relative change in diameter over the cardiac cycle, has been suggested as a measure of successful treatment.[11] Using ultrasound, pulsatile wall motion after endovascular repair was found to be higher in the presence of endoleak, but was also present without evidence of leakage. Using cine magnetic resonance imaging (cine MRI), Faries et al.[12] have also shown that the diameter pulsatility was reduced after EVAR. To the contrary, a 2-dimensional (2D) method measuring the change in cross-sectional sac area over the cardiac cycle has shown only an insignificant reduction after EVAR.[13]

A method has previously been suggested for measuring cyclic strain along the circumference of the abdominal aortic aneurysm (AAA) in vivo from cross-sectional ultrasound images.[14] The method revealed inhomogeneous strain along the circumference, suggesting that additional information is obtained compared to recording the relative change in diameter. Generally, strain is a measure of relative displacement of particles in an elastic object exposed to a force, i.e., the deformation of an object. Soft materials will experience larger strains than stiff materials when subjected to the same load. Strain imaging has been used for detecting stiff tumors in softer tissue.[15,16] In cardiology, strain is used to investigate the contractility of the left ventricle myocardium.[17] Because aneurysm growth is associated with changes in the tissue's material properties, strain may provide information that could assist in identifying varying rupture potentials of equally sized aneurysms. Further investigation is necessary to reveal the clinical interpretation and significance of strain in AAA.

Because cyclic strain depends on the pulsatile load imposed on the aneurysm wall, we believe that strain could provide an additional criterion in determining the need for secondary intervention. The objective of this study was to investigate the immediate changes in circumferential strain in the AAA wall before and after EVAR.

METHODS

Study Design, Patient Sample, and Data Acquisition

The study was approved by an Institutional Review Board, the Regional Committee for Medical Research Ethics, and the Norwegian Social Science Data Services. From March to November 2006, 25 patients underwent elective endovascular repair of AAA at our department. Investigators were available to examine 13 of these patients, who all gave informed consent to participate in the study. Of these 13, the first 2 were considered technical pilot cases and excluded from the study. One patient left the hospital before the post-EVAR examination had been carried out, leaving 10 patients (9 men; median age 76 years, range 61–83) who had an ultrasound examination the day before and 2 days after the intervention. The majority were present or former smokers (Table); 5 had coronary heart disease, 7 were being treated medically for hypertension, 3 used beta-blockers, and none used cortisone. All patients had a bifurcated stent-graft (Zenith Trifab; William Cook Europe ApS, Denmark) implanted. In 2 cases, endoleak was observed in routine computed tomography (CT) 2 days after the treatment. In both cases, the endoleak sealed without secondary intervention.

TABLE
Patient Data and Physiological Parameters

Pt	Age, y/ Gender	Risk Factors	Blood Pressure, mmHg		Heart Rate, bpm		Maximum Strain, %		Peak Average Strain, %		AAA Diameter, cm	Endoleak
			Pre	Post	Pre	Post	Pre	Post	Pre	Post		
1	75/M	SMK, HTN	180/105	160/80	103	94	3.8	2.1	0.82	0.21	75	0
2	68/M	SMK, HD	130/80	135/85	77	107	2.9	1.8	0.98	0.38	58	Type I
3	73/M	SMK, HTN, BB, HD	155/85	145/70	67	95	4.3	1.6	1.40	0.53	55	0
4	83/M	SMK	130/70	125/65	70	84	2.5	1.0	0.72	0.05	60	0
5	78/M	SMK, HTN	160/90	150/70	61	66	4.2	—	0.70	—	60	0
6	81/F	SMK, HTN	175/85	140/70	59	72	3.7	2.4	1.30	0.12	59	Type II
7	77/M	SMK, HTN, HD	125/80	120/70	73	60	2.6	1.6	0.75	0.44	64	0
8	61/M	SMK, HTN, BB	150/95	140/85	80	80	3.2	1.9	0.58	0.16	62	0
9	74/M	SMK, BB, HD	115/60	125/75	54	84	2.9	1.7	0.80	0.44	56	0
10	79/M	HTN, HD	175/70	140/70	59	68	3.2	1.3	0.54	0.18	62	0

AAA: abdominal aortic aneurysm, SMK: smoker (past or present), HTN: hypertension (all treated medically), BB: beta-blockers, HD: heart disease.

Ultrasound Examination

The examinations were performed by a vascular surgeon with experience in ultrasound imaging. The patients were supine, and brachial blood pressure was measured immediately before each examination. The echocardiogram (ECG) was recorded simultaneously with the B-mode ultrasound data, which was acquired with a digital ViVid7 ultrasound scanner (GE Vingmed Ultrasound, Horten, Norway) and a 3.5-MHz curved linear array probe. With the ultrasound probe placed in an anterior position, fundamental imaging was done at 3.5 MHz for the first patient, but for the others, data were acquired by harmonic imaging at 2.2/4.7 MHz. In each examination, which took ~20 minutes, data from several consecutive cardiac cycles (≥3) were acquired for each of 3 aneurysm cross sections: at the largest diameter and some centimeters proximal and distal to the largest diameter, depending on the length of the aneurysm. The image depth and width were adjusted to cover each aneurysm cross section. To achieve a high frame rate (40 to 50 per second) for robust postprocessing, only one transmit focus depth was used. Data were stored for later strain processing on an external computer.

Strain Processing and Data Analysis

Regional linear strain was used for quantifying the relative cyclic elongation and contraction of the wall tissue imposed by the pulsatile blood pressure. Subdividing the circumference of the wall into N segments, the linear strain (ε) in each segment was defined as:

$$\varepsilon(t)_i = \frac{L(t)_i - L_{0,i}}{L_{0,i}},\ L_{0,i} = L(0)_i,\quad i = 1 \ldots N$$

where $L(t)_i$ was the distance between the 2 endpoints of segment i and t was the time instance corresponding to each frame through the cardiac cycle. L varied with time due to the pulsatile aortic blood flow. The reference time (t=0) was set at the point between 2 passing blood pulses. The number of segments was chosen so that the initial length of each segment was ~2 cm. The strain processing method, described in detail by Brekken et al.,[14] is summarized below.

One cycle without apparent respiratory motion or probe displacement was selected from each dataset for processing. A vital part of the processing method was to measure L(t), which required tracing the (2D) position of the endpoints of each segment through the cardiac cycle. The tracing algorithm consisted of 3 parts. Firstly, the aneurysm wall was manually identified by placing a number of points (typically 10) along the wall. Based on these points, spline interpolation was used to obtain a curve representing the aneurysm wall in the initial frame. Secondly, this curve was automatically traced through the cardiac cycle,

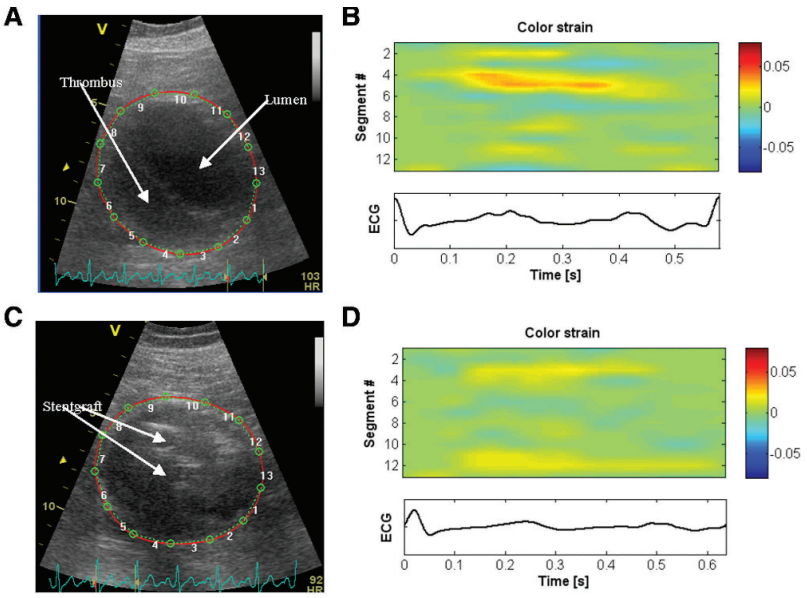

Figure 1 ◆ In these ultrasound images acquired (**A**) before and (**C**) after EVAR, the segments around the wall are indicated along with the thrombus and lumen. (**B**, **D**) The color-coded strain values along the circumference of the aneurysm over the cardiac cycle indicated in the ECG tracing; the numbers on the y-axis correspond to the segments in **A** and **C**, respectively. Note that strain is clearly reduced after EVAR. Due to the possibility of different positioning of the ultrasound probe in the examinations before and after EVAR, the segments are not necessarily at the exact same anatomical location.

resulting in a sequence of curves following the radial pulsation of the aorta. Finally, a number of equidistant points were automatically traced along the curves representing the wall, giving the tangential motion component.

This processing resulted in a time series of points representing the endpoints of each segment. Based upon visual evaluation of how well these points followed the motion of the aneurysm wall as displayed by the underlying ultrasound movie, the results of the tracing were either approved as being correct or the initial curve was edited and the tracing process run again. By calculating the distance L between each neighboring point in each frame, strain was found from the equation above. Because strain was calculated for each segment, a spatial resolution was obtained along the circumference of the AAA defined by the number of points traced, the number being a tradeoff between resolution and suppression of noise and method inaccuracies. To further reduce the influence of noise, the strain values were smoothed over 5 frames by applying a Gaussian low-pass filter.

Strain varied over time (cardiac cycle) and anatomical location (segment). A color M-mode was used for visualizing strain in all segments over all frames in the cardiac cycle in 1 view. The M-mode was generated by color coding the strain values along the circumference in each consecutive frame and drawing these as consecutive columns in the M-mode. The ECG tracing was drawn together with the M-mode to relate the strain values to the cardiac cycle (Fig. 1). Strain was color coded from red (+8%) to blue (−8%), with the reference value parameterized as green. The strain values were interpolated to give a more visually appealing image.

To quantify the reduction in strain, the maximum and average strain values over

the circumference were calculated for each frame. The temporal maximum of these 2 parameters are referred to as the maximum strain and the peak average strain, respectively. Physically, the peak average strain is a measure of the cyclic expansion/contraction of the aneurysm cross section and may therefore be compared to measuring the relative changes in mean cross-sectional diameter over the cardiac cycle.

One engineer processed each dataset several ($\geq$3) times, but on different days. Results are reported as medians. The values before and after treatment were compared using non-parametric methods. Specifically, data were paired before and after EVAR for the individual patient and compared using the Wilcoxon signed-rank test for paired data. The Mann-Whitney U test was used for group comparisons. The level of statistical significance was chosen as $p<0.05$.

RESULTS

The quality of the ultrasound images was subjectively determined to be sufficient for strain processing in 26 (87%) of the datasets before and 18 (60%) after EVAR (73% in all). In the remaining datasets, parts of the aneurysm wall could not be identified. For 1 patient, none of the datasets obtained after EVAR had sufficient quality for further processing, so strain was processed in at least 1 cross section both before and after endovascular repair in 9 patients. Figure 1 shows an example of strain in corresponding datasets before and after insertion of a stent-graft.

Comparing the strain values for each patient, the median reduction (difference) in maximum strain after EVAR was 1.3% (range 1%–2.7%), whereas the median reduction in peak average strain was 0.6% (range 0.3%–1.2%). These reductions were statistically significant for both parameters ($p<0.01$). The relative reductions in maximum strain and peak average strain were 41% (range 35%–63%) and 68% (range 41%–93%), respectively. The values were clearly reduced in every case.

In addition to measuring the overall reduction in strain for each aneurysm, the reduction was also analyzed (pairwise) for corresponding cross sections before and after

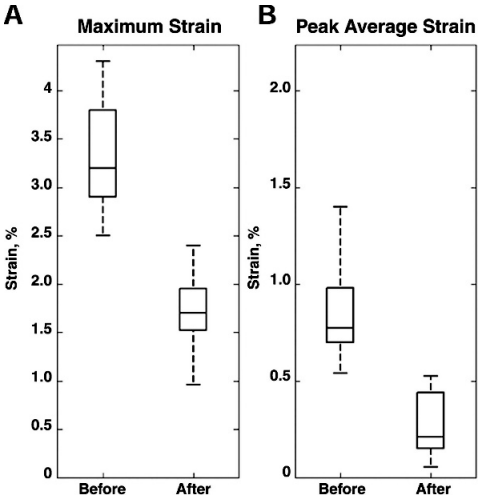

Figure 2 ◆ (**A**) The maximum strain and (**B**) the peak average strain before and after EVAR. Note that the y-axis is scaled by a factor 0.5 in **B** compared to **A**. The box plots show range, upper and lower quartiles, and the median value.

treatment. Maximum strain was reduced by 1.2% (range 0.3%–2.7%) and peak average strain by 0.5% (range 0.02%–1.2%; $p<0.01$ for both). The relative reduction values were 39% (range 17%–63%) and 71% (range 5%–99%), respectively. Strain was reduced in all cross sections.

Figure 2 shows a graphical representation of the maximum strain and peak average strain before and after endovascular repair. The sample median values of maximum strain and peak average strain were reduced from 3.2% (range 2.5%–4.3%) to 1.6% (range 1.0%–2.4%) and from 0.8% (range 0.5%–1.4%) to 0.2% (range 0.1%–0.5%), respectively ($p<0.01$ for both).

Although strain was clearly reduced for all patients, a certain level of strain was still observed after treatment. A further result was that strain was found to be inhomogeneous along the circumference of the aneurysm both before and after insertion of a stent-graft.

In the 2 cases where endoleak was identified by CT, the relative reduction in maximum strain was slightly less (35% and 38%) compared to those without endoleak (median 45%, range 38%–63%). No difference was

found in peak average strain reduction (61% and 90% in the endoleak patients compared to the median 68%, range 41%–93%).

DISCUSSION

The ultrasound images were collected from a random sampling of patients undergoing elective EVAR and are therefore assumed to give a good indication of the expected image quality for patients with this disease. The quality varied from patient to patient due to obesity, inhomogeneities in the intraperitoneal fat, calcification, and bowel gas. Also, the image quality in the posterior circumference of the wall was reduced in some cases after EVAR, which may partly be caused by artifacts due to the metal in the stent-graft. To minimize the inconvenience to the patients, fasting was not required before the examination; however, fasting may have the potential to improve ultrasound data quality, and we will implement this for future studies. Emerging advances in ultrasound imaging technology are expected to improve data quality and may therefore further increase the applicability of the strain processing method.

The first patient included in the study was examined using fundamental imaging at 3.5 MHz. When examining the second patient, we used an ultrasound probe that was able to do harmonic imaging at frequencies low enough to avoid overly high attenuation. Harmonic imaging reduces the acoustic noise in the images, although a possible drawback may be loss of sensitivity. The image quality was judged to be somewhat better in this setting. Because there is no expected bias in the strain estimates related to this change of the ultrasound probe, we still chose to include the results from the first patient.

The processing depends on manual initialization of a curve defining the aneurysm wall and also on certain parameters used in the tracing algorithm. Furthermore, because the regional strain represents an average strain over each segment, the initial length of the segments may affect the maximum strain value observed. The peak average strain is, however, not affected. The initial length was set to $\sim$2 cm, which in this material resulted in 10 (range 7–13) segments. With this length, a hypothetical tracking error $<$0.2 mm would correspond to an estimation error $<$1.0 (0.2/20) for maximum strain, which is less than the smallest value observed in this study (all $\geq$1.0, see the Table). This was regarded as being a fair tradeoff between accuracy and resolution. Although the processing results were visually evaluated, the accuracy of the method and the observer variability must be systematically evaluated before the method can be used in clinical practice. To account for variability and inaccuracies, the processing was performed several ($\geq$3) times for each dataset, and the median values were used in the analysis. To evaluate the repeatability of the processing, the standard deviation was calculated for each valid dataset (26 before, 18 after). On average, the standard deviation in maximum strain was 0.47% before EVAR and 0.25% after. Applying a 1-sided 2-sample *t* test with unknown and unequal variance, it was found that differences of 0.18% could be resolved with a significance level of $p=0.05$. For peak average strain, the same value was 0.10%. We therefore concluded that the variability was acceptable compared to the reductions of 1.3% and 0.6%, respectively. This conclusion was further supported by the fact that stain was reduced in every case.

Based on this study, we cannot conclude whether or not the method is sufficiently sensitive to identify endoleak, although a slightly smaller reduction in maximum strain was observed in the 2 cases with proven endoleak. To further reduce the operator dependency, a fully automatic method should be implemented.

Although the strain values were significantly reduced after EVAR, we found that the wall was still exposed to a certain level of strain, meaning that the aneurysm sac was not fully shielded from pulsatile blood pressure. Most likely, pulse pressure was transmitted through the stent-graft and thrombus mass. These findings are consistent with a study reporting a reduction in pulsatile wall motion of 75% (range 63% to 84%) without evidence of endoleak[11] compared to the 68% reduction in peak average strain in the present study. Another study, using cine MRI, reported a reduction in mean cyclic diameter change from 3.51 mm before repair to 0.12 mm after

(without endoleak). With a mean aneurysm diameter of 64 mm, it could be inferred that pulsatile wall motion was reduced from about 5.5% before to about 0.2% after.[12] We found a smaller pulsatility (peak average strain) before, while the value after EVAR was consistent with that obtained in our study.

Cine MRI has also been used for measuring change in cross-sectional area over the cardiac cycle. One study, including 7 patients, reported a change from 0.25 cm^2 before EVAR to 0.17 cm^2 at 34 days after (range 14–660; $p=0.79$).[13] Another study involving 21 patients reported that change in cross-sectional area over the cardiac cycle was negligible compared to the variation of measurements; they concluded that this could not be used as a measure to predict success of EVAR. However, local wall displacements up to 2 mm were observed.[18] Compared to measuring cyclic change in diameter or area over the cardiac cycle, applying our method further indicated inhomogeneity of strain along the circumference of the aneurysm both before and after insertion of the stent-graft, which means that some segments of the aneurysm may have higher elasticity or experience a larger pulsatile load compared to other parts of the wall. This is consistent with results from a study investigating the mechanical properties of 5 freshly excised whole aneurysms, showing that different regions of the aneurysm have different strains.[19] An interesting point is that the reduction in maximum strain was only 41% compared to the 68% reduction in peak average strain.

Cyclic strain gives a measure of the effects of the pulse pressure. Although this indicates how well the aneurysm wall is excluded from the pulse pressure, the mean pressure may still be high even if the (cyclic) strain values are low. High pressure could be a result of phenomena other than transmission of pulse pressure, e.g., hygroma.[20,21] Experiments performed on an aneurysm model suggested that pulsatility was dependent on lumbar branch outflow and could not be used for predicting aneurysm sac pressurization.[22] A study combining strain with pressure transducer measurements may be of interest for further investigation.

In this study, strain was measured in a limited number of cross sections, which means that the entire aneurysm was not covered. One consequence is that the data might not necessarily be acquired from the exact same part of the aneurysm before and after EVAR. This may be a limitation of the study because the mechanical properties of the aneurysm are spatially varying. However, because the variation in measurement location before and after EVAR was random, no bias was introduced in the strain estimates. Further, because strain was reduced following EVAR in every case, the results suggest that the reduction caused by EVAR significantly dominated the local spatial variations. By implementing the method on an ultrasound scanner for online processing, it would be possible to also analyze several cross sections without having to store data for later processing.

Even if strain were measured in the entire aneurysm, the deformation is, in general, a tensor composed of linear strains and shear strains. To fully describe the deformation of the aneurysm wall, the full strain tensor should be investigated as opposed to the regional linear method used in this work. To achieve this, the strain method might be combined with finite element modeling to obtain an interpolation scheme for estimating the strain tensor in the entire aneurysm. Finite element analysis has been applied to AAA to investigate the potential of using wall stress as an indicator for aneurysm rupture risk.[23,24] Because the wall stress method assumes certain boundary conditions and material properties, a direct comparison to measured strain is not straightforward, but relevant knowledge may be obtained by combining the two methods.

Reduced strain after EVAR may be systematically influenced by factors other than insertion of a stent-graft. For example, the systolic pressure was significantly reduced at the time of examination 2 days after EVAR compared to the day before ($p=0.04$). Linear regression suggested that there might be a correlation between systolic blood pressure and maximum strain before EVAR ($R^2=0.47$, $p=0.03$), while this relationship seemed to be less significant after ($R^2=0.24$, $p=0.18$). This observation could be explained by the aneu-

rysm being more shielded from systemic blood pressure after EVAR. The difference in maximum strain (pre/post EVAR) did not correlate to the difference in systolic blood pressure (R^2=0.1, p=0.40) nor did peak average strain correlate to blood pressure. The same trends were observed when analyzing the relation between strain and the pulse pressure. Because the study was not designed to investigate these relationships thoroughly, the number and range of observations may not empower firm conclusions regarding these points.

In studies comprising larger patient series, multivariate analysis may be used to account for potential confounding factors, such as blood pressure, heart rate, and aneurysm geometry. Because the pulse pressure is probably transmitted to the aneurysm wall through the stent-graft, strain may also depend on the type of stent-graft used. It may be of interest to compare different stent-grafts to each other for investigating whether the proposed method could provide any implications for stent-graft design. Because a low standard deviation was expected compared to the reduction of strain following EVAR, a relatively small series of patients was included in this study, a decision that is supported by the high significance level observed. To further evaluate the method's potential for early prediction of outcome after endovascular repair, a larger study must be performed to relate strain or reduction in strain to aneurysm size and enlargement, presence of endoleak, and postoperative rupture.

Conclusion

Using a method for measuring strain in the AAA wall before and after endovascular repair, we have demonstrated that strain was significantly reduced after EVAR. Despite this reduction, the aneurysm wall still experienced some cyclic strain. Further, inhomogeneous strain values were found along the circumference of the AAA both before and after the treatment. The results encourage further research to evaluate the method's potential for early prediction of outcome after endovascular aneurysm repair.

REFERENCES

1. Rhee RY, Eskandari MK, Zajko AB, et al. Long-term fate of the aneurysmal sac after endoluminal exclusion of abdominal aortic aneurysms. *J Vasc Surg*. 2000;32:689–696.
2. Wolf YG, Hill BR, Rubin GD, et al. Rate of change in abdominal aortic aneurysm diameter after endovascular repair. *J Vasc Surg*. 2000;32:108–115.
3. White GH, May J, Petrasek P, et al. Endotension: an explanation for continued AAA growth after successful endoluminal repair. *J Endovasc Surg*. 1999;6:308–315.
4. Heikkinen MA, Arko FR, Zarins CK. What is the significance of endoleaks and endotension. *Surg Clin N Am*. 2004;84:1337–1352.
5. Zarins CK, Bloch DA, Crabtree T, et al. Aneurysm enlargement following endovascular aneurysm repair: AneuRx clinical trial. *J Vasc Surg*. 2004;39:109–117.
6. Chaikof EL, Blankensteijn JD, Harris PL, et al. Reporting standards for endovascular aortic aneurysm repair. *J Vasc Surg*. 2002;35:1048–1060.
7. Veith FJ, Baum RA, Ohki T, et al. Nature and significance of endoleaks and endotension: summary of opinions expressed at an international conference. *J Vasc Surg*. 2002;35:1029–1038.
8. Alimi YS, Chakfe N, Rivoal E, et al. Rupture of an abdominal aortic aneurysm after endovascular graft placement and aneurysm size reduction. *J Vasc Surg*. 1998;28:178–183.
9. Gawenda M, Heckenkamp J, Zaehringer M, et al. Intra-aneurysm sac pressure - the holy grail of endoluminal grafting. *Eur J Vasc Endovasc Surg*. 2002;24:139–145.
10. Dias NV, Ivancev K, Malina M, et al. Intra-aneurysm sac pressure measurements after endovascular aneurysm repair: differences between shrinking, unchanged, and expanding aneurysms with and without endoleaks. *J Vasc Surg*. 2004;39:1229–1235.
11. Malina M, Länne T, Ivancev K, et al. Reduced pulsatile wall motion of abdominal aortic aneurysms after endovascular repair. *J Vasc Surg*. 1998;27:624–631.
12. Faries PL, Agarwal G, Lookstein R, et al. Use of cine magnetic resonance angiography in quantifying aneurysm pulsatility associated with endoleak. *J Vasc Surg*. 2003;38:652–656.
13. Vos AW, Wisselink W, Marcus JT, et al. Cine MRI assessment of aortic aneurysm dynamics before and after endovascular repair. *J Endovasc Ther*. 2003;10:433–439.

14. Brekken R, Bang J, Ødegård A, et al. Strain estimation in abdominal aortic aneurysms from 2D ultrasound. *Ultrasound Med Biol*. 2006;32:33–42.
15. Ophir J, Céspedes I, Ponnekanti H, et al. Elastography: a quantitative method for imaging the elasticity of biological tissues. *Ultrason Imaging*. 1991;13:111–134.
16. Selbekk T, Bang J, Unsgaard G. Strain processing of intraoperative ultrasound images of brain tumours: initial results. *Ultrasound Med Biol*. 2005;31:45–51.
17. Heimdal A, Støylen A, Torp H, et al. Real-time strain rate imaging of the left ventricle by ultrasound. *J Am Soc Echocardiogr*. 1998;11: 1013–1019.
18. Vos AW, Wisselink W, Marcus JT, et al. Aortic aneurysm wall motion imaged by cine MRI: a tool to evaluate efficacy of endovascular aneurysm repair? *Eur J Vasc Endovasc Surg*. 2002;23:158–161.
19. Thubrikar MJ, Labrosse M, Robicsek F, et al. Mechanical properties of abdominal aortic aneurysm wall. *J Med Eng Techn*. 2001;25: 133–142.
20. Mehta M, Darling RC, Chang BB, et al. Does sac size matter? Findings based on surgical exploration of excluded abdominal aortic aneurysms. *J Endovasc Ther*. 2005;12:183–188.
21. Risberg B, Delle M, Eriksson E, et al. Aneurysm sac hygroma: a cause of endotension. *J Endovasc Ther*. 2001;8:447–453.
22. Mehta M, Veith FJ, Ohki T, et al. Significance of endotension, endoleak, and aneurysm pulsatility after endovascular repair. *J Vasc Surg*. 2003;37:842–846.
23. Raghavan ML, Vorp D, Federle MP, et al. Wall stress distribution on three-dimensionally reconstructed models of human abdominal aortic aneurysm. *J Vasc Surg*. 2000;31: 760–769.
24. Fillinger MF, Marra SP, Raghavan ML, et al. Prediction of rupture risk in abdominal aortic aneurysm during observation: wall stress versus diameter. *J Vasc Surg*. 2003;37: 724–732.

Paper III

3D visualization of strain in abdominal aortic aneurysms based on navigated ultrasound imaging

Reidar Brekken*[1], Jon Harald Kaspersen[1], Geir Arne Tangen[1], Torbjørn Dahl[2,3], Toril AN Hernes[1,3], Hans Olav Myhre[2,3]
[1] SINTEF Health Research, N-7465 Trondheim, Norway.
[2] St Olav's Hospital, University Hospital of Trondheim, N-7006 Trondheim, Norway.
[3] Norwegian University of Science and Technology, N-7491 Trondheim, Norway.

ABSTRACT

The criterion for recommending treatment of an abdominal aortic aneurysm is that the diameter exceeds 50-55 mm or shows a rapid increase. Our hypothesis is that a more accurate prediction of aneurysm rupture is obtained by estimating arterial wall strain from patient specific measurements. Measuring strain in specific parts of the aneurysm reveals differences in load or tissue properties. We have previously presented a method for in vivo estimation of circumferential strain by ultrasound. In the present work, a position sensor attached to the ultrasound probe was used for combining several 2D ultrasound sectors into a 3D model. The ultrasound was registered to a computed-tomography scan (CT), and the strain values were mapped onto a model segmented from these CT data. This gave an intuitive coupling between anatomy and strain, which may benefit both data acquisition and the interpretation of strain. In addition to potentially provide information relevant for assessing the rupture risk of the aneurysm in itself, this model could be used for validating simulations of fluid-structure interactions. Further, the measurements could be integrated with the simulations in order to increase the amount of patient specific information, thus producing a more reliable and accurate model of the biomechanics of the individual aneurysm. This approach makes it possible to extract several parameters potentially relevant for predicting rupture risk, and may therefore extend the basis for clinical decision making.

Keywords: abdominal aortic aneurysm, biomechanics, strain, ultrasound, rupture risk, navigation, multi-modal imaging

1. INTRODUCTION

An abdominal aortic aneurysm (AAA) is a local dilatation of the abdominal aorta. The high mortality associated with rupture of AAA motivates the use of elective repair when the risk of rupture exceeds the risk involved with the treatment. The current clinical guideline is to recommend treatment of asymptomatic AAA when the maximum diameter exceeds 50-55 mm or shows a rapid expansion [1], [2]. This criterion is however known to be inaccurate [3], [4] and other approaches have therefore been suggested for assessing the risk of rupture. These include computer simulations of biomechanical properties based on computed tomography scan (CT) [5], [6] and measurement of compliance or elasticity from real-time ultrasound [7], [8], [9].

The motivation for doing patient-specific simulations is that, from a biomechanical point of view, rupture occurs when the load imposed on the aneurysm exceeds the strength of the vessel wall. Measuring the diameter gives an idealized estimate of the load, assuming that wall stress is proportional to diameter and blood pressure. However, this assumption is valid only for simple geometries. Improved estimates of wall stress are expected to be obtained by taking into account the patient specific geometry, the effect of the thrombus mass, the hemodynamic conditions and specific modeling of tissue properties. This leads to advanced model equations to be solved with numerical simulation methods.

Direct measurement of the dynamic properties of the aneurysm wall is an alternative or supplement to modeling and simulation. Following this approach, in-vivo estimation of 2D circumferential strain in AAA has recently been presented as a novel approach for assessing rupture risk [7]. The purpose of the present work was to combine strain images from several cross-sections into a 3D model for improved interpretation of strain by enhancing the relation between the aneurysm anatomy and strain.

Medical Imaging 2007: Physiology, Function, and Structure from Medical Images, edited by Armando Manduca, Xiaoping P. Hu, Proc. of SPIE Vol. 6511, 65111H, (2007) · 1605-7422/07/$18 · doi: 10.1117/12.708776

2. METHOD

A 3D model of strain in the aneurysm was generated by processing strain from 2D ultrasound recordings and color-parameterizing the results onto a 3D geometry segmented from contrast enhanced CT data (illustrated in Fig 1). The 3D positioning of the ultrasound images was found by attaching a position sensor to the ultrasound probe and tracking the position using a navigation system.

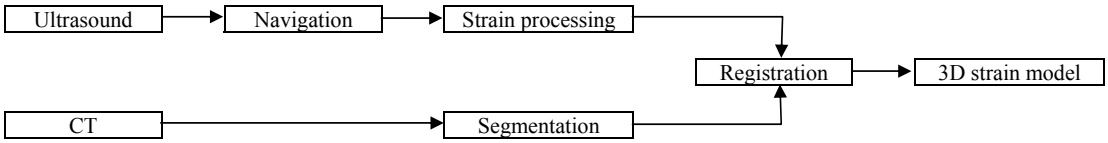

Fig 1 Workflow. Ultrasound was acquired while using a navigation system for positioning the ultrasound sectors in 3D space. Strain was processed for each 2D ultrasound sector, and registered to a 3D model segmented from CT data. The result was a 3D model visualizing strain in the aneurysm.

2.1 Data acquisition

Data was acquired from five patients undergoing elective endovascular treatment of AAA at St. Olav's Hospital (Trondheim, Norway). The patients gave informed consent to participate in the study, and underwent an extra ultrasound examination the day before the intervention.

Ultrasound B-mode data was recorded using the ViVid7 ultrasound scanner (GE Vingmed Ultrasound, Horten, Norway). A position sensor was attached to the ultrasound probe for acquiring the relative position of several ultrasound sectors from each patient [10]. Data was acquired using a 3.5 MHz curved linear array probe transmitting at 2.2MHz and receiving at 4.7MHz. The image depth and width was adjusted to cover the aneurysm cross-section. To achieve a frame rate in the order of 40 to 50 fps, which is necessary for the processing method to succeed, only one focal point was used. Data was stored for later strain-processing on an external PC. In addition to the ultrasound data, echocardiogram (ECG) was recorded simultaneously and blood pressure was measured immediately before each examination.

The examinations were performed by a vascular surgeon with experience in ultrasound imaging. The ultrasound probe was placed in an anterior position. Data was acquired from three aneurysm cross-sections. Several consecutive cycles (≥3) were recorded for each cross-section, and only cycles without apparent respiratory motion or probe displacement were chosen for further processing.

The CT datasets from the last routine examination before the treatment were used in this study. These datasets were recorded within a range of 1 to 27 weeks (average 14) before the ultrasound examination, and it is therefore possible that they did not exactly reflect the current anatomy at that time. The difference was however considered to be too small to justify the extra radiation dose of performing a separate CT scan for this study. The CT data had a resolution of 512x512 pixels with graylevels represented by 16 bit unsigned integers. Typical voxelsize was 0.45x0.45x5 mm.

2.2 Processing

Ultrasound strain processing

Linear strain was estimated along the circumference of the aneurysm in each 2D ultrasound image. Strain quantifies the relative elongation and contraction of the wall tissue imposed by the passing blood pulse. Subdividing the circumference of the aortic wall into N segments, the linear strain (ε) in each segment is defined as

$$\varepsilon(t)_i = \frac{L(t)_i - L_{0,i}}{L_{0,i}} \qquad , L_{0,i} = L(0)_i \qquad , i = 1...N$$

$L(t)_i$ is the distance between the two endpoints of segment i, and t is the time instance corresponding to each frame through the cardiac cycle. L is a time varying quantity due to the expansion and contraction imposed by the blood pulse passing through the aorta. The reference time (t=0) was chosen as a time instance between two passing blood pulses. To calculate L, and hence estimate strain, the endpoints of each segment were traced through the cardiac cycle. The method is described in detail by Brekken et al (2006) [7].

Segmentation

Medical segmentation is the process of extracting the geometry of organs relevant for an examination, either for visualization or for quantitative analysis. Medical data are noisy, contain regions with overlapping image intensity and drop-outs. Therefore, despite of the wish for a general segmentation method, experience shows that the algorithms have to be adapted to the specific image modality and organ for accurate and robust segmentation results.

In this study, the lumen and aneurysm wall were segmented from contrast enhanced CT. We focus on infrarenal AAA, and thus the relevant region is from below the renal arteries to the iliac bifurcation. The lumen segmentation was initialized by the user indicating one point in each of the iliac branches. An optimal ellipse approximation to the lumen was found in every CT slice (2D). These ellipses were then deformed by using an active contour method for minimizing an energy function [11]. The next slice was initialized with the result from the current slice. For segmenting the thrombus mass, the user indicated one point in the thrombus, and the same approach was used as for lumen, but with changed parameter settings.

Registration

Registration is the task of placing the ultrasound cross-sections correctly relative to the CT model (Fig 2), i.e. to align CT and ultrasound coordinate systems [12]. In this work registration was performed by means of manually indicating anatomical landmarks in both modalities. This information was further used for calculating the transformation matrix that describes the translation and rotation necessary for aligning the coordinate systems.

Having aligned the ultrasound and CT coordinate systems, a 3D visualization of strain was obtained by using the position data from the navigation system for mapping strain values onto the geometric model segmented from CT. A color parameterization was used for visualizing the level of strain.

The navigation system CustusX (SINTEF Health Research, Trondheim, Norway) [13] was used for positioning and registration. Matlab (The Mathworks Inc, Natick, MA, USA) was used for processing and concept development.

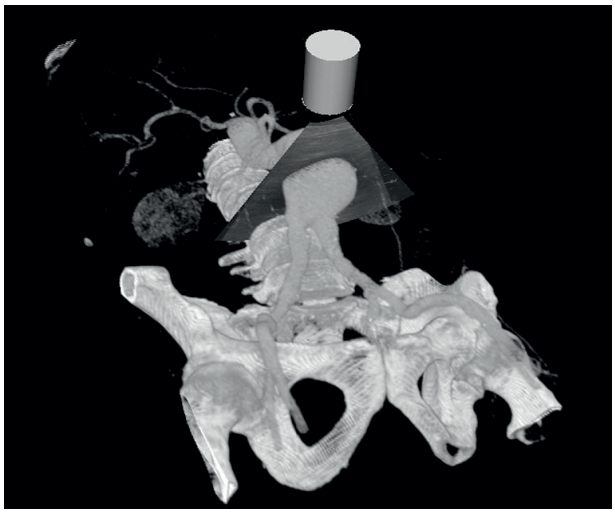

Fig 2. Example of an ultrasound image positioned in a 3D CT scene (CustusX, SINTEF, Trondheim, Norway).

3. RESULTS

The results of each processing task are illustrated in Fig 3. The first panel shows strain as calculated in three cross-sectional ultrasound images. The strain values are color parameterized and positioned in 3D space using the position output from the navigation system. Next, the results of segmenting the lumen and the aneurysm wall from CT data are shown as black and green surfaces, respectively. Finally, the strain surface is mapped onto the segmented model by manual registration between CT and ultrasound.

Given the limited selection of patients, no clinical results should be inferred from this study. We state, however, that maximum strain values were typically found to be less than 5%. Also, as illustrated in Fig 3, strain was found to be inhomogeneous along the circumference of the aneurysm, indicating that the method gives a measure of the varying load conditions and tissue properties.

Figure 4 shows the color parameterized strain surface visualized in the CT scene for improved anatomical interpretation, giving an intuitive visualization of strain.

4. DISCUSSION

The reasons for developing the 3D model were considered threefold. First, since strain quantifies the relative elongation and contraction of the tissue imposed by the pulsatile blood flow, strain depends on the load on the vessel wall and the tissue characteristics. This is believed to be information relevant for predicting rupture risk, and clinical studies should be performed to evaluate the clinical interpretation of strain. An intuitive 3D visualization could be of assistance in evaluating strain in clinics. Second, the model could be used for validating fluid structure interaction (FSI) simulations. The measurements could be used for calibrating the model parameters and hence improve the simulation results, especially the biomechanical tissue model. Third, the 3D model based on measured strain could be more closely integrated into the simulations thereby increasing the amount of patient specific information. Retrieving biomechanical properties from a model containing a maximum of information specific of the individual aneurysm has potential of being the method to provide the most precise assessment of rupture risk.

4.1 Accuracy

The accuracy of the method is influenced by several factors. Geometrical factors include positioning of the ultrasound probe, registration of ultrasound to CT and the segmentation of the aneurysm from the CT data. The accuracy of the registration could be improved by acquiring CT and ultrasound at the same time, and by using fiducials for registration. The manual registration method could be replaced by an automatic method, e.g. by sampling positions from the patient's stomach to produce a surface that could be mapped to the same surface as segmented from the CT data. In addition, non-rigid registration could be considered [14]. Also, the segmentation method may be improved, e.g. by using a 3D method for segmenting the thrombus-wall interface [15], [16] or by increased manual interaction. Better accuracy would also be obtained by using CT data with increased resolution. These factors influence the accuracy of the 3D geometry and the anatomical positioning of strain. Because the 3D geometry is used only for visualization, i.e. to get an overview of the 3D anatomy, we consider these factors to be less critical for this application, and the optimization of these subtasks has therefore not been the focus of the present work.

Another question is the accuracy of the strain processing method. This method is based on tracing wall motion from transabdominal ultrasound image sequences of varying quality. The accuracy of this method is more critical, hypothesing that diagnostic information could be drawn from determining the correct level of strain. There is a need for further studies evaluating the accuracy and reproducibility of the method. Also, further attention should be paid to the fact that the strain processing method gives strain only in 2D, thereby neglecting the longitudinal motion component. Generally, strain is a tensor value; in this work we measure only linear strain.

In this work the strain model is visualized at one particular time instance. However, because strain is calculated for each frame through the cardiac cycle, the model can be visualized as a movie showing how strain relates to the ECG through the cycle.

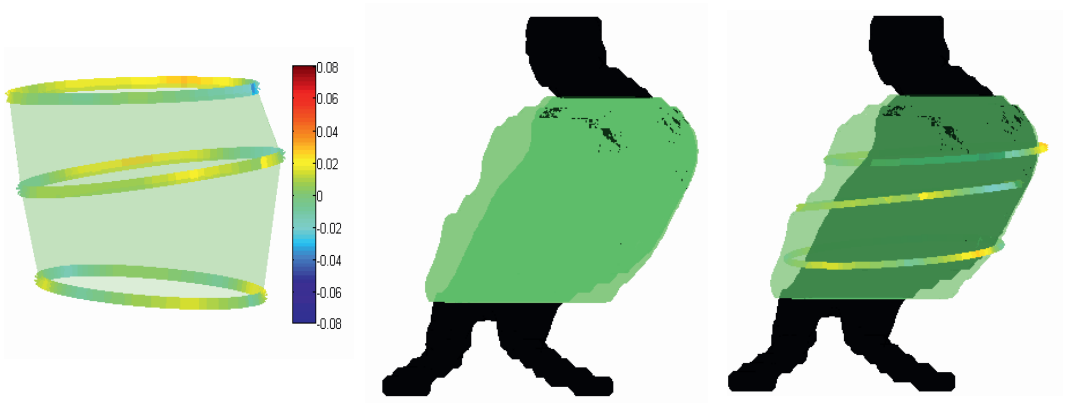

Fig 3. Left: Strain is processed from three 2D ultrasound images positioned in 3D by using a navigation system. The strain values are color-coded according to the indicated scale. A transparent green surface is drawn between the ultrasound planes for enhanced 3D perception. Middle: The black structure represents the blood flow volume (lumen), whereas the transparent green structure is the surface of the aneurysm as segmented from CT. Right: The strain model and the segmented model are combined using registration.

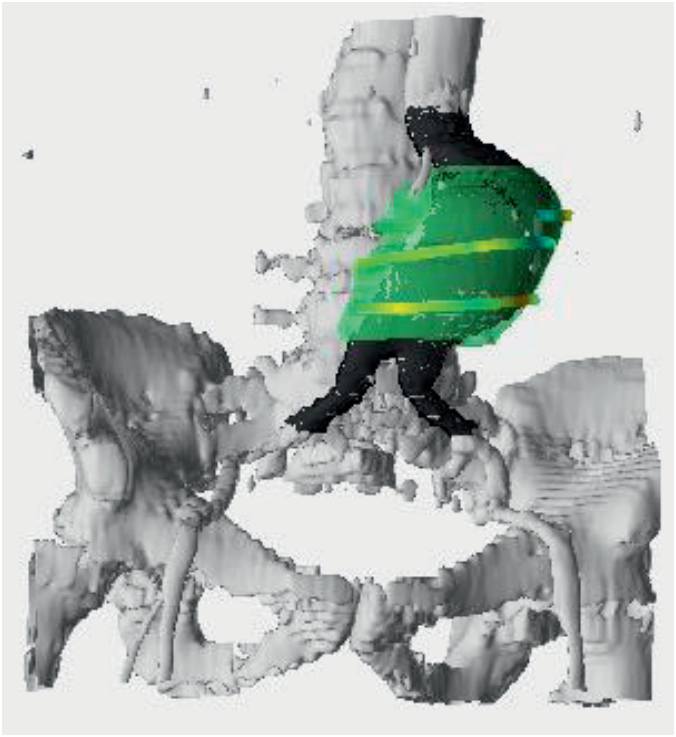

Fig 4. 3D strain model. The model from Fig 3 is placed in a CT scene for enhanced anatomical interpretation. Strain is shown in one time-instance, but it is possible to generate a video showing how strain changes through the cardiac cycle (synchronized with ECG).

4.2 Model based imaging

Previous research for alternative means of assessing rupture risk of AAA has mainly been focusing either on mathematical simulation or ultrasound measurement. We believe that the model suggested in this work provides the opportunity for a unified approach, in which simulation and measurements are integrated to introduce a model based imaging concept. The motivation for this is the recognition that measurements may not be sufficient on its own. For example, referring to Fig 3, strain is measured only in a limited number of slices. Here, modeling and simulation could be considered an "advanced interpolation method" that could provide simulated strain values in between the measured values. Also, other clinically relevant parameters could more easily be extracted from a mathematical model than from direct measurements. The aim is to combine as much relevant information as possible from theoretical consideration and patient specific data and measurements into one model supporting clinical decision making. As a next step towards this concept, the ultrasound based 3D strain model could be used for validation and possibly calibration of FSI simulations (Fig 5).

It should be noted that the accuracy of positioning, registration and segmentation becomes more critical when the results are to be further processed numerically as compared to visualization only.

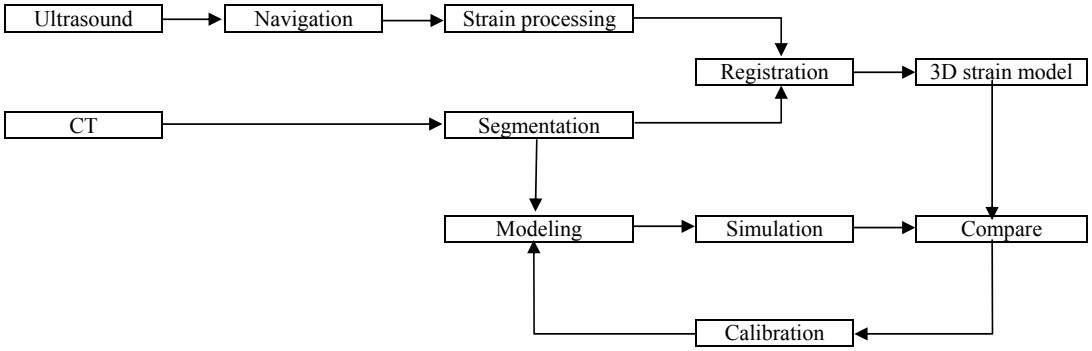

Fig 5 Workflow. The upper half of the figure equals Fig 1. In addition a loop describing the integration of the dynamic measurements into a modeling and simulation approach is included. The 3D strain model is compared to the model produced by numerical simulations, and the biomechanical simulation model is iteratively updated until the simulated values converge to the measured values.

4.3 Future work

Future work includes 1) evaluation and further development of the ultrasound strain processing method, 2) development of a model based imaging approach combining ultrasound measurements with computer simulations and 3) evaluation of the clinical relevance of strain or related parameters for predicting rupture of AAA.

5. CONCLUSIONS

We have presented a 3D visualization of strain in AAA. This approach gave a more intuitive visualization and improved the geometric interpretation of strain compared to a 2D visualization. We believe that the 3D strain model could provide relevant diagnostic information. The model may also be valuable for validation and calibration of FSI simulations, or even for providing input values to a simulation approach more closely integrated with patient specific measurements.

ACKNOWLEDGEMENT

This work was supported by SINTEF Health Research and by the Norwegian Ministry of Health and Social Affairs through the National Centre for 3D Ultrasound in Surgery.

REFERENCES

1. Brewster DC, Cronenwett JL, Hallett JW et al. Guidelines for the treatment of abdominal aortic aneurysms. J Vasc Surg 2003;37:1106-1117.
2. Brady AR, Brown LC, Fowkes FGR et al. Long-term outcomes of immediate repair compared with surveillance of small abdominal aortic aneurysms. N Engl J Med 2002;346:1445-1452.
3. Lederle FA, Johnson GR, Wilson SE et al. Rupture rate of large abdominal aortic aneurysms in patients refusing or unfit for elective repair. JAMA 2002;287:2968-2972.
4. Nicholls SC, Gardner JB, Meissner MH, Johansen HK. Rupture in small abdominal aortic aneurysms. J Vasc Surg 1998;28:884-888.
5. Wolters BJBM, Rutten MCM, Schurink GWH, Kose U, de Hart J, van de Vosse FN. A patient-specific computational model of fluid-structure interaction in abdominal aortic aneurysms. Med Eng Phys 2005;27:871-883.
6. Fillinger MF, Marra SP, Raghavan ML, Kennedy FB. Prediction of rupture risk in abdominal aortic aneurysm during observation: Wall stress versus diameter. J Vasc Surg 2003;37:724-732.
7. Brekken R, Bang J, Ødegård A, Aasland J, Hernes TAN, Myhre HO. Strain estimation in abdominal aortic aneurysms from 2D Ultrasound. Ultrasound Med Biol 2006;32:33-42.
8. Long A, Rouet L, Bissery A, Rossignol P, Mouradian D, Sapoval M. Compliance of abdominal aortic aneurysms evaluated by tissue Doppler imaging: Correlation with aneurysm size. J Vasc Surg 2005;42:18-26.
9. Wilson K, Lee AJ, Hoskins P et al. The relationship between aortic distensibility and rupture of infrarenal abdominal aortic aneurysm. J Vasc Surg 2003;37:112-117.
10. Kaspersen JH, Sjølie E, Wesche J, Åsland J, Lundbom J, Ødegård A, Lindseth F, Hernes TAN. Three-dimensional ultrasound-based navigation combined with preoperative CT during abdominal interventions: A feasibility study. Cardiovasc Intervent Radiol 2003;26:347-356.
11. Kass M, Witkin A, Terzepoulus. Snakes: Active contour models. Int J Comput Vision 1988;1:321-331.
12. Lindseth F, Kaspersen JH, Ommedal S, Langø T, Unsgaard G, Hernes TAN. Multimodal image fusion in ultrasound-based neuronavigation: improving overview and interpretation by integrating preoperative MRI with intraoperative 3D ultrasound. Comp Aided Surg 2003, 8:2:49-69.
13. Langø T, Tangen GA, Mårvik R, Ystgaard B, Kaspersen JH, Hernes TAN Navigation in laparoscopy – Prototype research platform CustusX for improved image-guided surgery. Submitted 2006.
14. Hernes TAN, Lindseth F, Selbekk T, et.al. Computer-assisted 3D ultrasound-guided neurosurgery: technological contributions, including multimodal registration and advanced display, demonstrating future perspectives. Int J Med Robotics Comput Assist Surg 2006;2:45-59.
15. de Bruijne M, van Ginneken B, Niessen WJ, Maintz JBA, Viergever MA. Active shape modell based segmentation of abdominal aortic aneurysms in CTA images. Proc SPIE Medial Imaging. 2002;4684:463-474.
16. Subasic M, Loncaric S, Sortantin E. 3D image analysis of abdominal aortic aneurysm. Proc SPIE Medical Imaging. 2002;4684:1681-1689.

Paper IV

Ultrasound in Med. & Biol., Vol. 38, No. 5, pp. 889–896, 2012

0301-5629/$ - see front matter

ELSEVIER

doi:10.1016/j.ultrasmedbio.2012.01.007

● *Technical Note*

SIMULATION MODEL FOR ASSESSING QUALITY OF ULTRASOUND STRAIN ESTIMATION IN ABDOMINAL AORTIC ANEURYSM

REIDAR BREKKEN,*† SÉBASTIEN MULLER,† SJUR U. GJERALD,* and TORIL A. NAGELHUS HERNES*†
*Department of Circulation and Medical Imaging, Norwegian University of Science and Technology, Trondheim, Norway; and †Department of Medical Technology, SINTEF, Trondheim, Norway

(*Received* 19 *June* 2011; *revised* 9 *January* 2012; *in final form* 9 *January* 2012)

Abstract—The purpose of this study was to develop a simulation model for evaluating methods for ultrasound strain estimation in abdominal aortic aneurysms. Wall geometry was obtained from a real ultrasound image and wall motion was simulated applying realistic blood pressures to a nonlinear viscoelastic wall model. The ultrasound simulation included speckle, absorption and angle dependent reflection. Gaussian white noise was added to simulate various noise levels. Despite not fully replicating real ultrasound images, the model simulated realistic circumferential variations in intensity and realistic speckle patterns and has potential for initial evaluation of strain estimation methods. (E-mail: reidar.brekken@sintef.no) © **2012 World Federation for Ultrasound in Medicine & Biology.**

Key Words: **Ultrasound, Strain, Simulation, Abdominal aortic aneurysm, Biomechanics.**

INTRODUCTION

Rupture of abdominal aortic aneurysm (AAA) causes high mortality, and elective surgery or endovascular therapy is, therefore, recommended when the risk of rupture exceeds the risk associated with treatment. Although indicators for rupture risk have been identified, predominantly the diameter exceeding 5.0–5.5 cm or increasing rapidly, rupture risk is still not evaluated on a patient-specific level with satisfying specificity and sensitivity (Brewster et al. 2003).

Ultrasound can be used for estimating dynamical properties of the aneurysm due to the pulsating blood pressure and, thereby, obtaining additional patient-specific information about the state of the aneurysm. Brekken et al. (2006) described a method for estimating circumferential strain over the cardiac cycle from cross-sectional ultrasound images. The level and distribution of strain depends on the wall stress and the material properties of the wall tissue. Since it has been shown that both wall stress (*e.g.*, Fillinger et al. 2003) and material properties (*e.g.*, Di Martino et al. 2006; Thubrikar et al. 2001) are relevant factors in AAA rupture, strain imaging may reveal additional information for assessing rupture risk.

Strain is generally estimated from ultrasound based on temporal correlation of images or signals. This correlation is degraded by noise, out-of-plane motion and deformation, which may lead to uncertainty in the strain estimates. Due to the varying quality of transcutaneous abdominal ultrasound images, it is, therefore, important to consider the validity of the strain measurements when using ultrasound strain in clinical studies on AAA. It is, however, technically challenging to obtain comparable true *in vivo* strain values for method evaluation.

To overcome this challenge, a controlled environment with known parameters could be obtained by combining biomechanical modeling with ultrasound image simulation. Swillens et al. (2009) suggested a computational fluid dynamics (CFD) model in combination with ultrasound simulation to simulate blood velocity imaging of a carotid artery. For evaluation of methods in echocardiography, Hergum et al. (2009) suggested a fast ultrasound simulation method in combination with a finite-element-model of an ellipsoidal left ventricle. Several authors have suggested using simulation to investigate methods for elastography and strain estimation (Crosby et al. 2009; D'Hooge et al. 2003; Gao et al. 2009; Maurice et al. 2004).

Address correspondence to: Reidar Brekken, SINTEF Medical Technology, MTFS, Box 4760 Sluppen, N-7465 Trondheim, Norway. E-mail: reidar.brekken@sintef.no

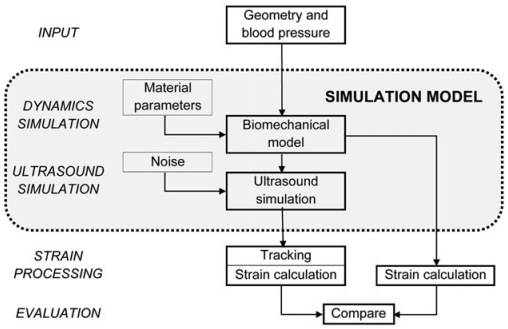

Fig. 1. Flowchart illustrating the simulation model and evaluation approach. Patient specific geometry and blood pressure were used together with material parameters as input to the simulation model producing dynamic ultrasound images with varying noise levels. Ultrasound strain processing methods could then be applied to these images, and evaluated by comparing results with similar strain measures calculated from the known dynamics of the synthetic aneurysm.

In this article, we suggest a simulation model that can be used as a first assessment of methods for ultrasound strain estimation in AAAs. The emphasis was on developing a model that simulated the main features of wall dynamics and image appearance, and at the same time was simple and allowed for fast repetition of simulations with different parameters.

MATERIALS AND METHODS

To simulate ultrasound of a dynamic AAA, a biomechanical model of aortic wall motion was combined with an ultrasound simulation method. The approach is illustrated in Figure 1 and further described in the following sections.

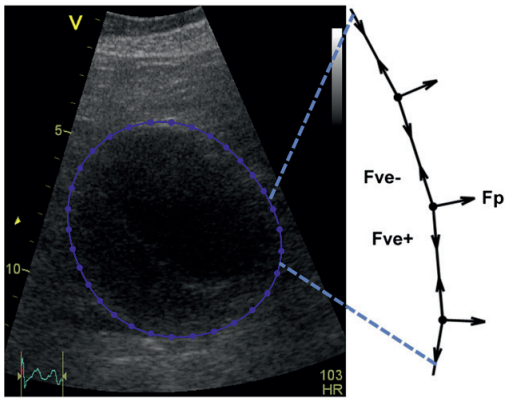

Fig. 2. Aneurysm model. Cross-sectional ultrasound image of an aneurysm, with a curve indicating the wall geometry. The right side illustrates in further detail part of the wall curve, with pressure (F_p) and viscoelastic forces (F_{ve}) acting at each node as illustrated by the arrows. The ECG-trace is shown in the lower left.

Geometry and blood pressure

To obtain realistic input values, we acquired ultrasound, systolic and diastolic brachial blood pressures, and electrocardiogram (ECG) from a (75-year-old male) patient scheduled for endovascular aneurysm repair. Ultrasound was acquired with a 3.5-MHz curved linear array (CLA) probe on a ViVid7 ultrasound scanner (GE Vingmed Ultrasound, Horten, Norway). The cross-sectional geometry of the aneurysm was obtained by manually indicating a curve within the wall in one diastolic ultrasound frame (Fig. 2). The wall was assumed to have a constant thickness of 2 mm, extending 1 mm at each side of the curve. A generic blood pressure profile, adapted from catheter measurements in the abdominal aorta of a healthy subject (Remington and Wood 1956) (Fig. 3), was scaled to match blood pressures and heart rate of the patient (blood pressure: 155/85 mm Hg, heart rate: 103 bpm). The Regional Committee for Medical Research Ethics approved the use of patient data.

Biomechanical model

The aneurysm wall was modeled as 1-D nonlinear viscoelastic elements connected at nodes. The force acting at each node was modeled as the sum of pressure force acting on the neighboring elements and viscoelastic forces due to stretching of the elements (Fig. 2). The pressure force acted normal to the wall and was calculated as the product of the blood pressure and the inner surface area around each node. The viscoelastic forces acted along the direction of the elements and were calculated as the product of the circumferential wall stress σ and the cut-plane area at each node. Stress was related to strain by a nonlinear viscoelastic material model:

$$\sigma = \mu_0 \cdot e^{\mu \cdot \varepsilon} + \tilde{\mu} \cdot \frac{\Delta \varepsilon}{\Delta t} \quad (1)$$

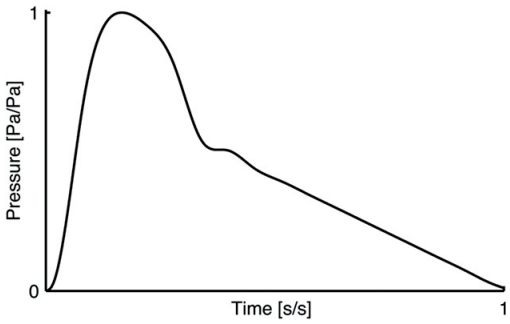

Fig. 3. Normalized blood pressure curve, adapted from Remington and Wood (1956).

Table 1. Ultrasound simulation parameters

Parameter	Description	Value	Unit
k_a	Ambient reflection coefficient	0.061	–
k_d	Diffuse reflection	0.282	–
n_d	coefficients	1	–
k_s	Specular reflection	0.657	–
n_s	coefficients	2.9	–
L_{dB}	Two-way absorption	0.4	(dB/cm)/MHz
c	Speed of sound	1540	m/s
f	Center frequency	3.5	MHz
$PSF_{-6dB\ ax}$	PSF dimensions at −6dB	±0.25	mm
$PSF_{-6dB\ lat}$		±0.0045	rad
$PSF_{-6dB\ ele}$		±2.0	mm
$d\Omega$	Neighborhood of sample point	$5 \cdot PSF_{-6dB}$	–
dr	Sampling resolution	1/20000	m
$d\theta$	Beam density	0.00225	rad

where $\mu_0, \mu, \tilde{\mu}$ are material parameters, and ε is the longitudinal strain of each element (circumferential strain for the aneurysm). The natural strain of a segment stretched from length L_0 to length L was separated into a constant diastolic and a dynamic cyclic strain component, respectively,

$$\begin{aligned}\varepsilon &= \ln\left(\frac{L}{L_0}\right) = \ln\left(\frac{L_D}{L_0}\cdot\frac{L}{L_D}\right) = \ln\left(\frac{L_D}{L_0}\right) + \ln\left(\frac{L}{L_D}\right) \\ &= \varepsilon_D + \Delta\varepsilon\end{aligned} \tag{2}$$

where L_D is the length of the segment in diastole. Inserted into eqn (1), this gives the following stress-strain relation

$$\begin{aligned}\sigma &= \mu_0 \cdot e^{\mu\cdot(\varepsilon_D+\Delta\varepsilon)} + \tilde{\mu}\cdot\frac{d\varepsilon}{dt} = \mu_0 \cdot e^{\mu\cdot\varepsilon_D}\cdot e^{\mu\cdot\Delta\varepsilon} + \tilde{\mu}\cdot\frac{d\varepsilon}{dt} \\ &= \sigma_D \cdot e^{\mu\cdot\Delta\varepsilon} + \tilde{\mu}\cdot\frac{d\varepsilon}{dt}\end{aligned} \tag{3}$$

where diastolic stress has been introduced as $\sigma_D = \mu_0 \cdot e^{\mu\cdot\varepsilon_D}$.

For simulating the wall motion, we further expressed wall stress as a function of segment length combining eqn (2) and eqn (3)

$$\sigma = \sigma_D \cdot \left(\frac{L}{L_D}\right)^{\mu} + \tilde{\mu}\cdot\frac{1}{L}\frac{dL}{dt} \tag{4}$$

The diastolic stress was estimated from Laplace law for a thin-walled cylinder, while parameter values were chosen as $\mu = 15$ (dimensionless) and $\tilde{\mu} = 1000$ Pa·s. Further details regarding the biomechanical simulation are included in the Appendix.

Ultrasound image simulation

The tissue was modeled as a collection of points with an associated acoustic backscattering coefficient (scatterers). The motion of each scatterer was deduced from the motion of the nodes by bilinear interpolation. The amplitude A_q of the backscattering coefficients was assigned Gaussian random values N and modified by taking into account that the reflection depends on the angle φ_q between the ultrasound beam and the normal vector of the object's surface. A model accounting for different types of reflection for shading in computer graphics (Phong 1975) was adapted to

$$\begin{aligned}A_q = A_q(\phi_q) = N \cdot \big(k_a + k_d \cdot \left|cos(\phi_q)\right|^{n_d} \\ + k_s \cdot max\big(0, cos2\phi_q\big)^{n_s}\big)\end{aligned} \tag{5}$$

where k and n are material parameters describing ambient, diffuse and specular reflection. We chose $n_d = 1$ to account for ideal diffuse reflection. The other parameters were determined by minimizing the square difference (least-square) between the model and the intensity from the wall in the real image, constraining $k_a + k_d + k_s = 1$ to avoid scaling. Values are included in Table 1.

Speckle was simulated as a convolution between the tissue (scatterer) model and the point-spread function (PSF) of the imaging system, similar to approaches described in more detail by *e.g.*, Gao et al. (2009). We simulated a CLA probe with 4.9 cm aperture and 4 cm radius of curvature. Using cylindrical coordinates, denoting each sample point by (r, θ, z_0) and the position of each scatterer in a neighborhood $d\Omega$ of the sample point by (r_q, θ_q, z_q), radio-frequency (rf) ultrasound signals were simulated by the following convolution

$$\begin{aligned}rf(r,\theta,z_0) = \sum_{q\in d\Omega} A_q \cdot PSF\big(r-r_q, \theta-\theta_q, z_0-z_q\big) \\ \cdot e^{i\cdot 2\pi f\cdot\left(d_q - r\right)/c}\end{aligned} \tag{6}$$

where d_q is the distance from the transducer to the scatterer, f is center frequency and c is speed of sound. Parameter values, along with radial and lateral sampling resolution (dr and $d\theta$), are included in Table 1. The PSF was modeled with Gaussian profiles in axial, lateral and elevation directions, defined by width at −6 dB for each direction (Table 1). In addition, we modeled a logarithmic absorption L_{dB} (intensity) per depth and frequency unit and Gaussian white noise with intensity levels ranging from −60 dB to −20 dB (with 0 dB defined as the signal level without absorption and with beam parallel to the normal vector of the aneurysm). B-mode images were obtained by time-gain-compensation (TGC), lateral interpolation of the simulated rf-signals, envelope detection, log-compression and scan-conversion. Interpolation between the rf-lines was done to improve image quality and reduce the risk of aliasing after the succeeding nonlinear signal processing. According to first-order speckle statistics, the ratio of the mean to the standard deviation (defined as signal-to-noise-ratio, SNR) of the

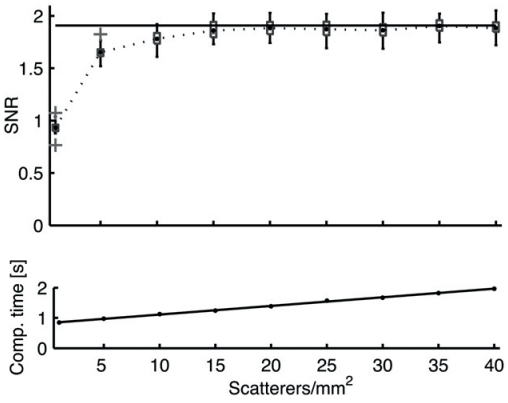

Fig. 4. Signal-to-noise ratio (SNR) and computation time as a function of scatterer density. A 1 cm × 1 cm speckle image was simulated. Upper: The SNR did not change significantly by increasing the density above 15 scatterers/mm^2. The boxplots show the lower and upper 25% percentile (box), range and outliers with the variation being due to 30 repetitive calculations with different random configurations of scatterers. Lower: The computation time increased linearly with scatter density ($R^2 > 0.99$).

speckle after detection should approach 1.91. (Cobbold 2007). We used eqn (6) to simulate a speckle pattern of size 1 cm × 1cm with varying scatterer densities. The computation time increased linearly with scatterer density (linear regression, R2 > 0.99) and the SNR did not improve significantly when increasing the density above 15 scatterers per mm^2 (analysis of variance [ANOVA] test showing no significant difference between groups with ≥15 scatterers per mm^2, $p = 0.24$) (Fig. 4). This density was, therefore, chosen when placing scatterers at random positions within the aneurysm wall, giving a total of approximately 7000 scatterers for the chosen aneurysm (approx. 7.3 cm diameter, 2 mm wall thickness). The simulation model was implemented in Matlab R2011a (The MathWorks Inc., Natick, MA, USA), and run on a MacBook Pro (Apple Inc., Cupertino, CA, USA) with operating system MaxOSX.6, dual core 2.66 GHz processor and 8 GB memory.

The temporal correlation of the speckle pattern was analyzed by choosing 2 mm × 2 mm regions-of-interest (ROI) in the aneurysm wall. The known motion of the underlying scatterers was used for aligning each ROI from frame to frame, and correlation was quantified by the temporal mean (over the cardiac cycle) of the normalized correlation coefficient between each succeeding frame. In addition, for illustration of tracking with different noise levels, a standard two-dimensional (2-D) normalized cross-correlation method was implemented for tracking the 2 mm × 2 mm ROIs from frame to frame according to the maximum correlation between the ROI and a 4 mm × 4 mm search area in the neighborhood of this ROI in the succeeding frame. Assuming that each ROI should return to the initial position after one cardiac cycle, linear correction was applied to adjust the position of the ROI in case of any deviation between the first and final frame. Tracking error was quantified by the root-mean-square (RMS) difference between the tracked position and the known true position over the cardiac cycle. To obtain analysis that were more robust to variation due to the stochastic scatterers, we simulated five different speckle realizations and reported the mean values.

RESULTS

Examples of simulated ultrasound images with different noise levels are shown in Figure 5a and b. The images differ from the corresponding real ultrasound for the same case, shown in Figure 2, since only the

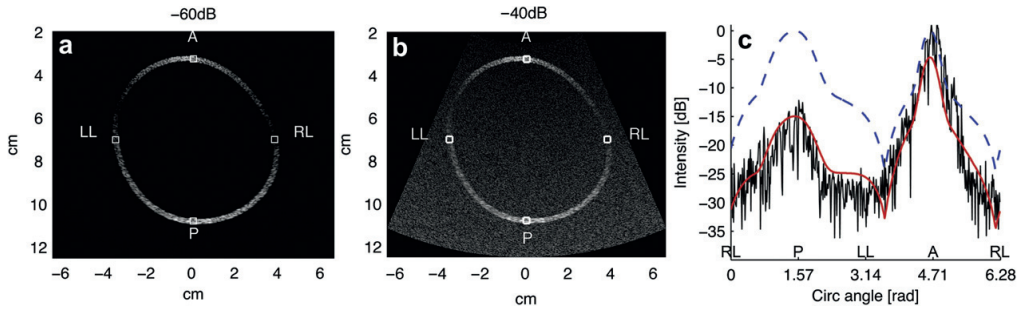

Fig. 5. Ultrasound simulation. (a) Simulated ultrasound image with noise −60 dB (b) noise −40 dB. (c) The intensity in the wall as a function of circumferential angle. The blue dashed curve shows intensity simulated according to eqn (5) while the solid red curve also includes absorption. The thin black curve is the intensity measured in a real ultrasound image (Fig. 2). The right lateral (RL), posterior (P), left lateral (LL) and anterior (A) regions-of-interest (ROIs) are indicated in each subplot.

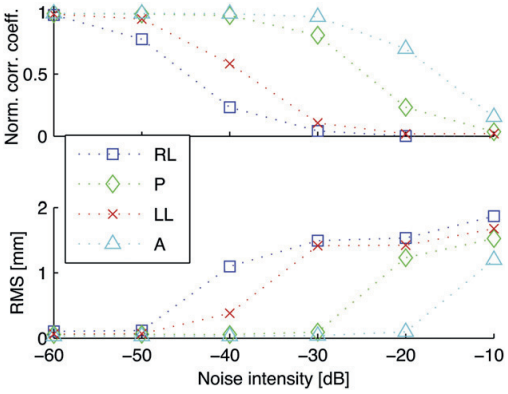

Fig. 6. Ultrasound images were simulated with different noise levels. Regions-of-interest (ROIs) (2 mm × 2 mm) were selected in the right lateral (RL), posterior (P), left lateral (LL) and anterior (A) wall (ref. Fig. 5). The upper panel shows the temporal mean value of the correlation coefficient calculated from frame to frame by using the known motion of the underlying scatterers. The lower panel shows the root-mean-square (RMS) difference between the tracked motion and the known true motion. The noise levels are relative to the highest possible intensity from the nonattenuated data. The data are mean values calculated over five different speckle realizations (random configuration of scatterers).

wall of the aneurysm was simulated, without thrombus or surrounding tissues. However, the intensity of the wall corresponded well. This is illustrated in Figure 5c by comparing the intensity of the wall from the real ultrasound image with the intensity theoretically predicted from eqn (5).

The temporal mean of normalized correlation coefficients were calculated and plotted as a function of different noise levels for ROIs in the right lateral (RL), posterior (P), left lateral (LL) and anterior (A) wall (Fig. 6). As expected, the correlation decreased with increasing noise. Due to different signal strength in the different parts of the wall (and therefore different SNR), the correlation was smallest in the lateral part and somewhat higher in the anterior part than in the posterior part. The tracking based on maximum correlation, therefore, failed for lower noise levels in the lateral wall than for the posterior and anterior wall, as illustrated by the RMS values in Figure 6.

The computation time depended linearly on the number of scatterers, the size of the imaging sector (*i.e.*, the number of samples) and the number of frames per cardiac cycle. For the aneurysm presented in this article, we simulated a blood pressure 155/85 mm Hg and heart rate of 103 bpm, imaged at 45 frames per second, resulting in 27 ultrasound frames over the cardiac cycle. The simulated imaging depth was 10 cm (2.5 cm–12.5 cm) and width was approximately 47 degrees, resulting in 361 beams and 2000 samples per beam. The simulation time was 38 s for the biomechanical simulation and 205 s for simulating the ultrasound images (*i.e.*, approximately a total of 4 min).

DISCUSSION

Before initiating clinical studies to investigate potential relations between ultrasound strain estimation and rupture risk in AAA, the quality of the strain estimation method should be assessed. In this article, we present a model for simulating dynamic ultrasound images of AAA, which may be used for this purpose.

The main advantage of a simulation model is that all parameters are known, thereby enabling direct comparison between estimated and true values. Also, parameters can be changed to test performance under different conditions. The disadvantage is that the model will not fully replicate true *in vivo* data and test results may, therefore, not be fully representative of the method's performance in clinical use. It is, therefore, reasonable to combine several means of evaluation, where a simulation model gives useful insight into specific aspects of the method to be evaluated.

To conveniently repeat simulations with different geometries and material properties, the simulation should be computationally fast. Computation time per cardiac cycle depended on the length of the cardiac cycle, frame rate and the size of the aneurysm (number of scatterers, beams and samples per beam). The patient-specific aneurysm shown in this article was simulated in approximately 4 min. Although it may be interesting to further optimize to achieve faster simulations, we considered the computation time obtained with the current implementation to be sufficient for our purpose.

Direction dependent reflections are prominent when imaging blood vessels by ultrasound, resulting in low signal from the lateral parts of the wall where the ultrasound beam is nearly tangential to the wall (see Fig. 2). Together with the acoustic noise from the abdominal wall and bowels, this leads to poor SNR in these parts of the images, making strain estimation especially challenging. This is, therefore, an important property that was well reproduced in the simulations (Fig. 5).

Only the wall was simulated, not including other organs, thrombus or surrounding tissues, which was a limitation because the identification of the wall is easier in the simulated images compared to real images. The simulation may, therefore, in some regard be a best-case scenario. However, except from immediate surroundings that may influence the local tracking, realistic simulation of the aneurysm wall is more important for evaluating tracking methods. Additional variations, *e.g.*, due to

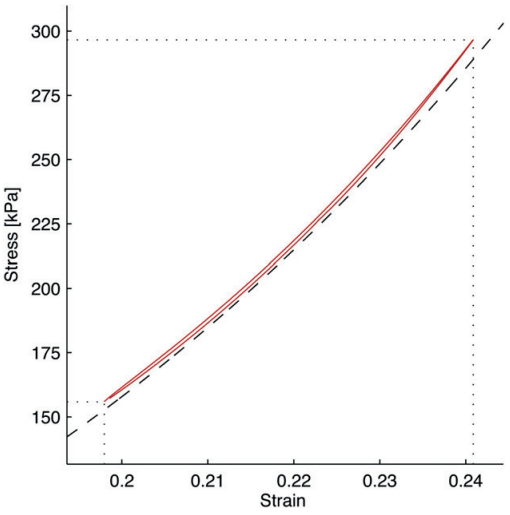

Fig. 7. Strain-stress relation for one element of a circular aneurysm with 5.5 cm diameter, 155/85 mm Hg blood pressure and heart rate 103 bpm. The solid curve shows the simulated response (with $\mu_0 = 8000$ Pa), including a small viscous effect (hysteresis). Diastolic and systolic stresses (156 kPa, 297 kPa) and strains (0.198, 0.241) are indicated. The model shows good agreement with a model suggested by Thubrikar et al. (2001) (dashed curve).

wall calcification, could be included in the model by altering the amplitude of scatterers in specific parts of the wall.

Because strain estimation is often based on speckle tracking, the simulation of a plausible speckle pattern is important. We chose to implement a fast simulation algorithm for producing fully developed speckle (Fig. 4). The algorithm produced a speckle pattern that was realistically correlated according to the motion of scatterers from frame to frame. Different SNRs were simulated by adding varying levels of Gaussian white noise. The noise levels in patients are varying, but the chosen range of -60 dB to -20 dB should represent extreme values to investigate at which noise levels a method fails, and to compare different tracking approaches for robustness to noise. Further research could include a more realistic simulation of acoustic artifacts to increase the realism of the simulated ultrasound. As shown in Figure 6, the simple maximum correlation tracking fails when the SNR in the different parts of the wall becomes too low. Regularization of the tracking according to physiologic constraints may increase the robustness of tracking with regard to noise. The simulation model could be used to optimize the size of ROIs and search areas and to test different regularization approaches. It is noted that the purpose of the implemented tracking method was to illustrate the potential evaluation by using the simulation model, rather than to evaluate or improve the tracking method itself.

Wall motion was simulated by assuming 1-D elements with nonlinear viscoelastic material properties. One-dimensional elements imply radially constant properties through the wall and were chosen because the wall is thin relative to the segment length, and because of lacking information of radial variation of parameters. Given the tubular thin wall structure, plane strain was assumed for the boundary conditions in the third dimension. Nonlinear (exponential) material models for AAA tissue have been suggested previously (*e.g.,* He and Roach 1994; Ragahavan et al. 1996; Thubrikar et al. 2001; Vande Geest et al. 2006). Because arterial tissue exhibits viscous properties, we also added a small viscous element to the material model, enabling *e.g.,* simulation of hysteresis. Figure 7 shows the simulated stress-strain relation of one element of a circular aneurysm of diameter 5.5 cm, with diastolic stress $\sigma_D = 156$ kPa and material parameters $\mu = 15$ and $\tilde{\mu} = 1000$Pa·s. The systolic wall stress was 297 kPa, which is consistent with values from literature on AAA wall stress simulation, *e.g.*, Fillinger et al. (2003), suggesting 440 kPa as a threshold for rupture prediction, and Raghavan et al. (2000) reporting peak wall stress among AAA patients from 290 kPa to 450 kPa. As illustrated in Figure 7, the model also shows good agreement with a model suggested by Thubrikar et al. (2001), based on *in vitro* strain-stress characterization of circumferentially oriented AAA tissue specimens. Additionally, *in vivo* ultrasound of stiffness, approximately corresponding to the parameter μ, has been reported to be in the order of 15–30 (Sonneson et al. 1999; Wilson et al. 2003).

The viscous effect means that the response of the model will depend not only on the amplitude but also on the rate of change of the blood pressure. Since the blood pressure profile may be affected by individual variations *e.g.*, due to age and presence of aneurysm, the response may change somewhat compared with the response when applying the profile described in this article. When evaluating tracking methods, it may, therefore, be interesting to apply different realistic or nonrealistic (*e.g.*, square or sinus) profiles to study potential effects on the performance of the tracking method.

Patient-specific simulations of AAA dynamics have previously been demonstrated based on three-dimensional (3-D) computed tomography (CT) scan to estimate parameters for predicting aneurysm rupture. These include fluid-structure interactions (FSI) simulating the motion of the wall when subject to pulsatile pressures (Di Martino et al. 2001; Wolters et al. 2005). Integration with an FSI model might be of interest for further research, especially to include out-of-plane motion and effects from surrounding

tissues and thrombus, and for investigating how the circumferential strain measure available from 2-D ultrasound corresponds to the underlying 3-D strain tensor.

Although only one example of AAA was shown in this article, the simulation model can be used for different patient specific or nonspecific AAA geometries or even for normal blood vessels by applying other geometries and material properties. The model could be used for investigating how different parameters, *e.g.*, frame rates, heart rates, blood pressures, noise-levels, geometries or stiffness affect the strain processing method.

In conclusion, we believe that the described model provides a simple and efficient first assessment of methods for ultrasound strain processing in AAA.

Acknowledgments—The work was funded by the Liaison Committee between the Central Norway Regional Health Authority and the Norwegian University of Science and Technology, SINTEF Department of Medical Technology and the National Center for 3-D Ultrasound in Surgery.

REFERENCES

Brekken R, Bang J, Ødegård A, Aasland JK, Hernes TAN, Myhre HO. Strain estimation in abdominal aortic aneurysms from 2-D ultrasound. Ultrasound Med Biol 2006;32:33–42.

Brewster DC, Cronenwett JL, Hallett JW Jr, Johnston KW, Krupski WC, Matsumura JS. Guidelines for the treatment of abdominal aortic aneurysms. Report of a subcommittee of the Joint Council of the American Association for Vascular Surgery and Society for Vascular Surgery. J Vasc Surg 2003;37:1106–1117.

Cobbold RSC. Foundations of biomedical ultrasound. New York: Oxford University Press; 2007:501.

Crosby J, Hergum T, Remme EW, Torp H. The effect of including myocardial anisotropy in simulated ultrasound images of the heart. IEEE Trans Ultrason Ferroelectr Freq Control 2009;56:326–333.

D'Hooge J, Rabben SI, Claus P, Irgens F, Thoen J, van de Werf F, Suetens P. A virtual environment for the evaluation, validation and optimization of strain and strain rate imaging. IEEE Symp Ultrason 2003;2:1839–1842.

Di Martino ES, Guadagni G, Fumero A, Ballerini G, Spirito R, Biglioli P, Redaelli A. Fluid-structure interaction within realistic three-dimensional models of the aneurysmatic aorta as a guidance to assess the risk of rupture of the aneurysm. Med Eng Phys 2001; 23:647–655.

Di Martino ES, Bohra A, Vande Geest JP, Gupta N, Makaroun MS, Vorp DA. Biomechanical properties of ruptured versus electively repaired abdominal aortic aneurysm wall tissue. J Vasc Surg 2006; 43:570–576.

Fillinger MF, Marra SP, Raghavan ML, Kennedy FB. Prediction of rupture risk in abdominal aortic aneurysm during observation: Wall stress versus diameter. J Vasc Surg 2003;37:724–732.

Gao H, Choi HF, Claus P, Boonen S, Jaecques S, Van Lenthe GH, Van der Perre G, Lauriks W, D'hooge J. A fast convolution-based methodology to simulate 2-D/3-D cardiac ultrasound images. IEEE Trans Ultrason Ferroelectr Freq Control 2009;56:404–409.

He CM, Roach MR. The composition and mechanical properties of abdominal aortic aneurysms. J Vasc Surg 1994;20:6–13.

Hergum T, Langeland S, Remme EW, Torp H. Fast ultrasound imaging simulation in K-space. IEEE Trans Ultrason Ferroelectr Freq Control 2009;56:1159–1167.

Maurice RL, Cloutier G, Ohayon J, Finet G. Adapting the Lagrangian speckle model estimator for endovascular elastography: Theory and validation with simulated radio-frequency data. J Acoust Soc Am 2004;116:1276–1286.

Phong BT. Illumination for computer generated pictures. J Commun ACM 1975;18:311–317.

Raghavan ML, Webster MW, Vorp DA. *Ex vivo* biomechanical behavior of abdominal aortic aneurysm: Assessment using a new mathematical model. Ann Biomed Eng 1996;24:573–582.

Raghavan ML, Vorp DA, Federle MP, Makaroun MS, Webster MW. Wall stress distribution on three-dimensionally reconstructed models of human abdominal aortic aneurysm. J Vasc Surg 2000; 31:760–769.

Remington JW, Wood EH. Formation of peripheral pulse contour in man. J Appl Physiol 1956;9:433–442.

Sonneson B, Sandgren T, Länne T. Abdominal aortic aneurysm wall mechanics and their relation to risk of rupture. Eur J Vasc Endovasc Surg 1999;18:487–493.

Swillens A, Løvstakken L, Kips J, Torp H, Segers P. Ultrasound simulation of complex flow velocity fields based on computational fluid dynamics. IEEE Trans Ultrason Ferroelectr Freq Control 2009;56: 546–556.

Thubrikar MJ, Labrosse M, Robicsek F, Al-Soudi J, Fowler B. Mechanical properties of abdominal aortic aneurysm wall. J Med Eng Techn 2001;25:133–142.

Vande Geest JP, Sacks MS, Vorp DA. The effects of aneurysm on the biaxial mechanical behavior of human abdominal aorta. J Biomech 2006;39:1324–1334.

Wilson KA, Lee AJ, Hoskins PR, Fowkes FG, Ruckley CV, Bradbury AW. The relationship between aortic distensibility and rupture of infrarenal abdominal aortic aneurysm. J Vasc Surg 2003;37:112–117.

Wolters BJBM, Rutten MCM, Schurink GWH, Kose U, de Hart J, van de Vosse FN. A patient-specific computational model of fluid–structure interaction in abdominal aortic aneurysms. Med Eng Phys 2005;27: 871–883.

APPENDIX

The aneurysm wall was modeled as one-dimensional (1-D) nonlinear viscoelastic elements connected at nodes. The force acting at each node was modeled as the sum of a blood pressure force F_p acting on the neighboring elements, and viscoelastic forces F_{ve} due to stretching of the elements (Fig. 2). Denoting mass m and acceleration a gives

$$m \cdot \vec{a} = \vec{F}_p + \vec{F}_{ve+} + \vec{F}_{ve-} \tag{A1}$$

In addition, the wall was constrained to return to the initial shape and position after a full cardiac cycle by adding an external force F_{ext} to eqn (A1).

$$\vec{F}_{ext} = -\left(\vec{F}_p + \vec{F}_{ve+} + \vec{F}_{ve-}\right)\Big|_{t=t^*} + T_{rbm} \tag{A2}$$

The first part represents a temporally constant, spatially varying force constraining the aneurysm to return to the initial shape after a cardiac cycle. It was defined by assuming equilibrium of eqn (A1) at a time t_*. T_{rbm} is a temporally varying transformation applied to exclude rigid body motion. The transformation was applied to all nodes and did, therefore, not influence the internal forces of the aneurysm wall. By applying other transformations, rigid body motion due to breathing and probe motion could be included in the simulation.

With initial positions given and assuming zero initial velocity in diastole, the dynamic positions of the nodes were found by temporal discretization and integration of eqns (A1) and (A2). As each node moves, the length of each segment changes continuously and the viscoelastic forces change correspondingly. Instead of assuming constant acceleration within each timestep Δt, we, therefore, chose a linearly varying acceleration

$$\hat{a}(t_n+u) = a(t_n)+\hat{\beta}\cdot u, \quad u \in [0, t_{n+1}-t_n = \Delta t] \tag{A3}$$

This acceleration predicts virtual positions $\underline{P}$ of the nodes in the next timestep

$$\underline{P}(t_{n+1}) = \underline{P}(t_n)+v(t_n)\cdot\Delta t+\frac{1}{2}a(t_n)\cdot\Delta t^2+\frac{1}{6}\hat{\beta}\cdot\Delta t^3 \tag{A4}$$

We chose to use $\Delta t \approx 30\ \mu s$. This value could be increased to save some computation time (*e.g.*, increasing Δt to 90 μs reduced computation time from 38 s to 22 s), but may compromise robustness for some combinations of geometry, material properties and blood pressures. From these predicted positions, the length of each segment was calculated. Wall stress was then calculated from eqn (4). With known blood pressures, the resulting forces and thus acceleration $a^*(t_{n+1})$ was calculated from eqns (A1) and (A2), and compared with the acceleration $\hat{a}(t_{n+1})$ predicted using eqn (A3). The calculations were run iteratively until $|\hat{a}(t_{n+1})-a^*(t_{n+1})|<\Delta$ (approaching zero), while updating

$$\hat{\beta} = \frac{a^*(t_{n+1})-a(t_n)}{t_{n+1}-t_n} \tag{A5}$$

Appendix: Ultrasound in AAA

7

Ultrasound in Abdominal Aortic Aneurysm

Reidar Brekken[1,2], Torbjørn Dahl[1,3] and Toril A. N. Hernes[1,2]
[1]*Norwegian University of Science and Technology, Dept. Circulation and Medical Imaging*
[2]*SINTEF, Dept. Medical Technology*
[3]*St. Olav's Hospital, The University Hospital of Trondheim*
Norway

1. Introduction

Formation and growth of abdominal aortic aneurysms (AAA) may lead to rupture resulting in life threatening haemorrhage. Elective treatment of asymptomatic AAA, either as open surgery or endovascular repair, is recommended when the maximum diameter of the aneurysm exceeds 50-55mm or increases rapidly (Brewster et al., 2003), whereas smaller aneurysms are recommended kept under surveillance. Risk factor modification, such as cessation of smoking, treatment of hypertension and pharmaceutical inhibition of inflammation and protease, could reduce growth in aneurysms kept under surveillance (Baxter et al., 2008; Chaikof et al., 2009; Moll et al., 2011).
The size and growth of the aneurysm is monitored using different radiological imaging modalities. Imaging is also important during image guided endovascular repair, and in follow-up examinations after treatment. In this chapter, we describe how ultrasound is currently used in management of abdominal aortic aneurysm, and discuss future potential and challenges of ultrasound for assisting in improved clinical management with regard to patient selection, treatment alternatives and follow-up.

2. Ultrasound

Ultrasound does not depend on ionizing radiation, and it is relatively inexpensive compared with other imaging modalities. Ultrasound equipment is also portable, and can be used both bedside as well as outside of hospitals. Ultrasound is a fast imaging modality, and presents images in real-time. Therefore, in addition to imaging anatomical structures, ultrasound can also be used for studying function by investigating blood flow or organ motion, e.g. dynamics of the heart. Being a real-time imaging modality, ultrasound further provides an opportunity to interactively investigate the anatomy and potential pathologies. Ultrasound has a certain operator dependency; specifically that it requires skills both to obtain good images, and to interpret the images. Also, in some cases, the image quality suffers from limited view due to bowel gas or obesity. Practical training and knowledge of principles and artefacts is therefore beneficial for successful application of ultrasound.
The physical foundation for medical ultrasound is high frequency waves that are transmitted into the body. The waves are reflected from structures within the body, and the echoes are analysed for retrieving diagnostic information. **Structural imaging** was first obtained using amplitude (A) mode, directly visualizing the amplitude of the echo as a

function of depth. Brightness (B)-line displays the amplitudes as grayscale values. In motion (M) mode imaging, several B-lines in the same direction are drawn consecutively as a function of time for examination of dynamical properties. By combining spatially adjacent B-lines, two-dimensional (2D) B-mode images are obtained and can be visualized in real time. More recently, new ultrasound probes and visualization techniques have made three-dimensional (3D) imaging of anatomical structures possible. 3D images (or volumes) are obtained either by mechanically sweeping the scanplane in the elevation direction to cover a 3D sector, or in real-time by steering the ultrasound beam in 3D using 2D transducer arrays.

In addition to structural imaging, ultrasound can be used for extracting information about function. One example is imaging of blood flow. The **Doppler** effect can be measured with ultrasound to quantify the velocity of blood and moving tissue. In short, the Doppler effect refers to a shift in frequency of a signal that is transmitted (or reflected) from a moving object. The frequency shift is proportional to the velocity of the moving object. By detecting the shift in frequency content of a reflected ultrasound signal relative to the transmitted signal, the velocity of the moving object can therefore be estimated. The velocity information can be presented either by visualizing the Doppler frequency spectrum as a function of time, or by visualizing the velocity as a colour-coded overlay on the B-mode image (Colour Doppler or Duplex imaging). Another example of functional imaging is **strain imaging or elastography**, which displays a quantitative measure of the response of tissues under compression (Garra, 2007; Ophir et al., 1991). The compression can be due to natural motion, e.g. heart contractions or pulsating arteries, or enforced by an external compression, e.g. movement of the ultrasound probe. The ultrasound pulse itself can also be used for enforcing compression, in which case the method is often referred to as artificial radiation force imaging (ARFI) (Nightingale et al., 2002). Clinical applications of strain imaging and elastography include assessment of left ventricular myocardial function, and differentiation of stiff tumours from surrounding normal tissues. Examples of B-mode and colour Doppler images of an abdominal aorta are shown in Fig. 1.

For some applications, it is beneficial to use contrast imaging by injecting **contrast agents** (microbubbles) in the blood to increase the echo obtained from blood. The microbubbles respond differently than human tissue under influence of the ultrasound pulse, thus allowing for specialized detection methods separating the contrast agents from surrounding tissues (Frinking et al., 2000; Hansen & Angelsen, 2009). Contrast agents may provide better images of the ventricles of the heart and larger blood vessels as well as visualization of microcirculation, which is interesting for detection of e.g. myocardial perfusion (Lindner et al., 2000). Targeted microbubbles that attach to specific molecular signatures may provide new possibilities for diagnosis of various diseases, e.g. tumours or atherosclerosis (Anderson et al., 2011; ten Kate et al., 2010).

Ultrasound is most commonly used for diagnostic purposes, but may also be used therapeutically. One application is ultrasound imaging for guidance during surgery, biopsy or needle insertion. Another therapeutic use of ultrasound is **high intensity focused ultrasound (HIFU)**, exploiting that ultrasound, being mechanical waves, can be used for focused delivery of high energies. Sonic waves (extracorporeal shock wave lithotripsy) can be used for destruction of kidney stones (Gallucci et al., 2001). Other applications include focused ultrasound surgery (FUS), thrombolysis and hemostasis (Kim et al., 2008; Vaezy et al., 2001). Burgess et al. (2007) reported HIFU for hemostasis in the posterior liver of 17 pigs. The probe was placed on the anterior surface of the liver and aimed at the bleeding. 17 became hemostatic, whereas 7 controls (sham-HIFU) did not become hemostatic, illustrating

the potential of HIFU as a pro-coagulant. Local treatment of various diseases may be possible by using nanotechnology for producing targeted microbubbles, which may be loaded with drugs or genes. The microbubbles can be monitored by ultrasound and destructed for local drug release. Bio-effects of the destruction can be used for disrupting cell membranes for killing malicious cells, or for increased drug uptake.

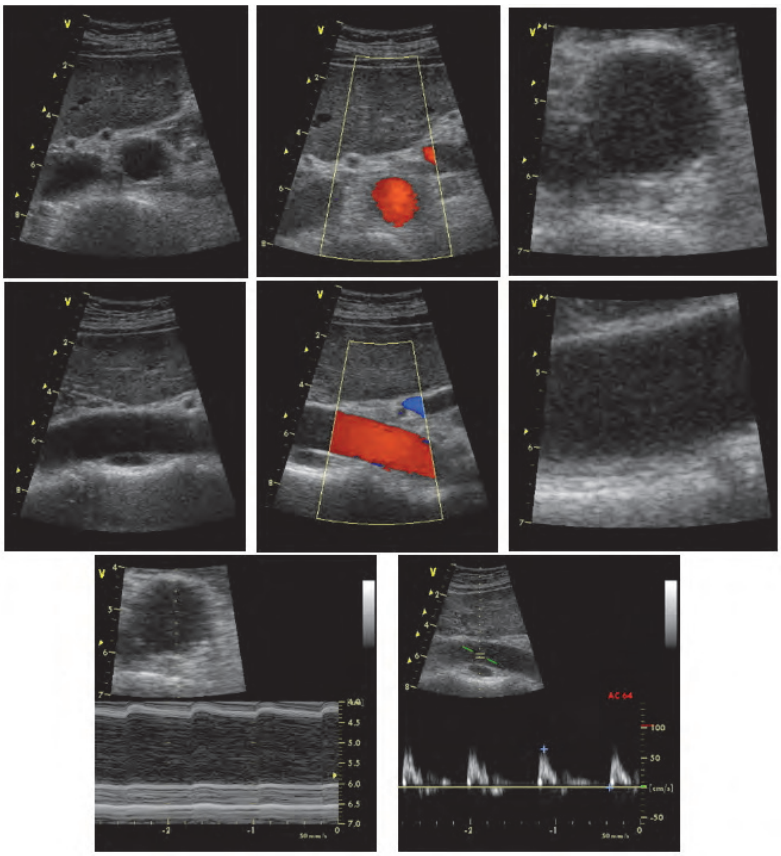

Fig. 1. Ultrasound images of abdominal aorta. Upper row: Cross-sectional view, 2D B-mode, colour Doppler (duplex) and zoomed B-mode image, respectively. Mid row: Same as upper row, but with longitudinal view. Lower row: M-mode (left) and Doppler velocity spectrum.

3. Ultrasound in AAA management

Use of ultrasound in the management of AAA was reported in the late 1960ies. Segal et al. (1966) published a case report of ultrasound for detection and size measurement of an AAA, and Goldberg et al. (1966) investigated 10 normal and 10 aneurysmal aortas. It was recognized that ultrasound could be used for detection of AAA, determination of size and monitoring of growth. During the following decade, several reports demonstrated favourable results for ultrasound in assessment of AAA, including analysis of pulsation,

detection of aneurysms, measurement of diameter and amount of thrombus (Brewster et al., 1977; Hassani & Bard, 1974; Lee et al., 1975; McGregor et al., 1975; Mulder et al., 1973; Wheeler et al., 1976; Winsberg & Cole, 1972). Bernstein et al. (1976) used ultrasound for studying growth rates of small AAA. During the recent decades, ultrasound has been dramatically improved through development of new technology and processing methods assisting in improved patient management in several clinical areas. We present an overview of the current clinical use, and discuss potential future use related to ultrasound in detection and monitoring of AAA, prediction of growth and rupture, and treatment and follow-up.

3.1 Detection and monitoring

AAA is most often asymptomatic until rupture, and coincidentally detected during examination for other diseases. Ultrasound has been recommended for detection of AAA in symptomatic patients and for asymptomatic patients in risk groups. A number of studies suggest that population screening reduces AAA mortality in subgroups with increased AAA susceptibility (Cosford & Leng, 2007; Ferket et al., 2011; Takagi et al., 2010). Screening may still represent an ethical dilemma because growth and rupture is difficult to predict, and it is therefore disputable when to recommend repair on a patient-specific basis, considering the risk involved in surgical or endovascular treatment.

High degree of validity of ultrasound for detection of AAA has been reported. Numbers indicate a sensitivity and specificity of almost 100% (Cosford & Leng, 2007; Lindholt et al., 1999). The accuracy and operator dependencies of size measurements are especially important in order to reliably monitor growth. Fig. 2 shows cross-sectional and longitudinal images of AAA. Singh et al. (1998) reported intra- and inter-observer variability less than 4mm, and concluded that maximal diameter could be measured by ultrasound with high degree of accuracy. Also Thomas et al. (1994) concluded that ultrasound diameter measurements were reproducible between ultrasonographers. However, compared to measurements from X-ray computed tomography (CT), ultrasound was found to consistently give lower values for maximum AAA diameter, with a mean underestimation of 4.4mm. Similar results were reported using duplex ultrasound (Dalainas et al., 2006; Manning et al., 2009). Sprouse et al. (2004) suggested that ultrasound is more accurate than axial CT in determining the true perpendicular diameter. This was based on use of orthogonally reconstructed CT, which varied insignificantly from US, while axial CT overestimated the diameter when the aortic angulation was high. It has also been noted that the variation using internal or external wall diameter would give discrepancies of 5-6mm (Thapar et al., 2010). It is important that measurements be carried out consistently, and being aware of differences between imaging modalities compared to evidence from different clinical trials (Lederle et al., 1995). When care is taken to adjust the critical limits for intervention for a modality, reproducibility is the most important characteristic.

Detection of AAA in emergencies

Emergency ultrasound is becoming more widespread as the development in ultrasound technology provides more portable and even handheld ultrasound scanners at an affordable cost. Ultrasound can be used bedside or in the ambulance for fast examination and early decision making. This development has a potential for reducing AAA mortality by early detection of ruptured (or otherwise symptomatic) aneurysms, allowing early surgery without having to use time for additional examinations in the emergency entrance. Sebesta et al. (1998) investigated the importance of fast treatment of ruptured aneurysms by

studying 103 patients with ruptured AAA. They concluded that "delay in surgical treatment caused both by time consuming confirmative evaluation and patient's lengthy transfers is responsible for ominous protraction of the original shock". Further, renal failure was found to be a leading cause of postoperative mortality. In combination with hemorrhagic shock, it should be considered that X-ray contrast material cause additional burden to renal function.

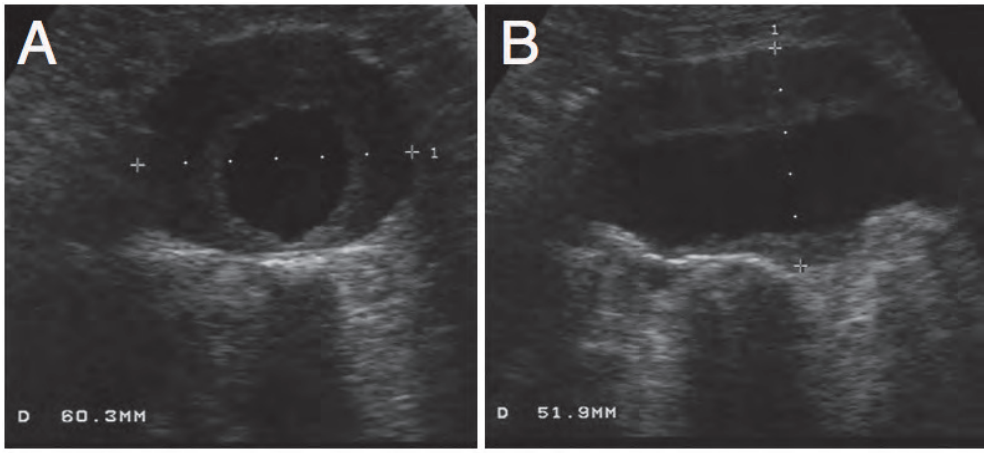

Fig. 2. Ultrasound images of AAA. Cross-sectional (A) and longitudinal (B) views. Courtesy of Asbjørn Ødegård, St. Olav's Hospital, Trondheim, Norway.

The sensitivity and specificity of detection of AAA in emergency medicine ultrasound is almost 100% (Kuhn et al., 2000). With appropriate training, emergency residents accurately determine both presence as well as size of AAA (Bentz & Jones, 2006; Costantino et al., 2005). Hoffmann et al. (2010) concluded that more experienced emergency department sonographers perform better in detecting aneurysms, and suggested training on more than 25 cases, including technically difficult cases, for credentialing personnel for the process. Although rupture of AAA could be indirectly diagnosed from clinical signs and symptoms and presence of an aneurysm, B-mode ultrasound can also reveal direct and indirect signs of rupture (Catalano & Siani, 2005a). Also, Catalano et al. (2005b) further examined 8 ruptured AAA using contrast-enhanced ultrasound, concluding that contrast-enhanced ultrasound may be as effective as CT in detecting rupture, and does not delay surgery significantly. Further considerations on AAA emergency ultrasound can be found in Reardon et al. (2008). The appearance of rupture in different modes of ultrasound images is shown in Fig. 3.

3.2 Prediction of growth and rupture

The validity of aneurysm size and growth as prognostic parameters has been questioned. Specifically, rupture does occur in aneurysm with diameter less than 5 to 5.5 cm, while on the other hand, several aneurysms with diameter larger than 5.5 cm are observed without rupture. Brewster et al. (2003) summarized findings from several studies, and estimated annual rupture risk versus size to be 0% (<4cm), 0.5-5% (4-5cm), 3-15% (5-6cm), 10-20% (6-7cm), 20-40% (7-8cm) and 30-50% (>8cm). Women appeared to have higher risk of rupture for a given diameter. These population-based values should be balanced against the expected risk associated with repair to determine appropriate time for intervention.

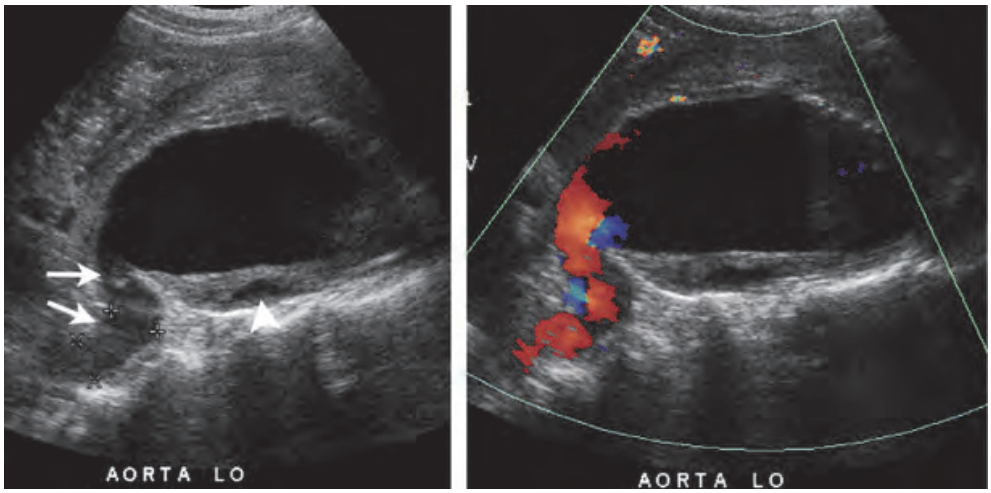

Fig. 3. Ultrasonic appearance of rupture. Left: Longitudinal B-mode image demonstrating a "tubular hypoechoic structure (arrows), which is continuous with the lumen of the aneurysm sac". The hypoechoic area in the thrombus (arrowhead) is a sign of aortic wall rupture. Right: Corresponding duplex image demonstrating an active bleeding. *In Bhatt et al. (2007), used with permission.*

Although diameter is currently the dominating population based indicator of rupture risk, additional indicators are warranted to predict rupture on an individual level. Improved patient specific assessment of rupture risk would provide better patient selection and reduce harm to patients as well as reducing societal cost. In a study by Hafez et al. (2008), 4308 patients were followed for research purpose after ultrasound screening showing a normal aorta. 3.9% (166/4308) were found to later develop AAA. Improved prediction of growth and rupture (prognostic monitoring) would 1) reduce the number of unnecessary examinations and interventions, and 2) make screening programs more favourable. Both would contribute to reduce AAA mortality.

Substantial efforts have been devoted to improved selection of patients for AAA repair through systematic assessment of risk factors of AAA growth and rupture, as well as individualized risk associated with repair. In this text, we will focus on image-based assessment of growth and rupture risk, specifically ultrasound imaging. Several groups have for more than a decade developed increasingly sophisticated numerical simulation tools for analysing the mechanical state of aneurysms, based on patient specific geometries. By applying solid-state stress analysis, Fillinger et al. (2003) found that peak wall stress was a better predictor of rupture than was maximum diameter. Further details on biomechanical analysis of AAA can be found in e.g. the reviews by Malkawi et al. (2010) and Vorp (2007).

Patient specific geometries applied for numerical analysis are most often based on CT, which is easily obtainable for AAA patients, and gives a good representation of the full 3D geometry of the aneurysm and blood vessels. Ultrasound imaging may be beneficial for early and consecutive measurements (i.e. screening/ detection and repeated monitoring). Real time 3D ultrasound imaging is used in cardiology, but gives a limited sector, and is not yet adapted to abdominal imaging. A possible alternative would be to obtain 3D volume by reconstruction of 2D ultrasound slices acquired with position tracking (Solberg et al., 2007).

An interesting application of ultrasound in analysis of AAA mechanics is due to the dynamical properties of ultrasound. Ultrasound is a fast imaging modality, which makes it possible to study the dynamical behaviour of the aneurysm when exposed to the blood pulse. Imura et al. (1986) presented a method using ultrasound for tracking the dynamic diameter of the abdominal aorta over the cardiac cycle in order to quantify the elastic properties of human abdominal aorta in vivo.

Analysis of the dynamical properties of the AAA may be motivated by the association between evolution of aneurysms and alteration of the elastic properties of the vessel wall. This alteration has been linked to matrix-metalloproteinase (MMP) activity (Freestone et al., 1995). It has been suggested that growth is associated with degradation of elastin, whereas rupture may be caused by degradation of collagen (Petersen et al., 2002). Consistent with this, it has been shown that aneurysm tissue is stiffer than normal tissue, but that softer aneurysm tissue is more prone to rupture than stiff aneurysm tissue (Di Martino et al., 2006).

Several authors have used ultrasound to study the elastic properties of AAA by tracking dynamical change in diameter over the cardiac cycle, and obtained interesting, but to some extent diverging, results. Wilson et al. (1998) reported results that might support the hypothesis of aneurysms being stiffer than normal tissue, while less stiff aneurysms may be more prone to rupture. Later studies reported that large aneurysms tended to be stiffer than smaller, but with large variations for equally sized aneurysms (Wilson et al., 1999), and that increased distensibility over time (compared to baseline) indicated significantly reduced time to rupture (Wilson et al., 2003). However, Long et al. (2005) used tissue Doppler imaging, and reported a trend toward increased distensibility with increased AAA diameter. Ultrasonic tracking of diameter has demonstrated that the aorta is stiffer in men than age-matched women, that stiffness increases with age, and that aneurysm tissue is much stiffer than normal aorta (Länne et al., 1992; Sonesson et al., 1993). However, Sonesson et al. (1999) studied 285 AAA patients and found no difference in "aneurysmal aortic wall mechanics in those AAAs that subsequently ruptured compared with electively operated AAAs. The results indicate that it is not possible to use aneurysmal aortic wall stiffness as a predictor of rupture."

Measuring the dynamical change in diameter over the cardiac cycle gives a stiffness measure representing an average over the cross section of the aneurysm wall. The mechanical properties of the wall are however known to vary heterogeneously over the wall (Thubrikar et al., 2001). Ultrasound strain imaging estimates local deformation of tissue due to applied load, and may therefore have a potential for better assessment and characterization of the local properties of the wall. In a study by Brekken et al. (2006), 2D cross-sectional ultrasound data with high frame rate (~40-50 fps, depending on the size of the aneurysm) was used to derive patient-specific information about in-vivo elastic properties of the aneurysm wall of 10 patients. For each dataset, points were semi-automatically selected along the aneurysm circumference in one ultrasound image. These points were then automatically traced over the cardiac cycle. A measure of cyclic circumferential strain was estimated by calculating the time varying distance between the points relative to the initial (diastolic) distance. (Fig. 4.) The preliminary patient study showed that the strain values were inhomogeneous along the circumference, thus indicating that additional information could be obtained as compared to maximum diameter alone. Further clinical trials are necessary to investigate the method's potential for improved prediction of growth and rupture.

In addition to potentially carry clinically relevant information in itself, the strain estimates could be integrated with computational methods to contribute to more patient specific analysis of wall stress. In order to relate the strain estimates to the geometry of the

aneurysm, and hence relate to biomechanical simulations based on 3D geometries, Brekken et al. (2007) reported attachment of a positioning sensor to the ultrasound probe for placing the ultrasound cross-section in a 3D space. The ultrasound data were then registered to CT data from the same patient, and strain was visualized together with the 3D geometry segmented from the CT data. (Fig. 5.) This allows for direct comparison of ultrasound based strain measurements with biomechanical simulations, and opens for more patient specific simulations by including elasticity measures from ultrasound.

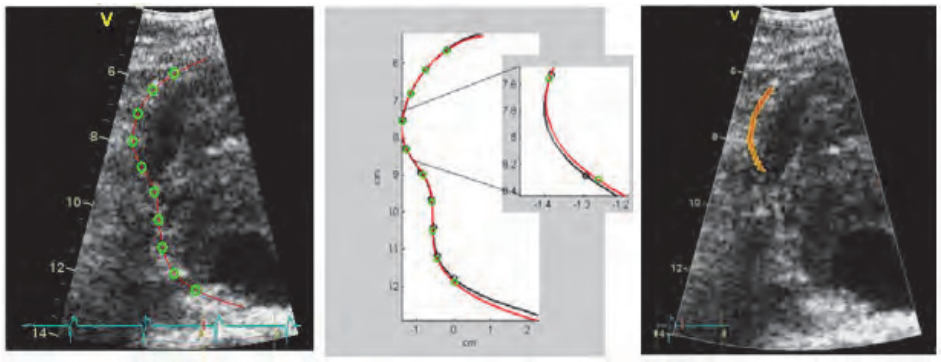

Fig. 4. Strain processing and ultrasound strain. Left: The aneurysm wall is manually identified (red line). A number of points (green) are placed equidistantly along the curve, and automatically traced over the cardiac cycle. Mid: Illustrating the points in diastole and systole. Right: Colour-coded strain in systole relative to diastole. It is noted that one part of the wall experiences elevated cyclic strain. *In Brekken et al. (2006), used with permission.*

Future research should be aimed at investigation also of longitudinal strain, and eventually estimation of full 3D strain, e.g. by developing probes and methods for 3D ultrasound acquisition and analysis. Also, low signal-to-noise ratio in abdominal ultrasound images reduces accuracy of tracking and thus strain estimation. Methods for noise reduction should therefore be explored. In addition, use of ultrasound Doppler for blood velocity estimation could provide further information to be used as input to patient specific simulations.

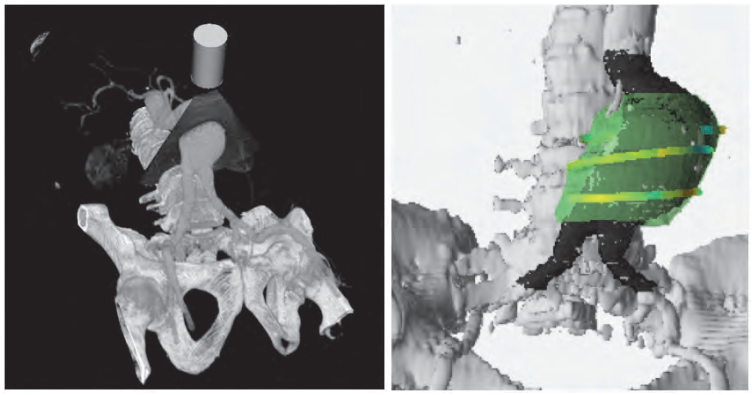

Fig. 5. Left: CT and ultrasound in the same scene. Right: 3D visualization of strain. *In Brekken et al. (2007), used with permission.*

3.3 Endovascular treatment and follow-up

Ultrasound in endovascular treatment

Radiological imaging is used in pre-operative planning of endovascular aneurysm repair (EVAR) and for intra-operative guidance and control. In pre-operative planning, imaging is used to get a measure of the 3D anatomy for investigating eligibility of EVAR and for choosing or customizing stentgrafts. A common imaging modality for this purpose is CT angiography (Broeders & Blankensteijn, 1999). CT has the advantage of visualizing the entire anatomical area of interest. Transabdominal 3D ultrasound offers only a limited sector, and, in addition, parts of the relevant anatomy will be obscured by acoustical shadows or absorption.

Some of these challenges are avoided in intravascular ultrasound (IVUS). IVUS has been used for pre-operative planning in combination with CT, for guidance and for control after device placement. (Fig. 6.) Several authors have concluded that IVUS gave accurate and reproducible measurements of the geometry of the aneurysm, and assisted in correct selection of stentgraft or final correction of stentgraft diameter or length. IVUS further assisted in rapid identification of fixation sites, and assessment of accuracy and patency of device placement (Eriksson et al., 2009; Garret et al., 2003; Tutein et al., 2000; van Essen et al., 1999; White et al., 1997; Zanchetta et al., 2003).

Ultrasound guidance during minimally invasive therapy has been reported and is in regular use within some clinical applications. Especially within neurosurgery ultrasound has been found beneficial for intra-operative imaging (Unsgaard et al., 2011). Intra-operative guidance during EVAR is usually performed with X-ray fluoroscopy. Both intraoperative CT (Dijkstra et al., 2011) as well as fluoroscopy in combination with navigation using electromagnetic sensors (Manstad-Hulaas et al., 2007) has been investigated for guiding insertion of fenestrated grafts. Some investigators have also reported transabdominal ultrasound for guidance of EVAR. Lie et al. (1997) studied the use of 2D transabdominal ultrasound during EVAR. They found that ultrasound could be useful for guiding the insertion of guidewire and control the wire position before connecting second graft limb to the main limb of bifurcated grafts (Fig. 6.). Kaspersen et al. (2003) reported a feasibility study registering ultrasound acquired during EVAR to pre-acquired CT data. This may be useful for updating the CT data used for navigation due to e.g. respiratory motion and deformation of the blood vessels during the procedure. With recent advances in ultrasound technology, we believe that real-time 3D ultrasound has potential for further advancing insertion of stentgraft, especially delivery of fenestrated stentgrafts. Specifically, it is easier to track e.g. the tip of guidewires in 3D, while simultaneously visualizing a focused area of the 3D anatomy in real-time, perhaps in combination with CT. Contrast-enhanced ultrasound has also been used intraoperatively for localization of fixation sites and identification of endoleaks (Kopp et al., 2010). The fixation sites were visualized in >80% of the 17 patients investigated with contrast-enhanced ultrasound, and more endoleaks were detected than with conventional EVAR. It was noted that ultrasound was especially beneficial in case of patients with contraindications for usage of X-ray contrast material.

Percutaneous EVAR, i.e. minimally invasive femoral access, is an alternative to open femoral access. A systematic review by Malkawi et al. (2010) concluded that percutaneous EVAR was associated with fewer access related complications and reduced operating time. In a study by Arthurs et al. (2008), it was shown that use of ultrasound guided access significantly reduced access-related complications compared to percutanous access without

ultrasound guidance. Successful ultrasound guidance in secondary interventions, for sealing endoleak after EVAR, has also been reported. Boks et al. (2005) described transabdominal embolization using duplex ultrasound guidance, and Kasthuri et al. (2005) used ultrasound for guiding percutaneous thrombin injection.

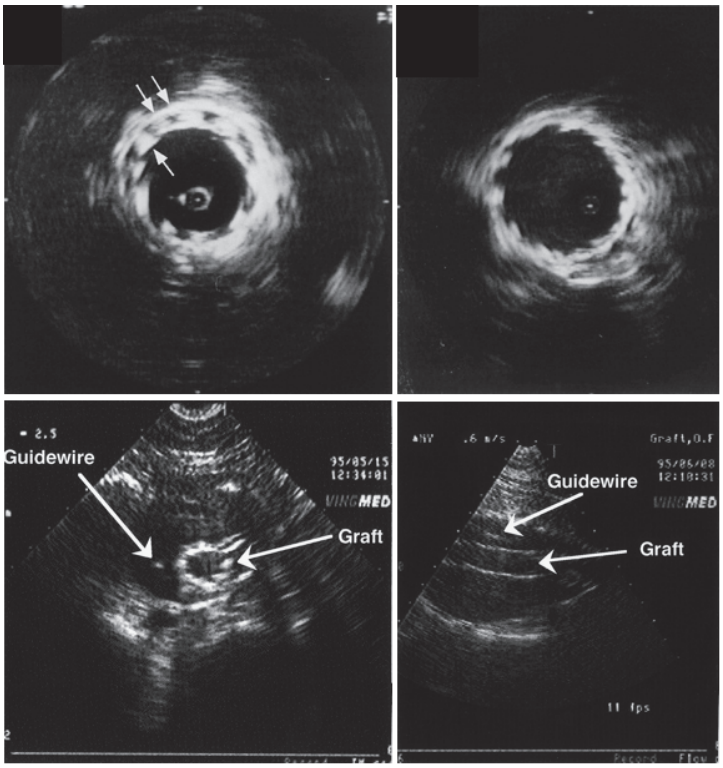

Fig. 6. Upper: IVUS during EVAR, left: incomplete stent expansion, right: stent correctly placed after additional dilation. *In White et al. (1995), used with permission*. Lower: Transabdominal ultrasound guidance during EVAR. Guidewire and stentgraft is visible inside the aneurysm. *In Lie et al. (1997), used with permission.*

Ultrasound in post-operative surveillance

Due to incidences of complications such as endoleak or continued growth after EVAR, it is necessary to conduct long-term follow-up. CT is in widespread use, but due to the repeated investigations, there is a significant radiation dose involved. Also, for some patients, the use of X-ray contrast material may cause allergic reactions or impair the renal function. Ultrasound has been suggested as an alternative that reduces these risks as well as the cost associated with follow-up of EVAR patients.

Several authors have investigated duplex ultrasound for detection of endoleak. In comparison with CT, duplex ultrasound is by some authors considered not to be sensitive or specific enough for replacing CT (Mirza et al., 2010; Sun, 2006). Other authors have found that duplex ultrasound may be sufficient in groups of patients, specifically those

with a stable aneurysm (Bargellini et al., 2009; Chaer et al., 2009; Nagre et al., 2011). Patel & Carpenter (2010) suggested that duplex ultrasound could be sufficient for long-term follow-up if the initial postoperative CT angiogaphy was normal. Collins et al. (2007) also compared duplex ultrasound with CT, and found that three endoleaks determined from CT could not be seen with ultrasound due to bowel gas, body habitus or hernia, whereas out of 41 endoleaks discovered by ultrasound, only 14 were visible on a CT scan. A number of studies have reported use of contrast-enhanced ultrasound for detection of endoleaks. Generally, it is considered to be more accurate than ultrasound without contrast, and similar to magnetic resonance imaging (MR) and CT (Cantisani et al., 2011; Iezzi et al., 2009; Mirza et al., 2010; Sun 2006). McWilliams et al. (2002) investigated 53 patients and found contrast enhanced ultrasound to be more sensitive than unenhanced ultrasound in detection of endoleak when compared to CT, but concluded that ultrasound (with or without contrast) was less reliable than CT. On the contrary, several other authors have concluded that contrast enhanced ultrasound may perform better than CT in detection of endoleak (Carrafiello et al., 2006; Clevert et al., 2008; Henao et al., 2006; Ten Bosch et al., 2010). Bakken & Illig (2010) presented a review summarizing use of ultrasound for detection of endoleak. They concluded that ultrasound was suitable for "monitoring the evolution of aneurysm sac post-EVAR and, in combination with endoleak evaluation, seems to provide follow-up comparable to CT and sufficient to identify complications requiring intervention". In addition to capture the majority of endoleaks, the authors suggested that ultrasound could also provide better characterization and localization of the endoleak than with CT. The sensitivity of ultrasound for endoleak detection is likely to be underestimated by comparing it to CT as the reference standard because some endoleaks are missed also by CT. Therefore, the validity of ultrasound for endoleak detection should ideally be tested against clinically relevant outcome measures rather than to CT. Operator dependency of ultrasound may be an additional cause for diverging results. The introduction of 3D ultrasound could provide simpler protocols for detection of endoleak, and reduce user dependency. Fig. 7 shows examples of endoleak appearance in duplex and contrast-enhanced ultrasound.

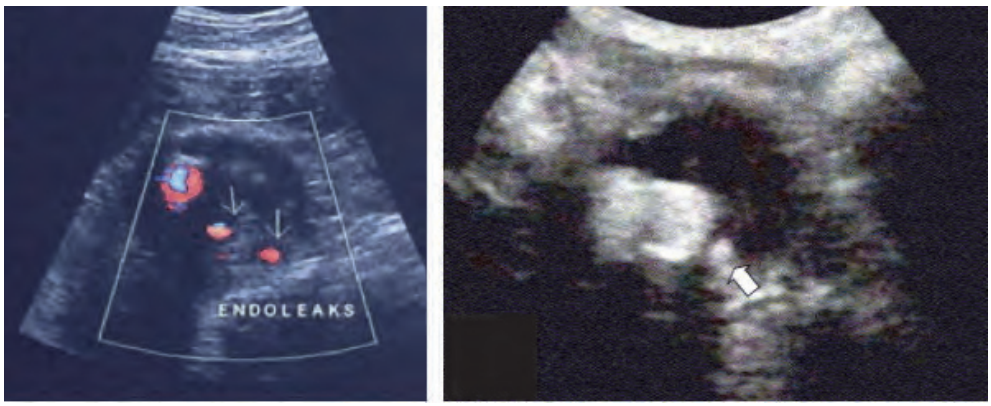

Fig. 7. Ultrasound for detection of endoleak. Left: Type II endoleaks with duplex ultrasound. *In Beeman et al. (2010), used with permission*. Right: Contrast-enhanced ultrasound illustrating flow inside the aneurysmal sac. *In Henao et al. (2006), used with permission*.

Another use of ultrasound in follow-up after EVAR is to study the pulsatile diameter. Malina et al. (1998) found that pulsatile wall motion was significantly reduced after EVAR as compared to before, and that endoleak was associated with smaller reduction. However, Lindblad et al. (2004) reported a similar study with more patients, and concluded that the reduction in pulsatile motion was not significantly different in the presence of endoleak. Using the ultrasound strain method previously described, Brekken et al. (2008) measured strain before and after insertion of stentgraft, confirming that the method detected a reduction in strain after endovascular repair. Pulsatility was observed after EVAR, and the strain values were heterogeneous along the circumference also after EVAR. It remains to investigate if the method is sensitive and accurate enough for detecting possible changes due to endoleak. Also, some aneurysms continue to grow without evidence of endoleak (Gilling-Smith et al., 2000). It is uncertain whether this is because of imaging modalities not being sensitive enough to detect all endoleaks, or other reasons. Therefore, in addition to monitor size, it is worth investigating if ultrasound strain could be used to predict growth or rupture, with or without endoleak, during follow-up after endovascular repair.

3.4 Functional and molecular imaging

The main pathophysiological mechanisms in development and progression of AAA are inflammation, proteolysis and apoptosis (Zankl et al., 2007). As these mechanisms and their role in AAA become more clear, new alternatives for detection, risk prediction and treatment may become available.

Compared to traditional imaging modalities, there is a need for alternative imaging to investigate pathophysiological mechanisms in-vivo, which could eventually identify high risk patients and monitor results of treatment. Hong et al. (2010) reviewed different modalities for imaging of AAA. They classified the modalities into anatomical, functional and molecular imaging. Anatomical imaging displays the structure of organs, whereas functional imaging can reveal physiological activities by detecting "changes in the metabolism, blood flow, regional chemical composition and absorption". Molecular imaging "introduces molecular agents (probes) to determine the expression of indicative molecular markers at different stages of disease." Functional and molecular imaging may be performed using SPECT, optical imaging and PET in combination with the appropriate contrast agents.

In addition to imaging functional properties using ultrasound Doppler or strain imaging, the use of ultrasound contrast agents constitutes a research area of great interest for imaging both functional and molecular properties. By injection of microbubbles in the blood stream, microcirculation has been imaged for investigation of myocardial perfusion and detection of neovascularization in relation to tumours and atherosclerosis (Fig. 8). (Anderson et al., 2011; Lindner et al., 2000 ; ten Kate et al., 2010). Staub et al. (2010a) demonstrated that adventitial vasa vasorum and plaque neovascularization of the carotid artery correlated with cardiovascular disease and past cardiovascular events using contrast-enhanced ultrasound in a retrospective study of 147 patients. Neovascularization or angiogenesis is also found in relation to AAA (Herron et al., 1991; Holmes et al., 1995; Thompson et al., 1996). Choke et al. (2006) found that rupture of AAA was associated with increased medial neovascularization. Assessment of neovascularization by contrast enhanced ultrasound may therefore have a significant potential for assisting in more accurate prediction of rupture.

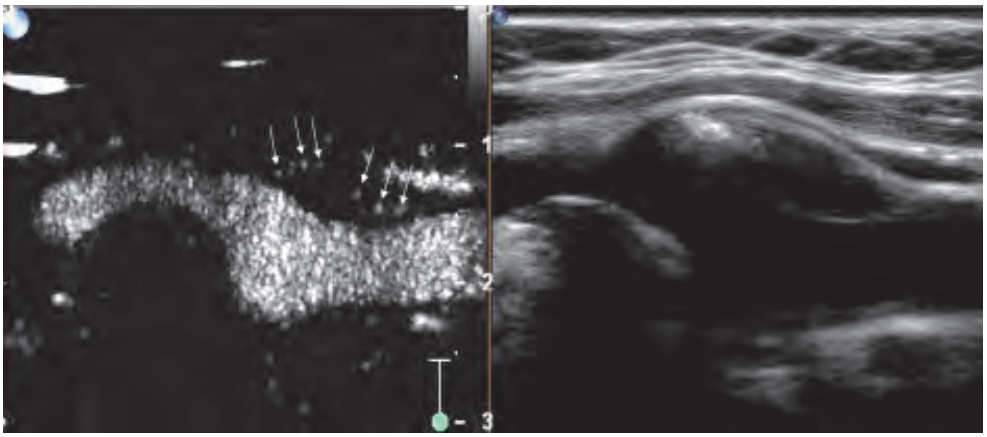

Fig. 8. Left: Contrast-enhanced ultrasound showing neovascularization in carotid artery plaque. Microbubbles within the plaque are indicated by arrows. Right: Corresponding B-mode ultrasound image without contrast. *In Staub et al. (2010b), used with permission.*

With recent advances in nanotechnology (nanomedicine), it is possible to produce targeted contrast agents, which connect to specific receptors. Due to current investigation of markers associated with AAA, targeted ultrasound imaging may be a future option (Moxon et al., 2010; Villanueva 2008). With increased knowledge of pathophysiological mechanisms, pharmacotherapy or gene therapy may be available for stabilization of aneurysms (Baxter et al., 2008; Cooper et al., 2009; Golledge et al., 2009; Raffetto & Khalil, 2008; Twine & Williams, 2011). It may then be interesting to apply drug- or gene-loaded contrast agents, which could be monitored and destructed using ultrasound for local drug delivery. Targeted drug delivery might benefit higher doses (locally) without increased risk of side effects.

4. Conclusions

The general aim of AAA research is to provide cost effective management for reducing mortality of AAA. Management includes screening/detection, monitoring, risk prediction, treatment and follow-up. We have described current and future potential of ultrasound for assisting in clinical management of AAA. Advantages of using ultrasound are that it is inexpensive, safe and portable, and allows for real-time dynamic imaging. New techniques, along with more widespread use of ultrasound, could contribute in several manners to improved AAA management.

Ultrasound is highly suitable for detection and monitoring of AAA size for screening and surveillance. In emergencies, ultrasound should be used for AAA detection and assessment of rupture as early as possible and preferably pre-hospital. Contrast enhanced ultrasound may be beneficial in detection of ruptured aneurysms. Early detection can provide early treatment and thereby reduce mortality of ruptured AAA. Ultrasound, and especially contrast enhanced ultrasound, is also a good alternative for detection of endoleak after EVAR. Ultrasound is cost-effective, does not include ionizing radiation or X-ray contrast material, and sensitivity may be better than CT. IVUS may be beneficial during EVAR for optimal measurement of stentgraft diameter, length and fixation site, as well as for post-operative control. Further research may find both IVUS and 3D transabdominal real-time

ultrasound guidance during EVAR to be useful in insertion of stentgrafts, especially fenestrated grafts. Ultrasound could also be used for guiding access to femoral artery in percutanuos EVAR.

A potential new application is to use ultrasound for analysing in-vivo mechanical properties of the aneurysm wall. This could provide additional parameters in predicting growth and rupture, or contribute to more patient-specific adaptation of numerical simulations both before and after EVAR. Improved prediction of growth and rupture would reduce the number of unnecessary examinations and interventions, reduce mortality and further benefit screening for detection of AAA. Another potential use of ultrasound in AAA management is in detection of neovascularization or other relevant markers by using general or targeted contrast agents. Contrast agents may also have a potential in treatment as drug carriers. Drug-loaded contrast agents can be monitored and destructed using ultrasound for local drug-delivery.

Obstacles for further use of ultrasound may be that ultrasound to some extent is operator dependent, and that abdominal ultrasound often is obscured from bowel gas, obesity and noise due to ultrasound propagation through the abdominal wall. Technology development will hopefully advance ultrasound image quality. An improvement was obtained with the introduction of tissue harmonic imaging (Caidahl et al., 1998). Several research groups are working on techniques for further improving quality of ultrasound images, such as suppression of reverberation and aberration correction. Due to operator dependencies, it might be necessary to investigate validity of ultrasound in the individual clinical surroundings before implementation in AAA management. Further, for ultrasound to become a widespread useful tool for AAA assessment, health personnel should be trained in focused assessment of presence and size of aneurysms, and detection of rupture and endoleak. Experts should be trained for more sophisticated examinations, such as analysis of wall mechanics and studies of microcirculation using contrast agents.

5. Acknowledgment

This work was funded by the Liaison Committee between the Central Norway Regional Health Authority and the Norwegian University of Science and Technology, SINTEF Department of Medical Technology and the National Centre for 3D Ultrasound in Surgery.

6. References

Anderson CR, Hu X, Zhang H, Tlaxca J, Declèves AE, Houghtaling R, Sharma K, Lawrence M, Ferrara KW, Rychak JJ. (2011). Ultrasound molecular imaging of tumor angiogenesis with an integrin targeted microbubble contrast agent. *Invest Radiol*. Vol.46, No.4, (April), pp. 215-224.

Arthurs ZM, Starnes BW, Sohn VY, Singh N, Andersen CA. (2008). Ultrasound-guided access improves rate of access-related complications for totally percutaneous aortic aneurysm repair. *Ann Vasc Surg*. Vol.22, No.6, (Nov), pp. 736-741.

Bakken AM, Illig KA. (2010). Long-term follow-up after endovascular aneurysm repair: is ultrasound alone enough? *Perspect Vasc Surg Endovasc Ther*. Vol.22, No.3, (Sep), pp. 145-151.

Bargellini I, Cioni R, Napoli V, Petruzzi P, Vignali C, Cicorelli A, Sardella S, Ferrari M, Bartolozzi C. (2009). Ultrasonographic surveillance with selective CTA after

endovascular repair of abdominal aortic aneurysm. *J Endovasc Ther*. Vol.16, No.1, (Feb), pp. 93-104.

Baxter BT, Terrin MC, Dalman RL. (2008) Medical management of small abdominal aortic aneurysms. *Circulation*. Vol.117, No.14, (Apr), pp. 1883-1889.

Beeman BR, Murtha K, Doerr K, McAfee-Bennett S, Dougherty MJ, Calligaro KD. (2010). Duplex ultrasound factors predicting persistent type II endoleak and increasing AAA sac diameter after EVAR. *J Vasc Surg*.Vol.51, No.5, (Nov), pp. 1147-1152.

Bentz S, Jones J. (2006). Towards evidence-based emergency medicine: best BETs from the Manchester Royal Infirmary. Accuracy of emergency department ultrasound scanning in detecting abdominal aortic aneurysm. *Emerg Med J*. Vol.23, No.10, (Oct), pp. 803-804.

Bernstein EF, Dilley RB, Goldberger LE, Gosink BB, Leopold GR. (1976). Growth rates of small abdominal aortic aneurysms. *Surgery*. Vol.80, No.6, (Dec), pp. 765-773.

Bhatt S, Ghazale H and Dogra VS. (2007). Sonographic Evaluation of the Abdominal Aorta. *Ultrasound Clin*. Vol.2, No.3, (Jul), pp. 437-453.

Boks SS, Andhyiswara T, de Smet AA, Vroegindeweij D. (2005). Ultrasound-guided percutaneous transabdominal treatment of a type 2 endoleak. *Cardiovasc Intervent Radiol*. Vol.28, No.4, (Jul-Aug), pp. 526-529.

Brekken R, Bang J, Ødegård A, Aasland J, Hernes TA, Myhre HO. (2006). Strain estimation in abdominal aortic aneurysms from 2D Ultrasound. *Ultrasound Med Biol*. Vol.32, No.1, (Jan), pp. 33-42.

Brekken R, Dahl T, Hernes TAN, Myhre HO. (2008). Reduced strain in abdominal aortic aneurysms after endovascular repair. *J Endovasc Ther*. Vol. 15, No.4, (Aug), pp. 453-461.

Brekken R, Kaspersen JH, Tangen GA, Dahl T, Hernes TAN, Myhre HO. (2007). 3D visualization of strain in abdominal aortic aneurysms based on navigated ultrasound imaging. *Proceedings of SPIE Medical Imaging: Physiology, Function, and Structure from Medical Images*, 65111H, San Diego, CA, USA, February 18, 2007.

Brewster DC, Cronenwett JL, Hallett JW Jr, Johnston KW, Krupski WC & Matsumura JS. (2003). Guidelines for the treatment of abdominal aortic aneurysms. Report of a subcommittee of the Joint Council of the American Association for Vascular Surgery and Society for Vascular Surgery. *J Vasc Surg*. Vol.37, No.5 (May), pp. 1106-1117.

Brewster DC, Darling RC, Raines JK, Sarno R, O'Donnell TF, Ezpeleta M, Athanasoulis C. (1977). Assessment of abdominal aortic aneurysm size. *Circulation*. Vol.56, No.3S, (Sep), pp. II164-II169.

Broeders IA, Blankensteijn JD. (1999). Preoperative imaging of the aortoiliac anatomy in endovascular aneurysm surgery. *Semin Vasc Surg*. Vol.12, No.4, (Dec), pp. 306-314.

Burgess S, Zderic V, Vaezy S. (2007). Image-guided acoustic hemostasis for hemorrhage in the posterior liver. *Ultrasound Med Biol*. Vol.33, No.1, (Jan), pp. 113-119.

Caidahl K, Kazzam E, Lidberg J, Neumann Andersen G, Nordanstig J, Rantapää Dahlqvist S, Waldenström A, Wikh R. (1998). New concept in echocardiography: harmonic imaging of tissue without use of contrast agent. *Lancet*. Vol.352, No.9136, (Oct), pp. 1264-1270.

Cantisani V, Ricci P, Grazhdani H, Napoli A, Fanelli F, Catalano C, Galati G, D'Andrea V, Biancari F, Passariello R. (2011). Prospective Comparative Analysis of Colour-

Doppler Ultrasound, Contrast-enhanced Ultrasound, Computed Tomography and Magnetic Resonance in Detecting Endoleak after Endovascular Abdominal Aortic Aneurysm Repair. *Eur J Vasc Endovasc Surg*. Vol. 41, No.2, (Feb), pp. 186-192.

Carrafiello G, Laganà D, Recaldini C, Mangini M, Bertolotti E, Caronno R, Tozzi M, Piffaretti G, Genovese EA, Fugazzola C. (2006). Comparison of contrast-enhanced ultrasound and computed tomography in classifying endoleaks after endovascular treatment of abdominal aorta aneurysms: preliminary experience. *Cardiovasc Intervent Radiol*. Vol.29, No.6, (Nov-Dec), pp. 969-974.

Catalano O and Siani A. (2005a). Ruptured Abdominal Aortic Aneurysm: Categorization of Sonographic Findings and Report of 3 New Signs. *J Ultrasound Med*. Vol.24, No.8, (Aug), pp. 1077-1083.

Catalano O, Lobianco R, Cusati B, Siani A. (2005b). Contrast-Enhanced Sonography for Diagnosis of Ruptured Abdominal Aortic Aneurysm. *Am J Roentgenol*. Vol.184, No.2, (Feb), pp. 423-427.

Chaer RA, Gushchin A, Rhee R, Marone L, Cho JS, Leers S, Makaroun MS. (2009). Duplex ultrasound as the sole long-term surveillance method post-endovascular aneurysm repair: a safe alternative for stable aneurysms. *J Vasc Surg*. Vol.49, No.4, (Apr), pp. 845-849.

Chaikof EL, Brewster DC, Dalman RL, Makaroun MS, Illig KA, Sicard GA, Timaran CH, Upchurch GR Jr, Veith FJ. (2009). The care of patients with an abdominal aortic aneurysm: the Society for Vascular Surgery practice guidelines. *J Vasc Surg*. Vol.50, No.4S, (Oct), pp. S2-S49.

Choke E, Thompson MM, Dawson J, Wilson WR, Sayed S, Loftus IM, Cockerill GW. (2006). Abdominal aortic aneurysm rupture is associated with increased medial neovascularization and overexpression of proangiogenic cytokines. *Arterioscler Thromb Vasc Biol*. Vol.26, No.9, (Sep), pp. 2077-2082.

Clevert DA, Minaifar N, Weckbach S, Kopp R, Meimarakis G, Clevert DA, Reiser M. (2008). Color duplex ultrasound and contrast-enhanced ultrasound in comparison to MS-CT in the detection of endoleak following endovascular aneurysm repair. *Clin Hemorheol Microcirc*. Vol.39, No.1-4, pp. 121-132.

Collins JT, Boros MJ, Combs K. (2007). Ultrasound surveillance of endovascular aneurysm repair: a safe modality versus computed tomography. *Ann Vasc Surg*. Vol.21, No.6, (Nov), pp. 671-675.

Cooper DG, King JA, Earnshaw JJ. (2009). Role of medical intervention in slowing the growth of small abdominal aortic aneurysms. *Postgrad Med J*. Vol.85, No.1010, (Dec), pp. 688-692.

Cosford PA, Leng GC. (2007). Screening for abdominal aortic aneurysm. *Cochrane Database Syst Rev*. Vol.18, No.2, (Apr), CD002945.

Costantino TG, Bruno EC, Handly N, Dean AJ. (2005). Accuracy of emergency medicine ultrasound in the evaluation of abdominal aortic aneurysm. *J Emerg Med*. Vol.29, No.4, (Nov), pp. 455-460.

Dalainas I, G. Nano, P. Bianchi, R. Casana, T. Lupattelli and S. Stegher, Malacrida G, Tealdi DG. (2006). Axial computed tomography and duplex scanning for the determination of the maximal abdominal aortic diameter in patients with abdominal aortic aneurysms. *Eur Surg*. Vol. 38, No.4, pp. 312-314.

Di Martino ES, Bohra A, Vande Geest JP, Gupta N, Makaroun MS,Vorp DA. (2006). Biomechanical properties of ruptured versus electively repaired abdominal aortic aneurysm wall tissue. *J Vasc Surg*. Vol.43, No.3, (Mar), pp. 570-576.

Dijkstra ML, Eagleton MJ, Greenberg RK, Mastracci T, Hernandez A. (2011). Intraoperative C-arm cone-beam computed tomography in fenestrated/branched aortic endografting. *J Vasc Surg*. Vol.53, No.3, (Mar), pp. 583-590.

Eriksson MO, Wanhainen A, Nyman R. (2009). Intravascular ultrasound with a vector phased-array probe (AcuNav) is feasible in endovascular abdominal aortic aneurysm repair. *Acta Radiol*. Vol.50, No.8, (Oct), pp. 870-875.

Ferket BS, Grootenboer N, Colkesen EB, Visser JJ, van Sambeek MR, Spronk S, Steyerberg EW, Hunink MG. (2011). Systematic review of guidelines on abdominal aortic aneurysm screening. *J Vasc Surg*. Epub: Feb 14.

Fillinger MF, Marra SP, Raghavan ML, Kennedy FE. (2003). Prediction of rupture risk in abdominal aortic aneurysm during observation: wall stress versus diameter. *J Vasc Surg*. Vol.37, No.4, (Apr), pp. 724-732.

Freestone T, Turner RJ, Coady A, Higman DJ, Greenhalgh RM, Powell JT. (1995). Inflammation and matrix metalloproteinases in the enlarging abdominal aortic aneurysm. *Arterioscler Thromb Vasc Biol*. Vol.15, No.8, (Aug), pp. 1145-1151.

Frinking PJ, Bouakaz A, Kirkhorn J, Ten Cate FJ, de Jong N. (2000). Ultrasound contrast imaging: current and new potential methods. *Ultrasound Med Biol*. Vol.26, No.6, (Jul), pp. 965-975.

Gallucci M, Vincenzoni A, Schettini M, Fortunato P, Cassanelli A, Zaccara A. (2001). Extracorporeal shock wave lithotripsy in ureteral and kidney malformations. *Urol Int*. Vol.66, No.2, pp. 61-65.

Garra BS. (2007). Imaging and estimation of tissue elasticity by ultrasound. *Ultrasound Q*. Vol.23, No.4, (Dec), pp. 255-268.

Garret HE Jr, Abdullah AH, Hodgkiss TD, Burgar SR. (2003). Intravascular ultrasound aids in the performance of endovascular repair of abdominal aortic aneurysm. *J Vasc Surg*. Vol.37, No.3, (Mar), pp. 615-618.

Gilling-Smith GL, Martin J, Sudhindran S, Gould DA, McWilliams RG, Bakran A, Brennan JA, Harris PL. (2000). Freedom from endoleak after endovascular aneurysm repair does not equal treatment success. *Eur J Vasc Endovasc Surg*. Vol.19, No.4, (Apr), pp. 421-425.

Goldberg BB, Ostrum BJ, Isard HJ. (1966). Ultrasonic aortography. *JAMA*. Vol.198, No.4, (Oct), pp. 353-358.

Golledge J, Dalman RL, Norman PE. (2009). Developments in non-surgical therapies for abdominal aortic aneurysm. *Curr Vasc Pharmacol*. Vol.7, No.2, (Apr), pp. 153-158.

Hafez H, Druce PS, Ashton HA. (2008). Abdominal aortic aneurysm development in men following a "normal" aortic ultrasound scan. *Eur J Vasc Endovasc Surg*. Vol.36, No.5, (Nov), pp. 553-558.

Hansen R, Angelsen BA. SURF imaging for contrast agent detection. (2009). *IEEE Trans Ultrason Ferroelectr Freq Control*. Vol.56, No.2, (Feb), pp. 280-290.

Hassani S, Bard R. (1974). Ultrasonic diagnosis of abdominal aortic aneurysms. *J Natl Med Assoc*. Vol.66, No.4, (Jul), pp. 298-299.

Henao EA, Hodge MD, Felkai DD, McCollum CH, Noon GP, Lin PH, Lumsden AB, Bush RL. (2006). Contrast-enhanced Duplex surveillance after endovascular abdominal

aortic aneurysm repair: improved efficacy using a continuous infusion technique. *J Vasc Surg*. Vol.43, No.2, (Feb), pp. 259-264.

Herron GS, Unemori E, Wong M, Rapp JH, Hibbs MH, Stoney RJ. (1991). Connective tissue proteinases and inhibitors in abdominal aortic aneurysms. Involvement of the vasa vasorum in the pathogenesis of aortic aneurysms. *Arterioscler Thromb*. Vol.11, No.6, (Nov-Dec), pp. 1667-1677.

Hoffmann B, Bessman ES, Um P, Ding R, McCarthy ML. (2010). Successful sonographic visualisation of the abdominal aorta differs significantly among a diverse group of credentialed emergency department providers. *Emerg Med J*. Epub: Aug 2.

Holmes DR, Liao S, Parks WC, Thompson RW. (1995). Medial neovascularization in abdominal aortic aneurysms: a histopathologic marker of aneurysmal degeneration with pathophysiologic implications. *J Vasc Surg*. Vol.21, No.5, (May), pp. 761-771.

Hong H, Yang Y, Liu B, Cai W. (2010). Imaging of Abdominal Aortic Aneurysm: the present and the future. *Curr Vasc Pharmacol*. Vol.8, No.6, (Nov), pp. 808-819.

Iezzi R, Basilico R, Giancristofaro D, Pascali D, Cotroneo AR, Storto ML. (2009). Contrast-enhanced ultrasound versus color duplex ultrasound imaging in the follow-up of patients after endovascular abdominal aortic aneurysm repair. *J Vasc Surg*. Vol.49, No.3, (Mar), pp. 552-560.

Imura T, Yamamoto K, Kanamori K, Mikami T, Yasuda H. (1986). Non-invasive ultrasonic measurement of the elastic properties of the human abdominal aorta. *Cardiovasc Res*. Vol.20, No.3, (Mar), pp. 208-214.

Kaspersen JH, Sjølie E, Wesche J, Asland J, Lundbom J, Odegård A, Lindseth F, Nagelhus Hernes TA. (2003). Three-dimensional ultrasound-based navigation combined with preoperative CT during abdominal interventions: a feasibility study. *Cardiovasc Intervent Radiol*. Vol.26, No.4, (Jul-Aug), pp. 347-356.

Kasthuri RS, Stivaros SM, Gavan D. (2005). Percutaneous ultrasound-guided thrombin injection for endoleaks: an alternative. *Cardiovasc Intervent Radiol*. Vol.28, No.1, (Jan-Feb), pp. 110-112.

Kim YS, Rhim H, Choi MJ, Lim HK, Choi D. (2008). High-intensity focused ultrasound therapy: an overview for radiologists. *Korean J Radiol*. Vol.9, No.4, (Aug), pp. 291-302.

Kopp R, Zürn W, Weidenhagen R, Meimarakis G, Clevert DA. (2010). First experience using intraoperative contrast-enhanced ultrasound during endovascular aneurysm repair for infrarenal aortic aneurysms. *J Vasc Surg*. Vol.51, No.5, (May), pp. 1103-1110.

Kuhn M, Bonnin RLL, Davey MJ, Rowland JL, Langlois S. (2000). Emergency Department Ultrasound Scanning for Abdominal Aortic Aneurysm: Accessible, Accurate, and Advantageous. *Ann Emerg Med* Vol.36, No.3, (Sep), pp. 219-223.

Länne T, Sonesson B, Bergqvist D, Bengtsson H, Gustafsson D. (1992). Diameter and compliance in the male human abdominal aorta: influence of age and aortic aneurysm. *Eur J Vasc Surg*. Vol.6, No.2, (Mar), pp. 178-184.

Lederle FA, Wilson SE, Johnson GR, Reinke DB, Littooy FN, Acher CW, Messina LM, Ballard DJ, Ansel HJ. (1995).Variability in measurement of abdominal aortic aneurysms. Abdominal Aortic Aneurysm Detection and Management Veterans Administration Cooperative Study Group. *J Vasc Surg*. Vol.21, No.6, (Jun), pp. 945-952.

Lee KR, Walls WJ, Martin NL, Templeton AW. (1975). A practical approach to the diagnosis of abdominal aortic aneurysms. *Surgery*. Vol.78, No.2, (Aug), pp. 195-201.

Lie T, Lundbom J, Hatlinghus S, Grønningsaeter A, Ommedal S, Aadahl P, Saether OD, Myhre HO. (1997). Ultrasound imaging during endovascular abdominal aortic aneurysm repair using the Stentor bifurcated endograft. *J Endovasc Surg*. Vol.4, No.3, (Aug), pp. 272-278.

Lindblad B, Dias N, Malina M, Ivancev K, Resch T, Hansen F, Sonesson B. (2004). Pulsatile wall motion (PWM) measurements after endovascular abdominal aortic aneurysm exclusion are not useful in the classification of endoleak. *Eur J Vasc Endovasc Surg*. Vol.28, No.6, (Dec), pp. 623-628.

Lindholt JS, Vammen S, Juul S, Henneberg EW, Fasting H. (1999). The validity of ultrasonographic scanning as screening method for abdominal aortic aneurysm. *Eur J Vasc Endovasc Surg*. Vol.17, No.6, (Jun), pp. 472-475.

Lindner JR, Villanueva FS, Dent JM, Wei K, Sklenar J, Kaul S. (2000). Assessment of resting perfusion with myocardial contrast echocardiography: theoretical and practical considerations. *Am Heart J*. Vol.139, No.2pt1, (Feb), pp. 231-240.

Long A, Rouet L, Bissery A, Rossignol P, Mouradian D, Sapoval M. (2005). Compliance of abdominal aortic aneurysms evaluated by tissue Doppler imaging: correlation with aneurysm size. *J Vasc Surg*. Vol.42, No.1, (Jul), pp. 18-26.

Malina M, Länne T, Ivancev K, Lindblad B, Brunkwall J. (1998). Reduced pulsatile wall motion of abdominal aortic aneurysms after endovascular repair. *J Vasc Surg*. Vol.27, No.4, (Apr), pp. 624-631.

Malkawi AH, Hinchliffe RJ, Holt PJ, Loftus IM, Thompson MM. (2010). Percutaneous access for endovascular aneurysm repair: a systematic review. *Eur J Vasc Endovasc Surg*. Vol.39, No.6, (Jun), pp. 676-682.

Malkawi AH, Hinchliffe RJ, Xu Y, Holt PJ, Loftus IM, Thompson MM. (2010). Patient-specific biomechanical profiling in abdominal aortic aneurysm development and rupture. *J Vasc Surg*. Vol.52, No.2, (Aug), pp. 489-488.

Manning BJ, Kristmundsson T, Sonesson B, Resch T. (2009). Abdominal aortic aneurysm diameter: a comparison of ultrasound measurements with those from standard and three-dimensional computed tomography reconstruction. *J Vasc Surg*. Vol.50, No.2, (Aug), pp. 263-268.

Manstad-Hulaas F, Ommedal S, Tangen GA, Aadahl P, Hernes TN. (2007). Side-branched AAA stent graft insertion using navigation technology: a phantom study. *Eur Surg Res*. Vol.39, No.6, (), pp. 364-371.

McGregor JC, Pollock JG, Anton HC. (1975). The value of ultrasonography in the diagnosis of abdominal aortic aneurysm. *Scott Med J*. Vol.20, No.3, (May), pp. 133-137.

McWilliams RG, Martin J, White D, Gould DA, Rowlands PC, Haycox A, Brennan J, Gilling-Smith GL, Harris PL. (2002). Detection of endoleak with enhanced ultrasound imaging: comparison with biphasic computed tomography. *J Endovasc Ther*..9, No.2, (Apr), pp. 170-179.

Mirza TA, Karthikesalingam A, Jackson D, Walsh SR, Holt PJ, Hayes PD, Boyle JR. (2010). Duplex ultrasound and contrast-enhanced ultrasound versus computed tomography for the detection of endoleak after EVAR: systematic review and bivariate meta-analysis. *Eur J Vasc Endovasc Surg*. Vol.39, No.4, (Apr), pp. 418-428.

Moll FL, Powell JT, Fraedrich G, Verzini F, Haulon S, Waltham M, van Herwaarden JA, Holt PJ, van Keulen JW, Rantner B, Schlösser FJ, Setacci F, Ricco JB. (2011). Management of abdominal aortic aneurysms clinical practice guidelines of the European society for vascular surgery. *Eur J Vasc Endovasc Surg*. Vol.41, No.S1, (Jan), pp. S1-S58.

Moxon JV, Parr A, Emeto TI, Walker P, Norman PE, Golledge J (2010). Diagnosis and Monitoring of Abdominal Aortic Aneurysm: Current Status and Future Prospects. *Curr Probl Cardiol*. Vol.35, No.10, (Oct), pp. 512-548.

Mulder DS, Winsberg F, Cole CM, Blundell PE, Scott HJ. (1973). Ultrasonic "B" scanning of abdominal aneurysms. *Ann Thorac Surg*. Vol.16, No.4, (Oct), pp. 361-367.

Nagre SB, Taylor SM, Passman MA, Patterson MA, Combs BR, Lowman BG, Jordan WD Jr. (2011). Evaluating outcomes of endoleak discrepancies between computed tomography scan and ultrasound imaging after endovascular abdominal aneurysm repair. *Ann Vasc Surg*. Vol.25, No.1, (Jan), pp. 94-100.

Nightingale K, Soo MS, Nightingale R, Trahey G. (2002). Acoustic radiation force impulse imaging: in vivo demonstration of clinical feasibility. *Ultrasound Med Biol*. Vol.28, No.2, (Feb), pp. 227-235.

Ophir J, Céspedes I, Ponnekanti H, Yazdi Y, Li X. (1991). Elastography: a quantitative method for imaging the elasticity of biological tissues. *Ultrason Imaging*. Vol.13, No.2, (Apr), pp. 111-134.

Patel MS, Carpenter JP. (2010). The value of the initial post-EVAR computed tomography angiography scan in predicting future secondary procedures using the Powerlink stent graft. *J Vasc Surg*. Vol.52, No.5, (Nov), pp. 1135-1139.

Petersen E, Wagberg F, Angquist KA. (2002). Proteolysis of the abdominal aortic aneurysm wall and the association with rupture. *Eur J Vasc Endovasc Surg*. Vol.23, No.2, (Feb), pp. 153-157.

Raffetto JD, Khalil RA. (2008). Matrix metalloproteinases and their inhibitors in vascular remodeling and vascular disease. *Biochem Pharmacol*. Vol.75, No.2, (Jan), pp. 346-359.

Reardon, RF; Cook, T; Plummer, D (2008). Abdominal aortic aneurysm, In *Emergency Ultrasound 2nd Edition*, O.J. Ma; J.R. Mateer; M. Blaivas (Eds), 149-167. The McGraw-Hill Companies, Inc. ISBN 978-0-07-147904-2. China.

Sebesta P, Klika T, Zdrahal P, Kramar J. (1998). Ruptured abdominal aortic aneurysm: role of initial delay on survival. *J Mal Vasc*. Vol.23, No.5, (Dec), pp. 361-367.

Segal BL, Likoff W, Asperger Z, Kingsley B. (1966). Ultrasound diagnosis of an abdominal aortic aneurysm. *Am J Cardiol*. Vol.17, No.1, (Jan), pp. 101-103.

Singh K, Bønaa KH, Solberg S, Sørlie DG, Bjørk L. (1998). Intra- and interobserver variability in ultrasound measurements of abdominal aortic diameter. The Tromsø Study. *Eur J Vasc Endovasc Surg*. Vol.15, No.6, (Jun), pp.497-504.

Solberg OV, Lindseth F, Torp H, Blake RE, Nagelhus Hernes TA. (2007). Freehand 3D ultrasound reconstruction algorithms--a review. *Ultrasound Med Biol*. Vol.33, No.7, (Jul), pp. 991-1009.

Sonesson B, Hansen F, Stale H, Länne T. (1993). Compliance and diameter in the human abdominal aorta--the influence of age and sex. *Eur J Vasc Surg*. Vol.7, No.6, (Nov), pp. 690-697.

Sonesson B, Sandgren T, Länne T. (1999). Abdominal aortic aneurysm wall mechanics and their relation to risk of rupture. *Eur J Vasc Endovasc Surg*. Vol.18, No.6, (Dec), pp. 487-493.

Sprouse L.R., G.H. Meier, F.N. Parent, R.J. DeMasi, M.H. Glickman and G.A. Barber. (2004). Is ultrasound more accurate than axial computed tomography for determination of maximal abdominal aortic aneurysm diameter? *Eur J Vasc Endovasc Surg*. Vol.28, No.1, (Jul), pp. 28-35.

Staub D, Patel MB, Tibrewala A, Ludden D, Johnson M, Espinosa P, Coll B, Jaeger KA, Feinstein SB. (2010a). Vasa vasorum and plaque neovascularization on contrast-enhanced carotid ultrasound imaging correlates with cardiovascular disease and past cardiovascular events. *Stroke*. Vol.41, No.1, (Jan), pp. 41-7.

Staub D, Schinkel AF, Coll B, Coli S, van der Steen AF, Reed JD, Krueger C, Thomenius KE, Adam D, Sijbrands EJ, ten Cate FJ, Feinstein SB. (2010b). Contrast-enhanced ultrasound imaging of the vasa vasorum: from early atherosclerosis to the identification of unstable plaques. *JACC Cardiovasc Imaging*. Vol.3, No.7, (Jul), pp. 761-771.

Sun Z. (2006). Diagnostic value of color duplex ultrasonography in the follow-up of endovascular repair of abdominal aortic aneurysm. *J Vasc Interv Radiol*. Vol.17, No.5, (May), pp. 759-764.

Takagi H, Goto SN, Matsui M, Manabe H, Umemoto T. (2010). A further meta-analysis of population-based screening for abdominal aortic aneurysm. *J Vasc Surg*. Vol.52, No.4, (Oct), pp. 1103-1108.

Ten Bosch JA, Rouwet EV, Peters CT, Jansen L, Verhagen HJ, Prins MH, Teijink JA. (2010). Contrast-enhanced ultrasound versus computed tomographic angiography for surveillance of endovascular abdominal aortic aneurysm repair. *J Vasc Interv Radiol*. Vol.21, No.5, (May), pp. 638-643.

ten Kate GL, Sijbrands EJ, Valkema R, ten Cate FJ, Feinstein SB, van der Steen AF, Daemen MJ, Schinkel AF. (2010). Molecular imaging of inflammation and intraplaque vasa vasorum: a step forward to identification of vulnerable plaques? *J Nucl Cardiol*. Vol.17, No.5, (), pp. 897-912.

Thapar A, Cheal D, Hopkins T, Ward S, Shalhoub J, Yusuf SW. (2010). Internal or external wall diameter for abdominal aortic aneurysm screening? *Ann R Coll Surg Engl*. Vol.92, No.6, (Sep), pp. 503-505.

Thomas PR, Shaw JC, Ashton HA, Kay DN, Scott RA. (1994). Accuracy of ultrasound in a screening programme for abdominal aortic aneurysms. *J Med Screen*. Vol.1, No.1, (Jan), pp. 3-6.

Thompson MM, Jones L, Nasim A, Sayers RD, Bell PR. (1996). Angiogenesis in abdominal aortic aneurysms. *Eur J Vasc Endovasc Surg*. Vol.11, No.4, (May), pp. 464-469.

Thubrikar MJ, Labrosse M, Robicsek F, Al-Soudi J, Fowler B. (2001). Mechanical properties of abdominal aortic aneurysm wall. *J Med Eng Technol*. Vol.25, No. 4, (Jul-Aug), pp. 133-142.

Tutein Nolthenius RP, van den Berg JC, Moll FL. (2000). The value of intraoperative intravascular ultrasound for determining stent graft size (excluding abdominal aortic aneurysm) with a modular system. *Ann Vasc Surg*. Vol.14, No.4, (Jul), pp. 311-317.

Twine CP, Williams IM. (2011). Systematic review and meta-analysis of the effects of statin therapy on abdominal aortic aneurysms. *Br J Surg*. Vol.98, No.3, (Mar), pp. 346-353.

Unsgård G, Solheim O, Lindseth F, Selbekk T. (2011). Intra-operative imaging with 3D ultrasound in neurosurgery. *Acta Neurochir Suppl*. Vol.109, pp. 181-186.

Vaezy S, Martin R, Crum L. (2001). High intensity focused ultrasound: a method of hemostasis. *Echocardiography*. Vol.18, No.4, (May), pp. 309-315.

van Essen JA, Gussenhoven EJ, van der Lugt A, Huijsman PC, van Muiswinkel JM, van Sambeek MR, van Dijk LC, van Urk H. (1999). Accurate assessment of abdominal aortic aneurysm with intravascular ultrasound scanning: validation with computed tomographic angiography. *J Vasc Surg*. Vol.29, No.4, (Apr), pp. 631-638.

Villanueva FS. (2008). Molecular imaging of cardiovascular disease using ultrasound. *J Nucl Cardiol*. Vol. 15, No.4, (Jul-Aug;). pp. 576-586.

Vorp DA. (2007). Biomechanics of abdominal aortic aneurysm. *J Biomech*. Vol.40, No.9, (), pp. 1887-1902.

Wheeler WE, Beachley MC, Ranniger K. (1976). Angiography and ultrasonography. A comparative study of abdominal aortic aneurysms. *Am J Roentgenol*. Vol.126, No.1, (Jan), pp. 95-100.

White RA, Donayre C, Kopchok G, Walot I, Wilson E, de Virgilio C. (1997). Intravascular ultrasound: the ultimate tool for abdominal aortic aneurysm assessment and endovascular graft delivery. *J Endovasc Surg*. Vol.4, No.1, (Feb), pp. 45-55.

White RA, Verbin C, Kopchok G, Scoccianti M, de Virgilio C, Donayre C. (1995). The role of cinefluoroscopy and intravascular ultrasonography in evaluating the deployment of experimental endovascular prostheses. *J Vasc Surg*. Vol.21, No.3, (Mar), pp. 365-74.

Wilson K, Bradbury A, Whyman M, Hoskins P, Lee A, Fowkes G, McCollum P, Ruckley CV. (1998). Relationship between abdominal aortic aneurysm wall compliance and clinical outcome: a preliminary analysis. *Eur J Vasc Endovasc Surg*. Vol.15, No.6, (Jun), pp. 472-477.

Wilson K, Whyman M, Hoskins P, Lee AJ, Bradbury AW, Fowkes FG, Ruckley CV. (1999). The relationship between abdominal aortic aneurysm wall compliance, maximum diameter and growth rate. *Cardiovasc Surg*. Vol.7, No.2, (Mar), pp. 208-213.

Wilson KA, Lee AJ, Lee AJ, Hoskins PR, Fowkes FG, Ruckley CV, Bradbury AW. (2003). The relationship between aortic wall distensibility and rupture of infrarenal abdominal aortic aneurysm. *J Vasc Surg*. Vol.37, No.1, (Jan), pp. 112-117.

Winsberg F, Cole CM. (1972). "Continuous ultrasound visualization of the pulsating abdominal aorta. *Radiology*. Vol.103, No.2, (May), pp. 455-457.

Zanchetta M, Rigatelli G, Pedon L, Zennaro M, Ronsivalle S, Maiolino P. (2003). IVUS guidance of thoracic and complex abdominal aortic aneurysm stent-graft repairs using an intracardiac echocardiography probe: preliminary report. *J Endovasc Ther*. Vol.10, No.2, (Apr), pp. 218-226.

Zankl AR, Schumacher H, Krumsdorf U, Katus HA, Jahn L, Tiefenbacher CP. (2007). Pathology, natural history and treatment of abdominal aortic aneurysms. *Clin Res Cardiol*. Vol.96, No.3, (Mar), pp-140-151.

Dissertations at the Faculty of Medicine, NTNU

1977

1. Knut Joachim Berg: EFFECT OF ACETYLSALICYLIC ACID ON RENAL FUNCTION
2. Karl Erik Viken and Arne Ødegaard: STUDIES ON HUMAN MONOCYTES CULTURED *IN VITRO*

1978

3. Karel Bjørn Cyvin: CONGENITAL DISLOCATION OF THE HIP JOINT.
4. Alf O. Brubakk: METHODS FOR STUDYING FLOW DYNAMICS IN THE LEFT VENTRICLE AND THE AORTA IN MAN.

1979

5. Geirmund Unsgaard: CYTOSTATIC AND IMMUNOREGULATORY ABILITIES OF HUMAN BLOOD MONOCYTES CULTURED IN VITRO

1980

6. Størker Jørstad: URAEMIC TOXINS
7. Arne Olav Jenssen: SOME RHEOLOGICAL, CHEMICAL AND STRUCTURAL PROPERTIES OF MUCOID SPUTUM FROM PATIENTS WITH CHRONIC OBSTRUCTIVE BRONCHITIS

1981

8. Jens Hammerstrøm: CYTOSTATIC AND CYTOLYTIC ACTIVITY OF HUMAN MONOCYTES AND EFFUSION MACROPHAGES AGAINST TUMOR CELLS *IN VITRO*

1983

9. Tore Syversen: EFFECTS OF METHYLMERCURY ON RAT BRAIN PROTEIN.
10. Torbjørn Iversen: SQUAMOUS CELL CARCINOMA OF THE VULVA.

1984

11. Tor-Erik Widerøe: ASPECTS OF CONTINUOUS AMBULATORY PERITONEAL DIALYSIS.
12. Anton Hole: ALTERATIONS OF MONOCYTE AND LYMPHOCYTE FUNCTIONS IN REALTION TO SURGERY UNDER EPIDURAL OR GENERAL ANAESTHESIA.
13. Terje Terjesen: FRACTURE HEALING AND STRESS-PROTECTION AFTER METAL PLATE FIXATION AND EXTERNAL FIXATION.
14. Carsten Saunte: CLUSTER HEADACHE SYNDROME.
15. Inggard Lereim: TRAFFIC ACCIDENTS AND THEIR CONSEQUENCES.
16. Bjørn Magne Eggen: STUDIES IN CYTOTOXICITY IN HUMAN ADHERENT MONONUCLEAR BLOOD CELLS.
17. Trond Haug: FACTORS REGULATING BEHAVIORAL EFFECTS OG DRUGS.

1985

18. Sven Erik Gisvold: RESUSCITATION AFTER COMPLETE GLOBAL BRAIN ISCHEMIA.
19. Terje Espevik: THE CYTOSKELETON OF HUMAN MONOCYTES.
20. Lars Bevanger: STUDIES OF THE Ibc (c) PROTEIN ANTIGENS OF GROUP B STREPTOCOCCI.
21. Ole-Jan Iversen: RETROVIRUS-LIKE PARTICLES IN THE PATHOGENESIS OF PSORIASIS.
22. Lasse Eriksen: EVALUATION AND TREATMENT OF ALCOHOL DEPENDENT BEHAVIOUR.
23. Per I. Lundmo: ANDROGEN METABOLISM IN THE PROSTATE.

1986

24. Dagfinn Berntzen: ANALYSIS AND MANAGEMENT OF EXPERIMENTAL AND CLINICAL PAIN.
25. Odd Arnold Kildahl-Andersen: PRODUCTION AND CHARACTERIZATION OF MONOCYTE-DERIVED CYTOTOXIN AND ITS ROLE IN MONOCYTE-MEDIATED CYTOTOXICITY.
26. Ola Dale: VOLATILE ANAESTHETICS.

1987

27. Per Martin Kleveland: STUDIES ON GASTRIN.
28. Audun N. Øksendal: THE CALCIUM PARADOX AND THE HEART.
29. Vilhjalmur R. Finsen: HIP FRACTURES

1988

30. Rigmor Austgulen: TUMOR NECROSIS FACTOR: A MONOCYTE-DERIVED REGULATOR OF CELLULAR GROWTH.
31. Tom-Harald Edna: HEAD INJURIES ADMITTED TO HOSPITAL.
32. Joseph D. Borsi: NEW ASPECTS OF THE CLINICAL PHARMACOKINETICS OF METHOTREXATE.
33. Olav F. M. Sellevold: GLUCOCORTICOIDS IN MYOCARDIAL PROTECTION.
34. Terje Skjærpe: NONINVASIVE QUANTITATION OF GLOBAL PARAMETERS ON LEFT VENTRICULAR FUNCTION: THE SYSTOLIC PULMONARY ARTERY PRESSURE AND CARDIAC OUTPUT.
35. Eyvind Rødahl: STUDIES OF IMMUNE COMPLEXES AND RETROVIRUS-LIKE ANTIGENS IN PATIENTS WITH ANKYLOSING SPONDYLITIS.
36. Ketil Thorstensen: STUDIES ON THE MECHANISMS OF CELLULAR UPTAKE OF IRON FROM TRANSFERRIN.
37. Anna Midelfart: STUDIES OF THE MECHANISMS OF ION AND FLUID TRANSPORT IN THE BOVINE CORNEA.
38. Eirik Helseth: GROWTH AND PLASMINOGEN ACTIVATOR ACTIVITY OF HUMAN GLIOMAS AND BRAIN METASTASES - WITH SPECIAL REFERENCE TO TRANSFORMING GROWTH FACTOR BETA AND THE EPIDERMAL GROWTH FACTOR RECEPTOR.
39. Petter C. Borchgrevink: MAGNESIUM AND THE ISCHEMIC HEART.
40. Kjell-Arne Rein: THE EFFECT OF EXTRACORPOREAL CIRCULATION ON SUBCUTANEOUS TRANSCAPILLARY FLUID BALANCE.
41. Arne Kristian Sandvik: RAT GASTRIC HISTAMINE.
42. Carl Bredo Dahl: ANIMAL MODELS IN PSYCHIATRY.

1989

43. Torbjørn A. Fredriksen: CERVICOGENIC HEADACHE.
44. Rolf A. Walstad: CEFTAZIDIME.
45. Rolf Salvesen: THE PUPIL IN CLUSTER HEADACHE.
46. Nils Petter Jørgensen: DRUG EXPOSURE IN EARLY PREGNANCY.
47. Johan C. Ræder: PREMEDICATION AND GENERAL ANAESTHESIA IN OUTPATIENT GYNECOLOGICAL SURGERY.
48. M. R. Shalaby: IMMUNOREGULATORY PROPERTIES OF TNF-α AND THE RELATED CYTOKINES.
49. Anders Waage: THE COMPLEX PATTERN OF CYTOKINES IN SEPTIC SHOCK.
50. Bjarne Christian Eriksen: ELECTROSTIMULATION OF THE PELVIC FLOOR IN FEMALE URINARY INCONTINENCE.
51. Tore B. Halvorsen: PROGNOSTIC FACTORS IN COLORECTAL CANCER.

1990

52. Asbjørn Nordby: CELLULAR TOXICITY OF ROENTGEN CONTRAST MEDIA.
53. Kåre E. Tvedt: X-RAY MICROANALYSIS OF BIOLOGICAL MATERIAL.
54. Tore C. Stiles: COGNITIVE VULNERABILITY FACTORS IN THE DEVELOPMENT AND MAINTENANCE OF DEPRESSION.
55. Eva Hofsli: TUMOR NECROSIS FACTOR AND MULTIDRUG RESISTANCE.
56. Helge S. Haarstad: TROPHIC EFFECTS OF CHOLECYSTOKININ AND SECRETIN ON THE RAT PANCREAS.
57. Lars Engebretsen: TREATMENT OF ACUTE ANTERIOR CRUCIATE LIGAMENT INJURIES.
58. Tarjei Rygnestad: DELIBERATE SELF-POISONING IN TRONDHEIM.
59. Arne Z. Henriksen: STUDIES ON CONSERVED ANTIGENIC DOMAINS ON MAJOR OUTER MEMBRANE PROTEINS FROM ENTEROBACTERIA.
60. Steinar Westin: UNEMPLOYMENT AND HEALTH: Medical and social consequences of a factory closure in a ten-year controlled follow-up study.
61. Ylva Sahlin: INJURY REGISTRATION, a tool for accident preventive work.
62. Helge Bjørnstad Pettersen: BIOSYNTHESIS OF COMPLEMENT BY HUMAN ALVEOLAR MACROPHAGES WITH SPECIAL REFERENCE TO SARCOIDOSIS.
63. Berit Schei: TRAPPED IN PAINFUL LOVE.
64. Lars J. Vatten: PROSPECTIVE STUDIES OF THE RISK OF BREAST CANCER IN A COHORT OF NORWEGIAN WOMAN.

1991

65. Kåre Bergh: APPLICATIONS OF ANTI-C5a SPECIFIC MONOCLONAL ANTIBODIES FOR THE ASSESSMENT OF COMPLEMENT ACTIVATION.
66. Svein Svenningsen: THE CLINICAL SIGNIFICANCE OF INCREASED FEMORAL ANTEVERSION.
67. Olbjørn Klepp: NONSEMINOMATOUS GERM CELL TESTIS CANCER: THERAPEUTIC OUTCOME AND PROGNOSTIC FACTORS.
68. Trond Sand: THE EFFECTS OF CLICK POLARITY ON BRAINSTEM AUDITORY EVOKED POTENTIALS AMPLITUDE, DISPERSION, AND LATENCY VARIABLES.
69. Kjetil B. Åsbakk: STUDIES OF A PROTEIN FROM PSORIATIC SCALE, PSO P27, WITH RESPECT TO ITS POTENTIAL ROLE IN IMMUNE REACTIONS IN PSORIASIS.
70. Arnulf Hestnes: STUDIES ON DOWN´S SYNDROME.
71. Randi Nygaard: LONG-TERM SURVIVAL IN CHILDHOOD LEUKEMIA.
72. Bjørn Hagen: THIO-TEPA.
73. Svein Anda: EVALUATION OF THE HIP JOINT BY COMPUTED TOMOGRAMPHY AND ULTRASONOGRAPHY.

1992

74. Martin Svartberg: AN INVESTIGATION OF PROCESS AND OUTCOME OF SHORT-TERM PSYCHODYNAMIC PSYCHOTHERAPY.
75. Stig Arild Slørdahl: AORTIC REGURGITATION.
76. Harold C Sexton: STUDIES RELATING TO THE TREATMENT OF SYMPTOMATIC NON-PSYCHOTIC PATIENTS.
77. Maurice B. Vincent: VASOACTIVE PEPTIDES IN THE OCULAR/FOREHEAD AREA.
78. Terje Johannessen: CONTROLLED TRIALS IN SINGLE SUBJECTS.
79. Turid Nilsen: PYROPHOSPHATE IN HEPATOCYTE IRON METABOLISM.
80. Olav Haraldseth: NMR SPECTROSCOPY OF CEREBRAL ISCHEMIA AND REPERFUSION IN RAT.
81. Eiliv Brenna: REGULATION OF FUNCTION AND GROWTH OF THE OXYNTIC MUCOSA.

1993

82. Gunnar Bovim: CERVICOGENIC HEADACHE.
83. Jarl Arne Kahn: ASSISTED PROCREATION.
84. Bjørn Naume: IMMUNOREGULATORY EFFECTS OF CYTOKINES ON NK CELLS.
85. Rune Wiseth: AORTIC VALVE REPLACEMENT.
86. Jie Ming Shen: BLOOD FLOW VELOCITY AND RESPIRATORY STUDIES.
87. Piotr Kruszewski: SUNCT SYNDROME WITH SPECIAL REFERENCE TO THE AUTONOMIC NERVOUS SYSTEM.
88. Mette Haase Moen: ENDOMETRIOSIS.
89. Anne Vik: VASCULAR GAS EMBOLISM DURING AIR INFUSION AND AFTER DECOMPRESSION IN PIGS.
90. Lars Jacob Stovner: THE CHIARI TYPE I MALFORMATION.
91. Kjell Å. Salvesen: ROUTINE ULTRASONOGRAPHY IN UTERO AND DEVELOPMENT IN CHILDHOOD.

1994

92. Nina-Beate Liabakk: DEVELOPMENT OF IMMUNOASSAYS FOR TNF AND ITS SOLUBLE RECEPTORS.
93. Sverre Helge Torp: *erb*B ONCOGENES IN HUMAN GLIOMAS AND MENINGIOMAS.
94. Olav M. Linaker: MENTAL RETARDATION AND PSYCHIATRY. Past and present.
95. Per Oscar Feet: INCREASED ANTIDEPRESSANT AND ANTIPANIC EFFECT IN COMBINED TREATMENT WITH DIXYRAZINE AND TRICYCLIC ANTIDEPRESSANTS.
96. Stein Olav Samstad: CROSS SECTIONAL FLOW VELOCITY PROFILES FROM TWO-DIMENSIONAL DOPPLER ULTRASOUND: Studies on early mitral blood flow.
97. Bjørn Backe: STUDIES IN ANTENATAL CARE.
98. Gerd Inger Ringdal: QUALITY OF LIFE IN CANCER PATIENTS.
99. Torvid Kiserud: THE DUCTUS VENOSUS IN THE HUMAN FETUS.
100. Hans E. Fjøsne: HORMONAL REGULATION OF PROSTATIC METABOLISM.
101. Eylert Brodtkorb: CLINICAL ASPECTS OF EPILEPSY IN THE MENTALLY RETARDED.
102. Roar Juul: PEPTIDERGIC MECHANISMS IN HUMAN SUBARACHNOID HEMORRHAGE.
103. Unni Syversen: CHROMOGRANIN A. Phsysiological and Clinical Role.

1995

104. Odd Gunnar Brakstad: THERMOSTABLE NUCLEASE AND THE *nuc* GENE IN THE DIAGNOSIS OF *Staphylococcus aureus* INFECTIONS.
105. Terje Engan: NUCLEAR MAGNETIC RESONANCE (NMR) SPECTROSCOPY OF PLASMA IN MALIGNANT DISEASE.
106. Kirsten Rasmussen: VIOLENCE IN THE MENTALLY DISORDERED.
107. Finn Egil Skjeldestad: INDUCED ABORTION: Timetrends and Determinants.
108. Roar Stenseth: THORACIC EPIDURAL ANALGESIA IN AORTOCORONARY BYPASS SURGERY.
109. Arild Faxvaag: STUDIES OF IMMUNE CELL FUNCTION *in mice infected with* MURINE RETROVIRUS.

1996

110. Svend Aakhus: NONINVASIVE COMPUTERIZED ASSESSMENT OF LEFT VENTRICULAR FUNCTION AND SYSTEMIC ARTERIAL PROPERTIES. Methodology and some clinical applications.
111. Klaus-Dieter Bolz: INTRAVASCULAR ULTRASONOGRAPHY.
112. Petter Aadahl: CARDIOVASCULAR EFFECTS OF THORACIC AORTIC CROSS-CLAMPING.
113. Sigurd Steinshamn: CYTOKINE MEDIATORS DURING GRANULOCYTOPENIC INFECTIONS.
114. Hans Stifoss-Hanssen: SEEKING MEANING OR HAPPINESS?
115. Anne Kvikstad: LIFE CHANGE EVENTS AND MARITAL STATUS IN RELATION TO RISK AND PROGNOSIS OF CANCER.
116. Torbjørn Grøntvedt: TREATMENT OF ACUTE AND CHRONIC ANTERIOR CRUCIATE LIGAMENT INJURIES. A clinical and biomechanical study.
117. Sigrid Hørven Wigers: CLINICAL STUDIES OF FIBROMYALGIA WITH FOCUS ON ETIOLOGY, TREATMENT AND OUTCOME.
118. Jan Schjøtt: MYOCARDIAL PROTECTION: Functional and Metabolic Characteristics of Two Endogenous Protective Principles.
119. Marit Martinussen: STUDIES OF INTESTINAL BLOOD FLOW AND ITS RELATION TO TRANSITIONAL CIRCULATORY ADAPATION IN NEWBORN INFANTS.
120. Tomm B. Müller: MAGNETIC RESONANCE IMAGING IN FOCAL CEREBRAL ISCHEMIA.
121. Rune Haaverstad: OEDEMA FORMATION OF THE LOWER EXTREMITIES.
122. Magne Børset: THE ROLE OF CYTOKINES IN MULTIPLE MYELOMA, WITH SPECIAL REFERENCE TO HEPATOCYTE GROWTH FACTOR.
123. Geir Smedslund: A THEORETICAL AND EMPIRICAL INVESTIGATION OF SMOKING, STRESS AND DISEASE: RESULTS FROM A POPULATION SURVEY.

1997

124. Torstein Vik: GROWTH, MORBIDITY, AND PSYCHOMOTOR DEVELOPMENT IN INFANTS WHO WERE GROWTH RETARDED *IN UTERO*.
125. Siri Forsmo: ASPECTS AND CONSEQUENCES OF OPPORTUNISTIC SCREENING FOR CERVICAL CANCER. Results based on data from three Norwegian counties.
126. Jon S. Skranes: CEREBRAL MRI AND NEURODEVELOPMENTAL OUTCOME IN VERY LOW BIRTH WEIGHT (VLBW) CHILDREN. A follow-up study of a geographically based year cohort of VLBW children at ages one and six years.
127. Knut Bjørnstad: COMPUTERIZED ECHOCARDIOGRAPHY FOR EVALUTION OF CORONARY ARTERY DISEASE.
128. Grethe Elisabeth Borchgrevink: DIAGNOSIS AND TREATMENT OF WHIPLASH/NECK SPRAIN INJURIES CAUSED BY CAR ACCIDENTS.
129. Tor Elsås: NEUROPEPTIDES AND NITRIC OXIDE SYNTHASE IN OCULAR AUTONOMIC AND SENSORY NERVES.
130. Rolf W. Gråwe: EPIDEMIOLOGICAL AND NEUROPSYCHOLOGICAL PERSPECTIVES ON SCHIZOPHRENIA.
131. Tonje Strømholm: CEREBRAL HAEMODYNAMICS DURING THORACIC AORTIC CROSSCLAMPING. An experimental study in pigs

1998

132. Martinus Bråten: STUDIES ON SOME PROBLEMS REALTED TO INTRAMEDULLARY NAILING OF FEMORAL FRACTURES.

133. Ståle Nordgård: PROLIFERATIVE ACTIVITY AND DNA CONTENT AS PROGNOSTIC INDICATORS IN ADENOID CYSTIC CARCINOMA OF THE HEAD AND NECK.
134. Egil Lien: SOLUBLE RECEPTORS FOR **TNF** AND **LPS**: RELEASE PATTERN AND POSSIBLE SIGNIFICANCE IN DISEASE.
135. Marit Bjørgaas: HYPOGLYCAEMIA IN CHILDREN WITH DIABETES MELLITUS
136. Frank Skorpen: GENETIC AND FUNCTIONAL ANALYSES OF DNA REPAIR IN HUMAN CELLS.
137. Juan A. Pareja: SUNCT SYNDROME. ON THE CLINICAL PICTURE. ITS DISTINCTION FROM OTHER, SIMILAR HEADACHES.
138. Anders Angelsen: NEUROENDOCRINE CELLS IN HUMAN PROSTATIC CARCINOMAS AND THE PROSTATIC COMPLEX OF RAT, GUINEA PIG, CAT AND DOG.
139. Fabio Antonaci: CHRONIC PAROXYSMAL HEMICRANIA AND HEMICRANIA CONTINUA: TWO DIFFERENT ENTITIES?
140. Sven M. Carlsen: ENDOCRINE AND METABOLIC EFFECTS OF METFORMIN WITH SPECIAL EMPHASIS ON CARDIOVASCULAR RISK FACTORES.

1999

141. Terje A. Murberg: DEPRESSIVE SYMPTOMS AND COPING AMONG PATIENTS WITH CONGESTIVE HEART FAILURE.
142. Harm-Gerd Karl Blaas: THE EMBRYONIC EXAMINATION. Ultrasound studies on the development of the human embryo.
143. Noèmi Becser Andersen:THE CEPHALIC SENSORY NERVES IN UNILATERAL HEADACHES. Anatomical background and neurophysiological evaluation.
144. Eli-Janne Fiskerstrand: LASER TREATMENT OF PORT WINE STAINS. A study of the efficacy and limitations of the pulsed dye laser. Clinical and morfological analyses aimed at improving the therapeutic outcome.
145. Bård Kulseng: A STUDY OF ALGINATE CAPSULE PROPERTIES AND CYTOKINES IN RELATION TO INSULIN DEPENDENT DIABETES MELLITUS.
146. Terje Haug: STRUCTURE AND REGULATION OF THE HUMAN UNG GENE ENCODING URACIL-DNA GLYCOSYLASE.
147. Heidi Brurok: MANGANESE AND THE HEART. A Magic Metal with Diagnostic and Therapeutic Possibilites.
148. Agnes Kathrine Lie: DIAGNOSIS AND PREVALENCE OF HUMAN PAPILLOMAVIRUS INFECTION IN CERVICAL INTRAEPITELIAL NEOPLASIA. Relationship to Cell Cycle Regulatory Proteins and HLA DQBI Genes.
149. Ronald Mårvik: PHARMACOLOGICAL, PHYSIOLOGICAL AND PATHOPHYSIOLOGICAL STUDIES ON ISOLATED STOMACS.
150. Ketil Jarl Holen: THE ROLE OF ULTRASONOGRAPHY IN THE DIAGNOSIS AND TREATMENT OF HIP DYSPLASIA IN NEWBORNS.
151. Irene Hetlevik: THE ROLE OF CLINICAL GUIDELINES IN CARDIOVASCULAR RISK INTERVENTION IN GENERAL PRACTICE.
152. Katarina Tunòn: ULTRASOUND AND PREDICTION OF GESTATIONAL AGE.
153. Johannes Soma: INTERACTION BETWEEN THE LEFT VENTRICLE AND THE SYSTEMIC ARTERIES.
154. Arild Aamodt: DEVELOPMENT AND PRE-CLINICAL EVALUATION OF A CUSTOM-MADE FEMORAL STEM.
155. Agnar Tegnander: DIAGNOSIS AND FOLLOW-UP OF CHILDREN WITH SUSPECTED OR KNOWN HIP DYSPLASIA.
156. Bent Indredavik: STROKE UNIT TREATMENT: SHORT AND LONG-TERM EFFECTS
157. Jolanta Vanagaite Vingen: PHOTOPHOBIA AND PHONOPHOBIA IN PRIMARY HEADACHES

2000

158. Ola Dalsegg Sæther: PATHOPHYSIOLOGY DURING PROXIMAL AORTIC CROSS-CLAMPING CLINICAL AND EXPERIMENTAL STUDIES
159. xxxxxxxxx (blind number)
160. Christina Vogt Isaksen: PRENATAL ULTRASOUND AND POSTMORTEM FINDINGS – A TEN YEAR CORRELATIVE STUDY OF FETUSES AND INFANTS WITH DEVELOPMENTAL ANOMALIES.
161. Holger Seidel: HIGH-DOSE METHOTREXATE THERAPY IN CHILDREN WITH ACUTE LYMPHOCYTIC LEUKEMIA: DOSE, CONCENTRATION, AND EFFECT CONSIDERATIONS.

162. Stein Hallan: IMPLEMENTATION OF MODERN MEDICAL DECISION ANALYSIS INTO CLINICAL DIAGNOSIS AND TREATMENT.
163. Malcolm Sue-Chu: INVASIVE AND NON-INVASIVE STUDIES IN CROSS-COUNTRY SKIERS WITH ASTHMA-LIKE SYMPTOMS.
164. Ole-Lars Brekke: EFFECTS OF ANTIOXIDANTS AND FATTY ACIDS ON TUMOR NECROSIS FACTOR-INDUCED CYTOTOXICITY.
165. Jan Lundbom: AORTOCORONARY BYPASS SURGERY: CLINICAL ASPECTS, COST CONSIDERATIONS AND WORKING ABILITY.
166. John-Anker Zwart: LUMBAR NERVE ROOT COMPRESSION, BIOCHEMICAL AND NEUROPHYSIOLOGICAL ASPECTS.
167. Geir Falck: HYPEROSMOLALITY AND THE HEART.
168. Eirik Skogvoll: CARDIAC ARREST Incidence, Intervention and Outcome.
169. Dalius Bansevicius: SHOULDER-NECK REGION IN CERTAIN HEADACHES AND CHRONIC PAIN SYNDROMES.
170. Bettina Kinge: REFRACTIVE ERRORS AND BIOMETRIC CHANGES AMONG UNIVERSITY STUDENTS IN NORWAY.
171. Gunnar Qvigstad: CONSEQUENCES OF HYPERGASTRINEMIA IN MAN
172. Hanne Ellekjær: EPIDEMIOLOGICAL STUDIES OF STROKE IN A NORWEGIAN POPULATION. INCIDENCE, RISK FACTORS AND PROGNOSIS
173. Hilde Grimstad: VIOLENCE AGAINST WOMEN AND PREGNANCY OUTCOME.
174. Astrid Hjelde: SURFACE TENSION AND COMPLEMENT ACTIVATION: Factors influencing bubble formation and bubble effects after decompression.
175. Kjell A. Kvistad: MR IN BREAST CANCER – A CLINICAL STUDY.
176. Ivar Rossvoll: ELECTIVE ORTHOPAEDIC SURGERY IN A DEFINED POPULATION. Studies on demand, waiting time for treatment and incapacity for work.
177. Carina Seidel: PROGNOSTIC VALUE AND BIOLOGICAL EFFECTS OF HEPATOCYTE GROWTH FACTOR AND SYNDECAN-1 IN MULTIPLE MYELOMA.

2001

178. Alexander Wahba: THE INFLUENCE OF CARDIOPULMONARY BYPASS ON PLATELET FUNCTION AND BLOOD COAGULATION – DETERMINANTS AND CLINICAL CONSEQUENSES
179. Marcus Schmitt-Egenolf: THE RELEVANCE OF THE MAJOR hISTOCOMPATIBILITY COMPLEX FOR THE GENETICS OF PSORIASIS
180. Odrun Arna Gederaas: BIOLOGICAL MECHANISMS INVOLVED IN 5-AMINOLEVULINIC ACID BASED PHOTODYNAMIC THERAPY
181. Pål Richard Romundstad: CANCER INCIDENCE AMONG NORWEGIAN ALUMINIUM WORKERS
182. Henrik Hjorth-Hansen: NOVEL CYTOKINES IN GROWTH CONTROL AND BONE DISEASE OF MULTIPLE MYELOMA
183. Gunnar Morken: SEASONAL VARIATION OF HUMAN MOOD AND BEHAVIOUR
184. Bjørn Olav Haugen: MEASUREMENT OF CARDIAC OUTPUT AND STUDIES OF VELOCITY PROFILES IN AORTIC AND MITRAL FLOW USING TWO- AND THREE-DIMENSIONAL COLOUR FLOW IMAGING
185. Geir Bråthen: THE CLASSIFICATION AND CLINICAL DIAGNOSIS OF ALCOHOL-RELATED SEIZURES
186. Knut Ivar Aasarød: RENAL INVOLVEMENT IN INFLAMMATORY RHEUMATIC DISEASE. A Study of Renal Disease in Wegener's Granulomatosis and in Primary Sjögren's Syndrome
187. Trude Helen Flo: RESEPTORS INVOLVED IN CELL ACTIVATION BY DEFINED URONIC ACID POLYMERS AND BACTERIAL COMPONENTS
188. Bodil Kavli: HUMAN URACIL-DNA GLYCOSYLASES FROM THE UNG GENE: STRUCTRUAL BASIS FOR SUBSTRATE SPECIFICITY AND REPAIR
189. Liv Thommesen: MOLECULAR MECHANISMS INVOLVED IN TNF- AND GASTRIN-MEDIATED GENE REGULATION
190. Turid Lingaas Holmen: SMOKING AND HEALTH IN ADOLESCENCE; THE NORD-TRØNDELAG HEALTH STUDY, 1995-97
191. Øyvind Hjertner: MULTIPLE MYELOMA: INTERACTIONS BETWEEN MALIGNANT PLASMA CELLS AND THE BONE MICROENVIRONMENT

192. Asbjørn Støylen: STRAIN RATE IMAGING OF THE LEFT VENTRICLE BY ULTRASOUND. FEASIBILITY, CLINICAL VALIDATION AND PHYSIOLOGICAL ASPECTS
193. Kristian Midthjell: DIABETES IN ADULTS IN NORD-TRØNDELAG. PUBLIC HEALTH ASPECTS OF DIABETES MELLITUS IN A LARGE, NON-SELECTED NORWEGIAN POPULATION.
194. Guanglin Cui: FUNCTIONAL ASPECTS OF THE ECL CELL IN RODENTS
195. Ulrik Wisløff: CARDIAC EFFECTS OF AEROBIC ENDURANCE TRAINING: HYPERTROPHY, CONTRACTILITY AND CALCUIM HANDLING IN NORMAL AND FAILING HEART
196. Øyvind Halaas: MECHANISMS OF IMMUNOMODULATION AND CELL-MEDIATED CYTOTOXICITY INDUCED BY BACTERIAL PRODUCTS
197. Tore Amundsen: PERFUSION MR IMAGING IN THE DIAGNOSIS OF PULMONARY EMBOLISM
198. Nanna Kurtze: THE SIGNIFICANCE OF ANXIETY AND DEPRESSION IN FATIQUE AND PATTERNS OF PAIN AMONG INDIVIDUALS DIAGNOSED WITH FIBROMYALGIA: RELATIONS WITH QUALITY OF LIFE, FUNCTIONAL DISABILITY, LIFESTYLE, EMPLOYMENT STATUS, CO-MORBIDITY AND GENDER
199. Tom Ivar Lund Nilsen: PROSPECTIVE STUDIES OF CANCER RISK IN NORD-TRØNDELAG: THE HUNT STUDY. Associations with anthropometric, socioeconomic, and lifestyle risk factors
200. Asta Kristine Håberg: A NEW APPROACH TO THE STUDY OF MIDDLE CEREBRAL ARTERY OCCLUSION IN THE RAT USING MAGNETIC RESONANCE TECHNIQUES

2002

201. Knut Jørgen Arntzen: PREGNANCY AND CYTOKINES
202. Henrik Døllner: INFLAMMATORY MEDIATORS IN PERINATAL INFECTIONS
203. Asta Bye: LOW FAT, LOW LACTOSE DIET USED AS PROPHYLACTIC TREATMENT OF ACUTE INTESTINAL REACTIONS DURING PELVIC RADIOTHERAPY. A PROSPECTIVE RANDOMISED STUDY.
204. Sylvester Moyo: STUDIES ON STREPTOCOCCUS AGALACTIAE (GROUP B STREPTOCOCCUS) SURFACE-ANCHORED MARKERS WITH EMPHASIS ON STRAINS AND HUMAN SERA FROM ZIMBABWE.
205. Knut Hagen: HEAD-HUNT: THE EPIDEMIOLOGY OF HEADACHE IN NORD-TRØNDELAG
206. Li Lixin: ON THE REGULATION AND ROLE OF UNCOUPLING PROTEIN-2 IN INSULIN PRODUCING ß-CELLS
207. Anne Hildur Henriksen: SYMPTOMS OF ALLERGY AND ASTHMA VERSUS MARKERS OF LOWER AIRWAY INFLAMMATION AMONG ADOLESCENTS
208. Egil Andreas Fors: NON-MALIGNANT PAIN IN RELATION TO PSYCHOLOGICAL AND ENVIRONTENTAL FACTORS. EXPERIENTAL AND CLINICAL STUDES OF PAIN WITH FOCUS ON FIBROMYALGIA
209. Pål Klepstad: MORPHINE FOR CANCER PAIN
210. Ingunn Bakke: MECHANISMS AND CONSEQUENCES OF PEROXISOME PROLIFERATOR-INDUCED HYPERFUNCTION OF THE RAT GASTRIN PRODUCING CELL
211. Ingrid Susann Gribbestad: MAGNETIC RESONANCE IMAGING AND SPECTROSCOPY OF BREAST CANCER
212. Rønnaug Astri Ødegård: PREECLAMPSIA – MATERNAL RISK FACTORS AND FETAL GROWTH
213. Johan Haux: STUDIES ON CYTOTOXICITY INDUCED BY HUMAN NATURAL KILLER CELLS AND DIGITOXIN
214. Turid Suzanne Berg-Nielsen: PARENTING PRACTICES AND MENTALLY DISORDERED ADOLESCENTS
215. Astrid Rydning: BLOOD FLOW AS A PROTECTIVE FACTOR FOR THE STOMACH MUCOSA. AN EXPERIMENTAL STUDY ON THE ROLE OF MAST CELLS AND SENSORY AFFERENT NEURONS

2003

216. Jan Pål Loennechen: HEART FAILURE AFTER MYOCARDIAL INFARCTION. Regional Differences, Myocyte Function, Gene Expression, and Response to Cariporide, Losartan, and Exercise Training.

217. Elisabeth Qvigstad: EFFECTS OF FATTY ACIDS AND OVER-STIMULATION ON INSULIN SECRETION IN MAN
218. Arne Åsberg: EPIDEMIOLOGICAL STUDIES IN HEREDITARY HEMOCHROMATOSIS: PREVALENCE, MORBIDITY AND BENEFIT OF SCREENING.
219. Johan Fredrik Skomsvoll: REPRODUCTIVE OUTCOME IN WOMEN WITH RHEUMATIC DISEASE. A population registry based study of the effects of inflammatory rheumatic disease and connective tissue disease on reproductive outcome in Norwegian women in 1967-1995.
220. Siv Mørkved: URINARY INCONTINENCE DURING PREGNANCY AND AFTER DELIVERY: EFFECT OF PELVIC FLOOR MUSCLE TRAINING IN PREVENTION AND TREATMENT
221. Marit S. Jordhøy: THE IMPACT OF COMPREHENSIVE PALLIATIVE CARE
222. Tom Christian Martinsen: HYPERGASTRINEMIA AND HYPOACIDITY IN RODENTS – CAUSES AND CONSEQUENCES
223. Solveig Tingulstad: CENTRALIZATION OF PRIMARY SURGERY FOR OVARAIN CANCER. FEASIBILITY AND IMPACT ON SURVIVAL
224. Haytham Eloqayli: METABOLIC CHANGES IN THE BRAIN CAUSED BY EPILEPTIC SEIZURES
225. Torunn Bruland: STUDIES OF EARLY RETROVIRUS-HOST INTERACTIONS – VIRAL DETERMINANTS FOR PATHOGENESIS AND THE INFLUENCE OF SEX ON THE SUSCEPTIBILITY TO FRIEND MURINE LEUKAEMIA VIRUS INFECTION
226. Torstein Hole: DOPPLER ECHOCARDIOGRAPHIC EVALUATION OF LEFT VENTRICULAR FUNCTION IN PATIENTS WITH ACUTE MYOCARDIAL INFARCTION
227. Vibeke Nossum: THE EFFECT OF VASCULAR BUBBLES ON ENDOTHELIAL FUNCTION
228. Sigurd Fasting: ROUTINE BASED RECORDING OF ADVERSE EVENTS DURING ANAESTHESIA – APPLICATION IN QUALITY IMPROVEMENT AND SAFETY
229. Solfrid Romundstad: EPIDEMIOLOGICAL STUDIES OF MICROALBUMINURIA. THE NORD-TRØNDELAG HEALTH STUDY 1995-97 (HUNT 2)
230. Geir Torheim: PROCESSING OF DYNAMIC DATA SETS IN MAGNETIC RESONANCE IMAGING
231. Catrine Ahlén: SKIN INFECTIONS IN OCCUPATIONAL SATURATION DIVERS IN THE NORTH SEA AND THE IMPACT OF THE ENVIRONMENT
232. Arnulf Langhammer: RESPIRATORY SYMPTOMS, LUNG FUNCTION AND BONE MINERAL DENSITY IN A COMPREHENSIVE POPULATION SURVEY. THE NORD-TRØNDELAG HEALTH STUDY 1995-97. THE BRONCHIAL OBSTRUCTION IN NORD-TRØNDELAG STUDY
233. Einar Kjelsås: EATING DISORDERS AND PHYSICAL ACTIVITY IN NON-CLINICAL SAMPLES
234. Arne Wibe: RECTAL CANCER TREATMENT IN NORWAY – STANDARDISATION OF SURGERY AND QUALITY ASSURANCE

2004

235. Eivind Witsø: BONE GRAFT AS AN ANTIBIOTIC CARRIER
236. Anne Mari Sund: DEVELOPMENT OF DEPRESSIVE SYMPTOMS IN EARLY ADOLESCENCE
237. Hallvard Lærum: EVALUATION OF ELECTRONIC MEDICAL RECORDS – A CLINICAL TASK PERSPECTIVE
238. Gustav Mikkelsen: ACCESSIBILITY OF INFORMATION IN ELECTRONIC PATIENT RECORDS; AN EVALUATION OF THE ROLE OF DATA QUALITY
239. Steinar Krokstad: SOCIOECONOMIC INEQUALITIES IN HEALTH AND DISABILITY. SOCIAL EPIDEMIOLOGY IN THE NORD-TRØNDELAG HEALTH STUDY (HUNT), NORWAY
240. Arne Kristian Myhre: NORMAL VARIATION IN ANOGENITAL ANATOMY AND MICROBIOLOGY IN NON-ABUSED PRESCHOOL CHILDREN
241. Ingunn Dybedal: NEGATIVE REGULATORS OF HEMATOPOIETEC STEM AND PROGENITOR CELLS
242. Beate Sitter: TISSUE CHARACTERIZATION BY HIGH RESOLUTION MAGIC ANGLE SPINNING MR SPECTROSCOPY
243. Per Arne Aas: MACROMOLECULAR MAINTENANCE IN HUMAN CELLS – REPAIR OF URACIL IN DNA AND METHYLATIONS IN DNA AND RNA

244. Anna Bofin: FINE NEEDLE ASPIRATION CYTOLOGY IN THE PRIMARY INVESTIGATION OF BREAST TUMOURS AND IN THE DETERMINATION OF TREATMENT STRATEGIES
245. Jim Aage Nøttestad: DEINSTITUTIONALIZATION AND MENTAL HEALTH CHANGES AMONG PEOPLE WITH MENTAL RETARDATION
246. Reidar Fossmark: GASTRIC CANCER IN JAPANESE COTTON RATS
247. Wibeke Nordhøy: MANGANESE AND THE HEART, INTRACELLULAR MR RELAXATION AND WATER EXCHANGE ACROSS THE CARDIAC CELL MEMBRANE

2005

248. Sturla Molden: QUANTITATIVE ANALYSES OF SINGLE UNITS RECORDED FROM THE HIPPOCAMPUS AND ENTORHINAL CORTEX OF BEHAVING RATS
249. Wenche Brenne Drøyvold: EPIDEMIOLOGICAL STUDIES ON WEIGHT CHANGE AND HEALTH IN A LARGE POPULATION. THE NORD-TRØNDELAG HEALTH STUDY (HUNT)
250. Ragnhild Støen: ENDOTHELIUM-DEPENDENT VASODILATION IN THE FEMORAL ARTERY OF DEVELOPING PIGLETS
251. Aslak Steinsbekk: HOMEOPATHY IN THE PREVENTION OF UPPER RESPIRATORY TRACT INFECTIONS IN CHILDREN
252. Hill-Aina Steffenach: MEMORY IN HIPPOCAMPAL AND CORTICO-HIPPOCAMPAL CIRCUITS
253. Eystein Stordal: ASPECTS OF THE EPIDEMIOLOGY OF DEPRESSIONS BASED ON SELF-RATING IN A LARGE GENERAL HEALTH STUDY (THE HUNT-2 STUDY)
254. Viggo Pettersen: FROM MUSCLES TO SINGING: THE ACTIVITY OF ACCESSORY BREATHING MUSCLES AND THORAX MOVEMENT IN CLASSICAL SINGING
255. Marianne Fyhn: SPATIAL MAPS IN THE HIPPOCAMPUS AND ENTORHINAL CORTEX
256. Robert Valderhaug: OBSESSIVE-COMPULSIVE DISORDER AMONG CHILDREN AND ADOLESCENTS: CHARACTERISTICS AND PSYCHOLOGICAL MANAGEMENT OF PATIENTS IN OUTPATIENT PSYCHIATRIC CLINICS
257. Erik Skaaheim Haug: INFRARENAL ABDOMINAL AORTIC ANEURYSMS – COMORBIDITY AND RESULTS FOLLOWING OPEN SURGERY
258. Daniel Kondziella: GLIAL-NEURONAL INTERACTIONS IN EXPERIMENTAL BRAIN DISORDERS
259. Vegard Heimly Brun: ROUTES TO SPATIAL MEMORY IN HIPPOCAMPAL PLACE CELLS
260. Kenneth McMillan: PHYSIOLOGICAL ASSESSMENT AND TRAINING OF ENDURANCE AND STRENGTH IN PROFESSIONAL YOUTH SOCCER PLAYERS
261. Marit Sæbø Indredavik: MENTAL HEALTH AND CEREBRAL MAGNETIC RESONANCE IMAGING IN ADOLESCENTS WITH LOW BIRTH WEIGHT
262. Ole Johan Kemi: ON THE CELLULAR BASIS OF AEROBIC FITNESS, INTENSITY-DEPENDENCE AND TIME-COURSE OF CARDIOMYOCYTE AND ENDOTHELIAL ADAPTATIONS TO EXERCISE TRAINING
263. Eszter Vanky: POLYCYSTIC OVARY SYNDROME – METFORMIN TREATMENT IN PREGNANCY
264. Hild Fjærtoft: EXTENDED STROKE UNIT SERVICE AND EARLY SUPPORTED DISCHARGE. SHORT AND LONG-TERM EFFECTS
265. Grete Dyb: POSTTRAUMATIC STRESS REACTIONS IN CHILDREN AND ADOLESCENTS
266. Vidar Fykse: SOMATOSTATIN AND THE STOMACH
267. Kirsti Berg: OXIDATIVE STRESS AND THE ISCHEMIC HEART: A STUDY IN PATIENTS UNDERGOING CORONARY REVASCULARIZATION
268. Björn Inge Gustafsson: THE SEROTONIN PRODUCING ENTEROCHROMAFFIN CELL, AND EFFECTS OF HYPERSEROTONINEMIA ON HEART AND BONE

2006

269. Torstein Baade Rø: EFFECTS OF BONE MORPHOGENETIC PROTEINS, HEPATOCYTE GROWTH FACTOR AND INTERLEUKIN-21 IN MULTIPLE MYELOMA
270. May-Britt Tessem: METABOLIC EFFECTS OF ULTRAVIOLET RADIATION ON THE ANTERIOR PART OF THE EYE
271. Anne-Sofie Helvik: COPING AND EVERYDAY LIFE IN A POPULATION OF ADULTS WITH HEARING IMPAIRMENT

272. Therese Standal: MULTIPLE MYELOMA: THE INTERPLAY BETWEEN MALIGNANT PLASMA CELLS AND THE BONE MARROW MICROENVIRONMENT
273. Ingvild Saltvedt: TREATMENT OF ACUTELY SICK, FRAIL ELDERLY PATIENTS IN A GERIATRIC EVALUATION AND MANAGEMENT UNIT – RESULTS FROM A PROSPECTIVE RANDOMISED TRIAL
274. Birger Henning Endreseth: STRATEGIES IN RECTAL CANCER TREATMENT – FOCUS ON EARLY RECTAL CANCER AND THE INFLUENCE OF AGE ON PROGNOSIS
275. Anne Mari Aukan Rokstad: ALGINATE CAPSULES AS BIOREACTORS FOR CELL THERAPY
276. Mansour Akbari: HUMAN BASE EXCISION REPAIR FOR PRESERVATION OF GENOMIC STABILITY
277. Stein Sundstrøm: IMPROVING TREATMENT IN PATIENTS WITH LUNG CANCER – RESULTS FROM TWO MULITCENTRE RANDOMISED STUDIES
278. Hilde Pleym: BLEEDING AFTER CORONARY ARTERY BYPASS SURGERY - STUDIES ON HEMOSTATIC MECHANISMS, PROPHYLACTIC DRUG TREATMENT AND EFFECTS OF AUTOTRANSFUSION
279. Line Merethe Oldervoll: PHYSICAL ACTIVITY AND EXERCISE INTERVENTIONS IN CANCER PATIENTS
280. Boye Welde: THE SIGNIFICANCE OF ENDURANCE TRAINING, RESISTANCE TRAINING AND MOTIVATIONAL STYLES IN ATHLETIC PERFORMANCE AMONG ELITE JUNIOR CROSS-COUNTRY SKIERS
281. Per Olav Vandvik: IRRITABLE BOWEL SYNDROME IN NORWAY, STUDIES OF PREVALENCE, DIAGNOSIS AND CHARACTERISTICS IN GENERAL PRACTICE AND IN THE POPULATION
282. Idar Kirkeby-Garstad: CLINICAL PHYSIOLOGY OF EARLY MOBILIZATION AFTER CARDIAC SURGERY
283. Linn Getz: SUSTAINABLE AND RESPONSIBLE PREVENTIVE MEDICINE. CONCEPTUALISING ETHICAL DILEMMAS ARISING FROM CLINICAL IMPLEMENTATION OF ADVANCING MEDICAL TECHNOLOGY
284. Eva Tegnander: DETECTION OF CONGENITAL HEART DEFECTS IN A NON-SELECTED POPULATION OF 42,381 FETUSES
285. Kristin Gabestad Nørsett: GENE EXPRESSION STUDIES IN GASTROINTESTINAL PATHOPHYSIOLOGY AND NEOPLASIA
286. Per Magnus Haram: GENETIC VS. AQUIRED FITNESS: METABOLIC, VASCULAR AND CARDIOMYOCYTE ADAPTATIONS
287. Agneta Johansson: GENERAL RISK FACTORS FOR GAMBLING PROBLEMS AND THE PREVALENCE OF PATHOLOGICAL GAMBLING IN NORWAY
288. Svein Artur Jensen: THE PREVALENCE OF SYMPTOMATIC ARTERIAL DISEASE OF THE LOWER LIMB
289. Charlotte Björk Ingul: QUANITIFICATION OF REGIONAL MYOCARDIAL FUNCTION BY STRAIN RATE AND STRAIN FOR EVALUATION OF CORONARY ARTERY DISEASE. AUTOMATED VERSUS MANUAL ANALYSIS DURING ACUTE MYOCARDIAL INFARCTION AND DOBUTAMINE STRESS ECHOCARDIOGRAPHY
290. Jakob Nakling: RESULTS AND CONSEQUENCES OF ROUTINE ULTRASOUND SCREENING IN PREGNANCY – A GEOGRAPHIC BASED POPULATION STUDY
291. Anne Engum: DEPRESSION AND ANXIETY – THEIR RELATIONS TO THYROID DYSFUNCTION AND DIABETES IN A LARGE EPIDEMIOLOGICAL STUDY
292. Ottar Bjerkeset: ANXIETY AND DEPRESSION IN THE GENERAL POPULATION: RISK FACTORS, INTERVENTION AND OUTCOME – THE NORD-TRØNDELAG HEALTH STUDY (HUNT)
293. Jon Olav Drogset: RESULTS AFTER SURGICAL TREATMENT OF ANTERIOR CRUCIATE LIGAMENT INJURIES – A CLINICAL STUDY
294. Lars Fosse: MECHANICAL BEHAVIOUR OF COMPACTED MORSELLISED BONE – AN EXPERIMENTAL IN VITRO STUDY
295. Gunilla Klensmeden Fosse: MENTAL HEALTH OF PSYCHIATRIC OUTPATIENTS BULLIED IN CHILDHOOD
296. Paul Jarle Mork: MUSCLE ACTIVITY IN WORK AND LEISURE AND ITS ASSOCIATION TO MUSCULOSKELETAL PAIN

297. Björn Stenström: LESSONS FROM RODENTS: I: MECHANISMS OF OBESITY SURGERY – ROLE OF STOMACH. II: CARCINOGENIC EFFECTS OF *HELICOBACTER PYLORI* AND SNUS IN THE STOMACH

2007

298. Haakon R. Skogseth: INVASIVE PROPERTIES OF CANCER – A TREATMENT TARGET ? IN VITRO STUDIES IN HUMAN PROSTATE CANCER CELL LINES
299. Janniche Hammer: GLUTAMATE METABOLISM AND CYCLING IN MESIAL TEMPORAL LOBE EPILEPSY
300. May Britt Drugli: YOUNG CHILDREN TREATED BECAUSE OF ODD/CD: CONDUCT PROBLEMS AND SOCIAL COMPETENCIES IN DAY-CARE AND SCHOOL SETTINGS
301. Arne Skjold: MAGNETIC RESONANCE KINETICS OF MANGANESE DIPYRIDOXYL DIPHOSPHATE (MnDPDP) IN HUMAN MYOCARDIUM. STUDIES IN HEALTHY VOLUNTEERS AND IN PATIENTS WITH RECENT MYOCARDIAL INFARCTION
302. Siri Malm: LEFT VENTRICULAR SYSTOLIC FUNCTION AND MYOCARDIAL PERFUSION ASSESSED BY CONTRAST ECHOCARDIOGRAPHY
303. Valentina Maria do Rosario Cabral Iversen: MENTAL HEALTH AND PSYCHOLOGICAL ADAPTATION OF CLINICAL AND NON-CLINICAL MIGRANT GROUPS
304. Lasse Løvstakken: SIGNAL PROCESSING IN DIAGNOSTIC ULTRASOUND: ALGORITHMS FOR REAL-TIME ESTIMATION AND VISUALIZATION OF BLOOD FLOW VELOCITY
305. Elisabeth Olstad: GLUTAMATE AND GABA: MAJOR PLAYERS IN NEURONAL METABOLISM
306. Lilian Leistad: THE ROLE OF CYTOKINES AND PHOSPHOLIPASE A_2s IN ARTICULAR CARTILAGE CHONDROCYTES IN RHEUMATOID ARTHRITIS AND OSTEOARTHRITIS
307. Arne Vaaler: EFFECTS OF PSYCHIATRIC INTENSIVE CARE UNIT IN AN ACUTE PSYCIATHRIC WARD
308. Mathias Toft: GENETIC STUDIES OF LRRK2 AND PINK1 IN PARKINSON'S DISEASE
309. Ingrid Løvold Mostad: IMPACT OF DIETARY FAT QUANTITY AND QUALITY IN TYPE 2 DIABETES WITH EMPHASIS ON MARINE N-3 FATTY ACIDS
310. Torill Eidhammer Sjøbakk: MR DETERMINED BRAIN METABOLIC PATTERN IN PATIENTS WITH BRAIN METASTASES AND ADOLESCENTS WITH LOW BIRTH WEIGHT
311. Vidar Beisvåg: PHYSIOLOGICAL GENOMICS OF HEART FAILURE: FROM TECHNOLOGY TO PHYSIOLOGY
312. Olav Magnus Søndenå Fredheim: HEALTH RELATED QUALITY OF LIFE ASSESSMENT AND ASPECTS OF THE CLINICAL PHARMACOLOGY OF METHADONE IN PATIENTS WITH CHRONIC NON-MALIGNANT PAIN
313. Anne Brantberg: FETAL AND PERINATAL IMPLICATIONS OF ANOMALIES IN THE GASTROINTESTINAL TRACT AND THE ABDOMINAL WALL
314. Erik Solligård: GUT LUMINAL MICRODIALYSIS
315. Elin Tollefsen: RESPIRATORY SYMPTOMS IN A COMPREHENSIVE POPULATION BASED STUDY AMONG ADOLESCENTS 13-19 YEARS. YOUNG-HUNT 1995-97 AND 2000-01; THE NORD-TRØNDELAG HEALTH STUDIES (HUNT)
316. Anne-Tove Brenne: GROWTH REGULATION OF MYELOMA CELLS
317. Heidi Knobel: FATIGUE IN CANCER TREATMENT – ASSESSMENT, COURSE AND ETIOLOGY
318. Torbjørn Dahl: CAROTID ARTERY STENOSIS. DIAGNOSTIC AND THERAPEUTIC ASPECTS
319. Inge-Andre Rasmussen jr.: FUNCTIONAL AND DIFFUSION TENSOR MAGNETIC RESONANCE IMAGING IN NEUROSURGICAL PATIENTS
320. Grete Helen Bratberg: PUBERTAL TIMING – ANTECEDENT TO RISK OR RESILIENCE ? EPIDEMIOLOGICAL STUDIES ON GROWTH, MATURATION AND HEALTH RISK BEHAVIOURS; THE YOUNG HUNT STUDY, NORD-TRØNDELAG, NORWAY
321. Sveinung Sørhaug: THE PULMONARY NEUROENDOCRINE SYSTEM. PHYSIOLOGICAL, PATHOLOGICAL AND TUMOURIGENIC ASPECTS
322. Olav Sande Eftedal: ULTRASONIC DETECTION OF DECOMPRESSION INDUCED VASCULAR MICROBUBBLES
323. Rune Bang Leistad: PAIN, AUTONOMIC ACTIVATION AND MUSCULAR ACTIVITY RELATED TO EXPERIMENTALLY-INDUCED COGNITIVE STRESS IN HEADACHE PATIENTS

324. Svein Brekke: TECHNIQUES FOR ENHANCEMENT OF TEMPORAL RESOLUTION IN THREE-DIMENSIONAL ECHOCARDIOGRAPHY
325. Kristian Bernhard Nilsen: AUTONOMIC ACTIVATION AND MUSCLE ACTIVITY IN RELATION TO MUSCULOSKELETAL PAIN
326. Anne Irene Hagen: HEREDITARY BREAST CANCER IN NORWAY. DETECTION AND PROGNOSIS OF BREAST CANCER IN FAMILIES WITH *BRCA1* GENE MUTATION
327. Ingebjørg S. Juel : INTESTINAL INJURY AND RECOVERY AFTER ISCHEMIA. AN EXPERIMENTAL STUDY ON RESTITUTION OF THE SURFACE EPITHELIUM, INTESTINAL PERMEABILITY, AND RELEASE OF BIOMARKERS FROM THE MUCOSA
328. Runa Heimstad: POST-TERM PREGNANCY
329. Jan Egil Afset: ROLE OF ENTEROPATHOGENIC *ESCHERICHIA COLI* IN CHILDHOOD DIARRHOEA IN NORWAY
330. Bent Håvard Hellum: *IN VITRO* INTERACTIONS BETWEEN MEDICINAL DRUGS AND HERBS ON CYTOCHROME P-450 METABOLISM AND P-GLYCOPROTEIN TRANSPORT
331. Morten André Høydal: CARDIAC DYSFUNCTION AND MAXIMAL OXYGEN UPTAKE MYOCARDIAL ADAPTATION TO ENDURANCE TRAINING

2008

332. Andreas Møllerløkken: REDUCTION OF VASCULAR BUBBLES: METHODS TO PREVENT THE ADVERSE EFFECTS OF DECOMPRESSION
333. Anne Hege Aamodt: COMORBIDITY OF HEADACHE AND MIGRAINE IN THE NORD-TRØNDELAG HEALTH STUDY 1995-97
334. Brage Høyem Amundsen: MYOCARDIAL FUNCTION QUANTIFIED BY SPECKLE TRACKING AND TISSUE DOPPLER ECHOCARDIOGRAPHY – VALIDATION AND APPLICATION IN EXERCISE TESTING AND TRAINING
335. Inger Anne Næss: INCIDENCE, MORTALITY AND RISK FACTORS OF FIRST VENOUS THROMBOSIS IN A GENERAL POPULATION. RESULTS FROM THE SECOND NORD-TRØNDELAG HEALTH STUDY (HUNT2)
336. Vegard Bugten: EFFECTS OF POSTOPERATIVE MEASURES AFTER FUNCTIONAL ENDOSCOPIC SINUS SURGERY
337. Morten Bruvold: MANGANESE AND WATER IN CARDIAC MAGNETIC RESONANCE IMAGING
338. Miroslav Fris: THE EFFECT OF SINGLE AND REPEATED ULTRAVIOLET RADIATION ON THE ANTERIOR SEGMENT OF THE RABBIT EYE
339. Svein Arne Aase: METHODS FOR IMPROVING QUALITY AND EFFICIENCY IN QUANTITATIVE ECHOCARDIOGRAPHY – ASPECTS OF USING HIGH FRAME RATE
340. Roger Almvik: ASSESSING THE RISK OF VIOLENCE: DEVELOPMENT AND VALIDATION OF THE BRØSET VIOLENCE CHECKLIST
341. Ottar Sundheim: STRUCTURE-FUNCTION ANALYSIS OF HUMAN ENZYMES INITIATING NUCLEOBASE REPAIR IN DNA AND RNA
342. Anne Mari Undheim: SHORT AND LONG-TERM OUTCOME OF EMOTIONAL AND BEHAVIOURAL PROBLEMS IN YOUNG ADOLESCENTS WITH AND WITHOUT READING DIFFICULTIES
343. Helge Garåsen: THE TRONDHEIM MODEL. IMPROVING THE PROFESSIONAL COMMUNICATION BETWEEN THE VARIOUS LEVELS OF HEALTH CARE SERVICES AND IMPLEMENTATION OF INTERMEDIATE CARE AT A COMMUNITY HOSPITAL COULD PROVIDE BETTER CARE FOR OLDER PATIENTS. SHORT AND LONG TERM EFFECTS
344. Olav A. Foss: "THE ROTATION RATIOS METHOD". A METHOD TO DESCRIBE ALTERED SPATIAL ORIENTATION IN SEQUENTIAL RADIOGRAPHS FROM ONE PELVIS
345. Bjørn Olav Åsvold: THYROID FUNCTION AND CARDIOVASCULAR HEALTH
346. Torun Margareta Melø: NEURONAL GLIAL INTERACTIONS IN EPILEPSY
347. Irina Poliakova Eide: FETAL GROWTH RESTRICTION AND PRE-ECLAMPSIA: SOME CHARACTERISTICS OF FETO-MATERNAL INTERACTIONS IN DECIDUA BASALIS
348. Torunn Askim: RECOVERY AFTER STROKE. ASSESSMENT AND TREATMENT; WITH FOCUS ON MOTOR FUNCTION
349. Ann Elisabeth Åsberg: NEUTROPHIL ACTIVATION IN A ROLLER PUMP MODEL OF CARDIOPULMONARY BYPASS. INFLUENCE ON BIOMATERIAL, PLATELETS AND COMPLEMENT

350. Lars Hagen: REGULATION OF DNA BASE EXCISION REPAIR BY PROTEIN INTERACTIONS AND POST TRANSLATIONAL MODIFICATIONS
351. Sigrun Beate Kjøtrød: POLYCYSTIC OVARY SYNDROME – METFORMIN TREATMENT IN ASSISTED REPRODUCTION
352. Steven Keita Nishiyama: PERSPECTIVES ON LIMB-VASCULAR HETEROGENEITY: IMPLICATIONS FOR HUMAN AGING, SEX, AND EXERCISE
353. Sven Peter Näsholm: ULTRASOUND BEAMS FOR ENHANCED IMAGE QUALITY
354. Jon Ståle Ritland: PRIMARY OPEN-ANGLE GLAUCOMA & EXFOLIATIVE GLAUCOMA. SURVIVAL, COMORBIDITY AND GENETICS
355. Sigrid Botne Sando: ALZHEIMER'S DISEASE IN CENTRAL NORWAY. GENETIC AND EDUCATIONAL ASPECTS
356. Parvinder Kaur: CELLULAR AND MOLECULAR MECHANISMS BEHIND METHYLMERCURY-INDUCED NEUROTOXICITY
357. Ismail Cüneyt Güzey: DOPAMINE AND SEROTONIN RECEPTOR AND TRANSPORTER GENE POLYMORPHISMS AND EXTRAPYRAMIDAL SYMPTOMS. STUDIES IN PARKINSON'S DISEASE AND IN PATIENTS TREATED WITH ANTIPSYCHOTIC OR ANTIDEPRESSANT DRUGS
358. Brit Dybdahl: EXTRA-CELLULAR INDUCIBLE HEAT-SHOCK PROTEIN 70 (Hsp70) – A ROLE IN THE INFLAMMATORY RESPONSE ?
359. Kristoffer Haugarvoll: IDENTIFYING GENETIC CAUSES OF PARKINSON'S DISEASE IN NORWAY
360. Nadra Nilsen: TOLL-LIKE RECEPTOR 2 –EXPRESSION, REGULATION AND SIGNALING
361. Johan Håkon Bjørngaard: PATIENT SATISFACTION WITH OUTPATIENT MENTAL HEALTH SERVICES – THE INFLUENCE OF ORGANIZATIONAL FACTORS.
362. Kjetil Høydal : EFFECTS OF HIGH INTENSITY AEROBIC TRAINING IN HEALTHY SUBJECTS AND CORONARY ARTERY DISEASE PATIENTS; THE IMPORTANCE OF INTENSITY,, DURATION AND FREQUENCY OF TRAINING.
363. Trine Karlsen: TRAINING IS MEDICINE: ENDURANCE AND STRENGTH TRAINING IN CORONARY ARTERY DISEASE AND HEALTH.
364. Marte Thuen: MANGANASE-ENHANCED AND DIFFUSION TENSOR MR IMAGING OF THE NORMAL, INJURED AND REGENERATING RAT VISUAL PATHWAY
365. Cathrine Broberg Vågbø: DIRECT REPAIR OF ALKYLATION DAMAGE IN DNA AND RNA BY 2-OXOGLUTARATE- AND IRON-DEPENDENT DIOXYGENASES
366. Arnt Erik Tjønna: AEROBIC EXERCISE AND CARDIOVASCULAR RISK FACTORS IN OVERWEIGHT AND OBESE ADOLESCENTS AND ADULTS
367. Marianne W. Furnes: FEEDING BEHAVIOR AND BODY WEIGHT DEVELOPMENT: LESSONS FROM RATS
368. Lene N. Johannessen: FUNGAL PRODUCTS AND INFLAMMATORY RESPONSES IN HUMAN MONOCYTES AND EPITHELIAL CELLS
369. Anja Bye: GENE EXPRESSION PROFILING OF *INHERITED* AND *ACQUIRED* MAXIMAL OXYGEN UPTAKE – RELATIONS TO THE METABOLIC SYNDROME.
370. Oluf Dimitri Røe: MALIGNANT MESOTHELIOMA: VIRUS, BIOMARKERS AND GENES. A TRANSLATIONAL APPROACH
371. Ane Cecilie Dale: DIABETES MELLITUS AND FATAL ISCHEMIC HEART DISEASE. ANALYSES FROM THE HUNT1 AND 2 STUDIES
372. Jacob Christian Hølen: PAIN ASSESSMENT IN PALLIATIVE CARE: VALIDATION OF METHODS FOR SELF-REPORT AND BEHAVIOURAL ASSESSMENT
373. Erming Tian: THE GENETIC IMPACTS IN THE ONCOGENESIS OF MULTIPLE MYELOMA
374. Ole Bosnes: KLINISK UTPRØVING AV NORSKE VERSJONER AV NOEN SENTRALE TESTER PÅ KOGNITIV FUNKSJON
375. Ola M. Rygh: 3D ULTRASOUND BASED NEURONAVIGATION IN NEUROSURGERY. A CLINICAL EVALUATION
376. Astrid Kamilla Stunes: ADIPOKINES, PEROXISOME PROFILERATOR ACTIVATED RECEPTOR (PPAR) AGONISTS AND SEROTONIN. COMMON REGULATORS OF BONE AND FAT METABOLISM
377. Silje Engdal: HERBAL REMEDIES USED BY NORWEGIAN CANCER PATIENTS AND THEIR ROLE IN HERB-DRUG INTERACTIONS
378. Kristin Offerdal: IMPROVED ULTRASOUND IMAGING OF THE FETUS AND ITS CONSEQUENCES FOR SEVERE AND LESS SEVERE ANOMALIES

379.Øivind Rognmo: HIGH-INTENSITY AEROBIC EXERCISE AND CARDIOVASCULAR HEALTH
380. Jo-Åsmund Lund: RADIOTHERAPY IN ANAL CARCINOMA AND PROSTATE CANCER

2009

381.Tore Grüner Bjåstad: HIGH FRAME RATE ULTRASOUND IMAGING USING PARALLEL BEAMFORMING
382.Erik Søndenaa: INTELLECTUAL DISABILITIES IN THE CRIMINAL JUSTICE SYSTEM
383.Berit Rostad: SOCIAL INEQUALITIES IN WOMEN'S HEALTH, HUNT 1984-86 AND 1995-97, THE NORD-TRØNDELAG HEALTH STUDY (HUNT)
384.Jonas Crosby: ULTRASOUND-BASED QUANTIFICATION OF MYOCARDIAL DEFORMATION AND ROTATION
385.Erling Tronvik: MIGRAINE, BLOOD PRESSURE AND THE RENIN-ANGIOTENSIN SYSTEM
386.Tom Christensen: BRINGING THE GP TO THE FOREFRONT OF EPR DEVELOPMENT
387.Håkon Bergseng: ASPECTS OF GROUP B STREPTOCOCCUS (GBS) DISEASE IN THE NEWBORN. EPIDEMIOLOGY, CHARACTERISATION OF INVASIVE STRAINS AND EVALUATION OF INTRAPARTUM SCREENING
388.Ronny Myhre: GENETIC STUDIES OF CANDIDATE TENE3S IN PARKINSON'S DISEASE
389.Torbjørn Moe Eggebø: ULTRASOUND AND LABOUR
390.Eivind Wang: TRAINING IS MEDICINE FOR PATIENTS WITH PERIPHERAL ARTERIAL DISEASE
391.Thea Kristin Våtsveen: GENETIC ABERRATIONS IN MYELOMA CELLS
392.Thomas Jozefiak: QUALITY OF LIFE AND MENTAL HEALTH IN CHILDREN AND ADOLESCENTS: CHILD AND PARENT PERSPECTIVES
393.Jens Erik Slagsvold: N-3 POLYUNSATURATED FATTY ACIDS IN HEALTH AND DISEASE – CLINICAL AND MOLECULAR ASPECTS
394.Kristine Misund: A STUDY OF THE TRANSCRIPTIONAL REPRESSOR ICER. REGULATORY NETWORKS IN GASTRIN-INDUCED GENE EXPRESSION
395.Franco M. Impellizzeri: HIGH-INTENSITY TRAINING IN FOOTBALL PLAYERS. EFFECTS ON PHYSICAL AND TECHNICAL PERFORMANCE
396.Kari Hanne Gjeilo: HEALTH-RELATED QUALITY OF LIFE AND CHRONIC PAIN IN PATIENTS UNDERGOING CARDIAC SURGERY
397.Øyvind Hauso: NEUROENDOCRINE ASPECTS OF PHYSIOLOGY AND DISEASE
398.Ingvild Bjellmo Johnsen: INTRACELLULAR SIGNALING MECHANISMS IN THE INNATE IMMUNE RESPONSE TO VIRAL INFECTIONS
399.Linda Tømmerdal Roten: GENETIC PREDISPOSITION FOR DEVELOPMENT OF PREEMCLAMPSIA – CANDIDATE GENE STUDIES IN THE HUNT (NORD-TRØNDELAG HEALTH STUDY) POPULATION
400.Trude Teoline Nausthaug Rakvåg: PHARMACOGENETICS OF MORPHINE IN CANCER PAIN
401.Hanne Lehn: MEMORY FUNCTIONS OF THE HUMAN MEDIAL TEMPORAL LOBE STUDIED WITH fMRI
402.Randi Utne Holt: ADHESION AND MIGRATION OF MYELOMA CELLS – IN VITRO STUDIES –
403.Trygve Solstad: NEURAL REPRESENTATIONS OF EUCLIDEAN SPACE
404.Unn-Merete Fagerli: MULTIPLE MYELOMA CELLS AND CYTOKINES FROM THE BONE MARROW ENVIRONMENT; ASPECTS OF GROWTH REGULATION AND MIGRATION
405.Sigrid Bjørnelv: EATING– AND WEIGHT PROBLEMS IN ADOLESCENTS, THE YOUNG HUNT-STUDY
406.Mari Hoff: CORTICAL HAND BONE LOSS IN RHEUMATOID ARTHRITIS. EVALUATING DIGITAL X-RAY RADIOGRAMMETRY AS OUTCOME MEASURE OF DISEASE ACTIVITY, RESPONSE VARIABLE TO TREATMENT AND PREDICTOR OF BONE DAMAGE
407.Siri Bjørgen: AEROBIC HIGH INTENSITY INTERVAL TRAINING IS AN EFFECTIVE TREATMENT FOR PATIENTS WITH CHRONIC OBSTRUCTIVE PULMONARY DISEASE
408.Susanne Lindqvist: VISION AND BRAIN IN ADOLESCENTS WITH LOW BIRTH WEIGHT
409.Torbjørn Hergum: 3D ULTRASOUND FOR QUANTITATIVE ECHOCARDIOGRAPHY

410. Jørgen Urnes: PATIENT EDUCATION IN GASTRO-OESOPHAGEAL REFLUX DISEASE. VALIDATION OF A DIGESTIVE SYMPTOMS AND IMPACT QUESTIONNAIRE AND A RANDOMISED CONTROLLED TRIAL OF PATIENT EDUCATION
411. Elvar Eyjolfsson: 13C NMRS OF ANIMAL MODELS OF SCHIZOPHRENIA
412. Marius Steiro Fimland: CHRONIC AND ACUTE NEURAL ADAPTATIONS TO STRENGTH TRAINING
413. Øyvind Støren: RUNNING AND CYCLING ECONOMY IN ATHLETES; DETERMINING FACTORS, TRAINING INTERVENTIONS AND TESTING
414. Håkon Hov: HEPATOCYTE GROWTH FACTOR AND ITS RECEPTOR C-MET. AUTOCRINE GROWTH AND SIGNALING IN MULTIPLE MYELOMA CELLS
415. Maria Radtke: ROLE OF AUTOIMMUNITY AND OVERSTIMULATION FOR BETA-CELL DEFICIENCY. EPIDEMIOLOGICAL AND THERAPEUTIC PERSPECTIVES
416. Liv Bente Romundstad: ASSISTED FERTILIZATION IN NORWAY: SAFETY OF THE REPRODUCTIVE TECHNOLOGY
417. Erik Magnus Berntsen: PREOPERATIV PLANNING AND FUNCTIONAL NEURONAVIGATION – WITH FUNCTIONAL MRI AND DIFFUSION TENSOR TRACTOGRAPHY IN PATIENTS WITH BRAIN LESIONS
418. Tonje Strømmen Steigedal: MOLECULAR MECHANISMS OF THE PROLIFERATIVE RESPONSE TO THE HORMONE GASTRIN
419. Vidar Rao: EXTRACORPOREAL PHOTOCHEMOTHERAPY IN PATIENTS WITH CUTANEOUS T CELL LYMPHOMA OR GRAFT-vs-HOST DISEASE
420. Torkild Visnes: DNA EXCISION REPAIR OF URACIL AND 5-FLUOROURACIL IN HUMAN CANCER CELL LINES

2010

421. John Munkhaugen: BLOOD PRESSURE, BODY WEIGHT, AND KIDNEY FUNCTION IN THE NEAR-NORMAL RANGE: NORMALITY, RISK FACTOR OR MORBIDITY ?
422. Ingrid Castberg: PHARMACOKINETICS, DRUG INTERACTIONS AND ADHERENCE TO TREATMENT WITH ANTIPSYCHOTICS: STUDIES IN A NATURALISTIC SETTING
423. Jian Xu: BLOOD-OXYGEN-LEVEL-DEPENDENT-FUNCTIONAL MAGNETIC RESONANCE IMAGING AND DIFFUSION TENSOR IMAGING IN TRAUMATIC BRAIN INJURY RESEARCH
424. Sigmund Simonsen: ACCEPTABLE RISK AND THE REQUIREMENT OF PROPORTIONALITY IN EUROPEAN BIOMEDICAL RESEARCH LAW. WHAT DOES THE REQUIREMENT THAT BIOMEDICAL RESEARCH SHALL NOT INVOLVE RISKS AND BURDENS DISPROPORTIONATE TO ITS POTENTIAL BENEFITS MEAN?
425. Astrid Woodhouse: MOTOR CONTROL IN WHIPLASH AND CHRONIC NON-TRAUMATIC NECK PAIN
426. Line Rørstad Jensen: EVALUATION OF TREATMENT EFFECTS IN CANCER BY MR IMAGING AND SPECTROSCOPY
427. Trine Moholdt: AEROBIC EXERCISE IN CORONARY HEART DISEASE
428. Øystein Olsen: ANALYSIS OF MANGANESE ENHANCED MRI OF THE NORMAL AND INJURED RAT CENTRAL NERVOUS SYSTEM
429. Bjørn H. Grønberg: PEMETREXED IN THE TREATMENT OF ADVANCED LUNG CANCER
430. Vigdis Schnell Husby: REHABILITATION OF PATIENTS UNDERGOING TOTAL HIP ARTHROPLASTY WITH FOCUS ON MUSCLE STRENGTH, WALKING AND AEROBIC ENDURANCE PERFORMANCE
431. Torbjørn Øien: CHALLENGES IN PRIMARY PREVENTION OF ALLERGY. THE PREVENTION OF ALLERGY AMONG CHILDREN IN TRONDHEIM (PACT) STUDY.
432. Kari Anne Indredavik Evensen: BORN TOO SOON OR TOO SMALL: MOTOR PROBLEMS IN ADOLESCENCE
433. Lars Adde: PREDICTION OF CEREBRAL PALSY IN YOUNG INFANTS. COMPUTER BASED ASSESSMENT OF GENERAL MOVEMENTS
434. Magnus Fasting: PRE- AND POSTNATAL RISK FACTORS FOR CHILDHOOD ADIPOSITY
435. Vivi Talstad Monsen: MECHANISMS OF ALKYLATION DAMAGE REPAIR BY HUMAN AlkB HOMOLOGUES
436. Toril Skandsen: MODERATE AND SEVERE TRAUMATIC BRAIN INJURY. MAGNETIC RESONANCE IMAGING FINDINGS, COGNITION AND RISK FACTORS FOR DISABILITY

437. Ingeborg Smidesang: ALLERGY RELATED DISORDERS AMONG 2-YEAR OLDS AND ADOLESCENTS IN MID-NORWAY – PREVALENCE, SEVERITY AND IMPACT. THE PACT STUDY 2005, THE YOUNG HUNT STUDY 1995-97
438. Vidar Halsteinli: MEASURING EFFICIENCY IN MENTAL HEALTH SERVICE DELIVERY: A STUDY OF OUTPATIENT UNITS IN NORWAY
439. Karen Lehrmann Ægidius: THE PREVALENCE OF HEADACHE AND MIGRAINE IN RELATION TO SEX HORMONE STATUS IN WOMEN. THE HUNT 2 STUDY
440. Madelene Ericsson: EXERCISE TRAINING IN GENETIC MODELS OF HEART FAILURE
441. Marianne Klokk: THE ASSOCIATION BETWEEN SELF-REPORTED ECZEMA AND COMMON MENTAL DISORDERS IN THE GENERAL POPULATION. THE HORDALAND HEALTH STUDY (HUSK)
442. Tomas Ottemo Stølen: IMPAIRED CALCIUM HANDLING IN ANIMAL AND HUMAN CARDIOMYOCYTES REDUCE CONTRACTILITY AND INCREASE ARRHYTHMIA POTENTIAL – EFFECTS OF AEROBIC EXERCISE TRAINING
443. Bjarne Hansen: ENHANCING TREATMENT OUTCOME IN COGNITIVE BEHAVIOURAL THERAPY FOR OBSESSIVE COMPULSIVE DISORDER: THE IMPORTANCE OF COGNITIVE FACTORS
444. Mona Løvlien: WHEN EVERY MINUTE COUNTS. FROM SYMPTOMS TO ADMISSION FOR ACUTE MYOCARDIAL INFARCTION WITH SPECIAL EMPHASIS ON GENDER DIFFERECES
445. Karin Margaretha Gilljam: DNA REPAIR PROTEIN COMPLEXES, FUNCTIONALITY AND SIGNIFICANCE FOR REPAIR EFFICIENCY AND CELL SURVIVAL
446. Anne Byriel Walls: NEURONAL GLIAL INTERACTIONS IN CEREBRAL ENERGY – AND AMINO ACID HOMEOSTASIS – IMPLICATIONS OF GLUTAMATE AND GABA
447. Cathrine Fallang Knetter: MECHANISMS OF TOLL-LIKE RECEPTOR 9 ACTIVATION
448. Marit Følsvik Svindseth: A STUDY OF HUMILIATION, NARCISSISM AND TREATMENT OUTCOME IN PATIENTS ADMITTED TO PSYCHIATRIC EMERGENCY UNITS
449. Karin Elvenes Bakkelund: GASTRIC NEUROENDOCRINE CELLS – ROLE IN GASTRIC NEOPLASIA IN MAN AND RODENTS
450. Kirsten Brun Kjelstrup: DORSOVENTRAL DIFFERENCES IN THE SPATIAL REPRESENTATION AREAS OF THE RAT BRAIN
451. Roar Johansen: MR EVALUATION OF BREAST CANCER PATIENTS WITH POOR PROGNOSIS
452. Rigmor Myran: POST TRAUMATIC NECK PAIN. EPIDEMIOLOGICAL, NEURORADIOLOGICAL AND CLINICAL ASPECTS
453. Krisztina Kunszt Johansen: GENEALOGICAL, CLINICAL AND BIOCHEMICAL STUDIES IN *LRRK2* – ASSOCIATED PARKINSON'S DISEASE
454. Pål Gjerden: THE USE OF ANTICHOLINERGIC ANTIPARKINSON AGENTS IN NORWAY. EPIDEMIOLOGY, TOXICOLOGY AND CLINICAL IMPLICATIONS
455. Else Marie Huuse: ASSESSMENT OF TUMOR MICROENVIRONMENT AND TREATMENT EFFECTS IN HUMAN BREAST CANCER XENOGRAFTS USING MR IMAGING AND SPECTROSCOPY
456. Khalid S. Ibrahim: INTRAOPERATIVE ULTRASOUND ASSESSMENT IN CORONARY ARTERY BYPASS SURGERY – WITH SPECIAL REFERENCE TO CORONARY ANASTOMOSES AND THE ASCENDING AORTA
457. Bjørn Øglænd: ANTHROPOMETRY, BLOOD PRESSURE AND REPRODUCTIVE DEVELOPMENT IN ADOLESCENCE OF OFFSPRING OF MOTHERS WHO HAD PREECLAMPSIA IN PREGNANCY
458. John Olav Roaldset: RISK ASSESSMENT OF VIOLENT, SUICIDAL AND SELF-INJURIOUS BEHAVIOUR IN ACUTE PSYCHIATRY – A BIO-PSYCHO-SOCIAL APPROACH
459. Håvard Dalen: ECHOCARDIOGRAPHIC INDICES OF CARDIAC FUNCTION – NORMAL VALUES AND ASSOCIATIONS WITH CARDIAC RISK FACTORS IN A POPULATION FREE FROM CARDIOVASCULAR DISEASE, HYPERTENSION AND DIABETES: THE HUNT 3 STUDY
460. Beate André: CHANGE CAN BE CHALLENGING. INTRODUCTION TO CHANGES AND IMPLEMENTATION OF COMPUTERIZED TECHNOLOGY IN HEALTH CARE
461. Latha Nrugham: ASSOCIATES AND PREDICTORS OF ATTEMPTED SUICIDE AMONG DEPRESSED ADOLESCENTS – A 6-YEAR PROSPECTIVE STUDY

462.Håvard Bersås Nordgaard: TRANSIT-TIME FLOWMETRY AND WALL SHEAR STRESS ANALYSIS OF CORONARY ARTERY BYPASS GRAFTS – A CLINICAL AND EXPERIMENTAL STUDY

Cotutelle with University of Ghent: Abigail Emily Swillens: A MULTIPHYSICS MODEL FOR IMPROVING THE ULTRASONIC ASSESSMENT OF LARGE ARTERIES

2011

463. Marte Helene Bjørk: DO BRAIN RHYTHMS CHANGE BEFORE THE MIGRAINE ATTACK? A LONGITUDINAL CONTROLLED EEG STUDY

464. Carl-Jørgen Arum: A STUDY OF UROTHELIAL CARCINOMA: GENE EXPRESSION PROFILING, TUMORIGENESIS AND THERAPIES IN ORTHOTOPIC ANIMAL MODELS

465. Ingunn Harstad: TUBERCULOSIS INFECTION AND DISEASE AMONG ASYLUM SEEKERS IN NORWAY. SCREENING AND FOLLOW-UP IN PUBLIC HEALTH CARE

466. Leif Åge Strand: EPIDEMIOLOGICAL STUDIES AMONG ROYAL NORWEGIAN NAVY SERVICEMEN. COHORT ESTABLISHMENT, CANCER INCIDENCE AND CAUSE-SPECIFIC MORTALITY

467. Katrine Høyer Holgersen: SURVIVORS IN THEIR THIRD DECADE AFTER THE NORTH SEA OIL RIG DISASTER OF 1980. LONG-TERM PERSPECTIVES ON MENTAL HEALTH

468. MarianneWallenius: PREGNANCY RELATED ASPECTS OF CHRONIC INFLAMMATORY ARTHRITIDES: DISEASE ONSET POSTPARTUM, PREGNANCY OUTCOMES AND FERTILITY. DATA FROM A NORWEGIAN PATIENT REGISTRY LINKED TO THE MEDICAL BIRTH REGISTRY OF NORWAY

469. Ole Vegard Solberg: 3D ULTRASOUND AND NAVIGATION – APPLICATIONS IN LAPAROSCOPIC SURGERY

470. Inga Ekeberg Schjerve: EXERCISE-INDUCED IMPROVEMENT OF MAXIMAL OXYGEN UPTAKE AND ENDOTHELIAL FUNCTION IN OBESE AND OVERWEIGHT INDIVIDUALS ARE DEPENDENT ON EXERCISE-INTENSITY

471. Eva Veslemøy Tyldum: CARDIOVASCULAR FUNCTION IN PREECLAMPSIA – WITH REFERENCE TO ENDOTHELIAL FUNCTION, LEFT VENTRICULAR FUNCTION AND PRE-PREGNANCY PHYSICAL ACTIVITY

472. Benjamin Garzón Jiménez de Cisneros: CLINICAL APPLICATIONS OF MULTIMODAL MAGNETIC RESONANCE IMAGING

473. Halvard Knut Nilsen: ASSESSING CODEINE TREATMENT TO PATIENTS WITH CHRONIC NON-MALIGNANT PAIN: NEUROPSYCHOLOGICAL FUNCTIONING, DRIVING ABILITY AND WEANING

474. Eiliv Brenner: GLUTAMATE RELATED METABOLISM IN ANIMAL MODELS OF SCHIZOPHRENIA

475. Egil Jonsbu: CHEST PAIN AND PALPITATIONS IN A CARDIAC SETTING; PSYCHOLOGICAL FACTORS, OUTCOME AND TREATMENT

476. Mona Høysæter Fenstad: GENETIC SUSCEPTIBILITY TO PREECLAMPSIA : STUDIES ON THE NORD-TRØNDELAG HEALTH STUDY (HUNT) COHORT, AN AUSTRALIAN/NEW ZEALAND FAMILY COHORT AND DECIDUA BASALIS TISSUE

477. Svein Erik Gaustad: CARDIOVASCULAR CHANGES IN DIVING: FROM HUMAN RESPONSE TO CELL FUNCTION

478. Karin Torvik: PAIN AND QUALITY OF LIFE IN PATIENTS LIVING IN NURSING HOMES

479. Arne Solberg: OUTCOME ASSESSMENTS IN NON-METASTATIC PROSTATE CANCER

480. Henrik Sahlin Pettersen: CYTOTOXICITY AND REPAIR OF URACIL AND 5-FLUOROURACIL IN DNA

481. Pui-Lam Wong: PHYSICAL AND PHYSIOLOGICAL CAPACITY OF SOCCER PLAYERS: EFFECTS OF STRENGTH AND CONDITIONING

482. Ole Solheim: ULTRASOUND GUIDED SURGERY IN PATIENTS WITH INTRACRANIAL TUMOURS

483. Sten Roar Snare: QUANTITATIVE CARDIAC ANALYSIS ALGORITHMS FOR POCKET-SIZED ULTRASOUND DEVICES

484. Marit Skyrud Bratlie: LARGE-SCALE ANALYSIS OF ORTHOLOGS AND PARALOGS IN VIRUSES AND PROKARYOTES

485.Anne Elisabeth F. Isern: BREAST RECONSTRUCTION AFTER MASTECTOMY – RISK OF RECURRENCE AFTER DELAYED LARGE FLAP RECONSTRUCTION – AESTHETIC OUTCOME, PATIENT SATISFACTION, QUALITY OF LIFE AND SURGICAL RESULTS;

HISTOPATHOLOGICAL FINDINGS AND FOLLOW-UP AFTER PROPHYLACTIC MASTECTOMY IN HEREDITARY BREAST CANCER

486. Guro L. Andersen: CEREBRAL PALSY IN NORWAY – SUBTYPES, SEVERITY AND RISK FACTORS

487. Frode Kolstad: CERVICAL DISC DISEASE – BIOMECHANICAL ASPECTS

488. Bente Nordtug: CARING BURDEN OF COHABITANTS LIVING WITH PARTNERS SUFFERING FROM CHRONIC OBSTRUCTIVE PULMONARY DISEASE OR DEMENTIA

489. Mariann Gjervik Heldahl: EVALUATION OF NEOADJUVANT CHEMOTHERAPY IN LOCALLY ADVANCED BREAST CANCER BASED ON MR METHODOLOGY

490. Lise Tevik Løvseth: THE SUBJECTIVE BURDEN OF CONFIDENTIALITY

491. Marie Hjelmseth Aune: INFLAMMATORY RESPONSES AGAINST GRAM NEGATIVE BACTERIA INDUCED BY TLR4 AND NLRP12

492. Tina Strømdal Wik: EXPERIMENTAL EVALUATION OF NEW CONCEPTS IN HIP ARTHROPLASTY

493. Solveig Sigurdardottir: CLINICAL ASPECTS OF CEREBRAL PALSY IN ICELAND. A POPULATION-BASED STUDY OF PRESCHOOL CHILDREN

494. Arne Reimers: CLINICAL PHARMACOKINETICS OF LAMOTRIGINE

495. Monica Wegling: KULTURMENNESKETS BYRDE OG SYKDOMMENS VELSIGNELSE. KAN MEDISINSK UTREDNING OG INTERVENSJON HA EN SELVSTENDIG FUNKSJON UAVHENGIG AV DET KURATIVE?

496. Silje Alvestad: ASTROCYTE-NEURON INTERACTIONS IN EXPERIMENTAL MESIAL TEMPORAL LOBE EPILEPSY – A STUDY OF UNDERLYING MECHANISMS AND POSSIBLE BIOMARKERS OF EPILEPTOGENESIS

497. Javaid Nauman: RESTING HEART RATE: A MATTER OF LIFE OR DEATH – PROSPECTIVE STUDIES OF RESTING HEART RATE AND CARDIOVASCULAR RISK (THE HUNT STUDY, NORWAY)

498. Thuy Nguyen: THE ROLE OF C-SRC TYROSINE KINASE IN ANTIVIRAL IMMUNE RESPONSES

499. Trine Naalsund Andreassen: PHARMACOKINETIC, PHARMACODYNAMIC AND PHARMACOGENETIC ASPECTS OF OXYCODONE TREATMENT IN CANCER PAIN

500. Eivor Alette Laugsand: SYMPTOMS IN PATIENTS RECEIVING OPIOIDS FOR CANCER PAIN – CLINICAL AND PHARMACOGENETIC ASPECTS

501. Dorthe Stensvold: PHYSICAL ACTIVITY, CARDIOVASCULAR HEALTH AND LONGEVITY IN PATIENTS WITH METABOLIC SYNDROME

502. Stian Thoresen Aspenes: PEAK OXYGEN UPTAKE AMONG HEALTHY ADULTS – CROSS-SECTIONAL DESCRIPTIONS AND PROSPECTIVE ANALYSES OF PEAK OXYGEN UPTAKE, PHYSICAL ACTIVITY AND CARDIOVASCULAR RISK FACTORS IN HEALTHY ADULTS (20-90 YEARS)

503. Reidar Alexander Vigen: PATHOBIOLOGY OF GASTRIC CARCINOIDS AND ADENOCARCINOMAS IN RODENT MODELS AND PATIENTS. STUDIES OF GASTROCYSTOPLASTY, GENDER-RELATED FACTORS, AND AUTOPHAGY

504. Halvard Høilund-Kaupang: MODELS AND METHODS FOR INVESTIGATION OF REVERBERATIONS IN NONLINEAR ULTRASOUND IMAGING

505. Audhild Løhre: WELLBEING AMONG SCHOOL CHILDREN IN GRADES 1-10: PROMOTING AND ADVERSE FACTORS

506. Torgrim Tandstad: VOX POPULI. POPULATION-BASED OUTCOME STUDIES IN TESTICULAR CANCER

507. Anna Brenne Grønskag: THE EPIDEMIOLOGY OF HIP FRACTURES AMONG ELDERLY WOMEN IN NORD-TRØNDELAG. HUNT 1995-97, THE NORD-TRØNDELAG HEALTH STUDY

508. Kari Ravndal Risnes: BIRTH SIZE AND ADULT MORTALITY: A SYSTEMATIC REVIEW AND A LONG-TERM FOLLOW-UP OF NEARLY 40 000 INDIVIDUALS BORN AT ST. OLAV UNIVERSITY HOSPITAL IN TRONDHEIM 1920-1960

509. Hans Jakob Bøe: LONG-TERM POSTTRAUMATIC STRESS AFTER DISASTER – A CONTROLLED STUDY OF SURVIVORS' HEALTH 27 YEARS AFTER THE CAPSIZED NORTH SEA OIL RIG

510. Cathrin Barbara Canto, Cotutelle with University of Amsterdam: LAYER SPECIFIC INTEGRATIVE PROPERTIES OF ENTORHINAL PRINCIPAL NEURONS

511. Ioanna Sandvig: THE ROLE OF OLFACTORY ENSHEATHING CELLS, MRI, AND BIOMATERIALS IN TRANSPLANT-MEDIATED CNS REPAIR

512. Karin Fahl Wader: HEPATOCYTE GROWTH FACTOR, C-MET AND SYNDECAN-1 IN MULTIPLE MYELOMA
513. Gerd Tranø: FAMILIAL COLORECTAL CANCER
514. Bjarte Bergstrøm: INNATE ANTIVIRAL IMMUNITY – MECHANISMS OF THE RIG-I-MEDIATED RESPONSE
515. Marie Søfteland Sandvei: INCIDENCE, MORTALITY, AND RISK FACTORS FOR ANEURYSMAL SUBARACHNOID HEMORRHAGE. PROSPECTIVE ANALYZES OF THE HUNT AND TROMSØ STUDIES
516. Mary-Elizabeth Bradley Eilertsen: CHILDREN AND ADOLESCENTS SURVIVING CANCER: PSYCHOSOCIAL HEALTH, QUALITY OF LIFE AND SOCIAL SUPPORT
517. Takaya Saito: COMPUTATIONAL ANALYSIS OF REGULATORY MECHANISM AND INTERACTIONS OF MICRORNAS

Godkjent for disputas, publisert post mortem: Eivind Jullumstrø: COLORECTAL CANCER AT LEVANGER HOSPITAL 1980-2004

518. Christian Gutvik: A PHYSIOLOGICAL APPROACH TO A NEW DECOMPRESSION ALGORITHM USING NONLINEAR MODEL PREDICTIVE CONTROL
519. Ola Storrø: MODIFICATION OF ADJUVANT RISK FACTOR BEHAVIOURS FOR ALLERGIC DISEASE AND ASSOCIATION BETWEEN EARLY GUT MICROBIOTA AND ATOPIC SENSITIZATION AND ECZEMA. EARLY LIFE EVENTS DEFINING THE FUTURE HEALTH OF OUR CHILDREN
520. Guro Fanneløb Giskeødegård: IDENTIFICATION AND CHARACTERIZATION OF PROGNOSTIC FACTORS IN BREAST CANCER USING MR METABOLOMICS
521. Gro Christine Christensen Løhaugen: BORN PRETERM WITH VERY LOW BIRTH WEIGHT – NEVER ENDING COGNITIVE CONSEQUENCES?
522. Sigrid Nakrem: MEASURING QUALITY OF CARE IN NURSING HOMES – WHAT MATTERS?
523. Brita Pukstad: CHARACTERIZATION OF INNATE INFLAMMATORY RESPONSES IN ACUTE AND CHRONIC WOUNDS

2012

524. Hans H. Wasmuth: ILEAL POUCHES
525. Inger Økland: BIASES IN SECOND-TRIMESTER ULTRASOUND DATING RELATED TO PREDICTION MODELS AND FETAL MEASUREMENTS
526. Bjørn Mørkedal: BLOOD PRESSURE, OBESITY, SERUM IRON AND LIPIDS AS RISK FACTORS OF ISCHAEMIC HEART DISEASE
527. Siver Andreas Moestue: MOLECULAR AND FUNCTIONAL CHARACTERIZATION OF BREAST CANCER THROUGH A COMBINATION OF MR IMAGING, TRANSCRIPTOMICS AND METABOLOMICS
528. Guro Aune: CLINICAL, PATHOLOGICAL, AND MOLECULAR CLASSIFICATION OF OVARIAN CARCINOMA
529. Ingrid Alsos Lian: MECHANISMS INVOLVED IN THE PATHOGENESIS OF PRE-ECLAMPSIA AND FETAL GROWTH RESTRICTION. TRANSCRIPTIONAL ANALYSES OF PLACENTAL AND DECIDUAL TISSUE
530. Karin Solvang-Garten: X-RAY REPAIR CROSS-COMPLEMENTING PROTEIN 1 – THE ROLE AS A SCAFFOLD PROTEIN IN BASE EXCISION REPAIR AND SINGLE STRAND BREAK REPAIR
531. Toril Holien: BONE MORPHOGENETIC PROTEINS AND MYC IN MULTIPLE MYELOMA
532. Rooyen Mavenyengwa: *STREPTOCOCCUS AGALACTIAE* IN PREGNANT WOMEN IN ZIMBABWE: EPIDEMIOLOGY AND SEROTYPE MARKER CHARACTERISTICS
533. Tormod Rimehaug: EMOTIONAL DISTRESS AND PARENTING AMONG COMMUNITY AND CLINIC PARENTS
534. Maria Dung Cao: MR METABOLIC CHARACTERIZATION OF LOCALLY ADVANCED BREAST CANCER – TREATMENT EFFECTS AND PROGNOSIS
535. Mirta Mittelstedt Leal de Sousa: PROTEOMICS ANALYSIS OF PROTEINS INVOLVED IN DNA BASE REPAIR AND CANCER THERAPY
536. Halfdan Petursson: THE VALIDITY AND RELEVANCE OF INTERNATIONAL CARDIOVASCULAR DISEASE PREVENTION GUIDELINES FOR GENERAL PRACTICE
537. Marit By Rise: LIFTING THE VEIL FROM USER PARTICIPATION IN CLINICAL WORK – WHAT IS IT AND DOES IT WORK?

538. Lene Thoresen: NUTRITION CARE IN CANCER PATIENTS. NUTRITION ASSESSMENT: DIAGNOSTIC CRITERIA AND THE ASSOCIATION TO SURVIVAL AND HEALTH-RELATED QUALITY OF LIFE IN PATIENTS WITH ADVANCED COLORECTAL CARCINOMA
539. Berit Doseth: PROCESSING OF GENOMIC URACIL IN MAN AND MOUSE
540. Gro Falkenér Bertheussen: PHYSICAL ACTIVITY AND HEALTH IN A GENERAL POPULATION AND IN CANCER SURVIVORS – METHODOLOGICAL, OBSERVATIONAL AND CLINICAL ASPECTS
541. Anne Kari Knudsen: CANCER PAIN CLASSIFICATION
542. Sjur Urdson Gjerald: A FAST ULTRASOUND SIMULATOR
543. Harald Edvard Mølmen Hansen: CARDIOVASCULAR EFFECTS OF HIGH INTENSITY AEROBIC INTERVAL TRAINING IN HYPERTENSITIVE PATIENTS, HEALTHY AGED AND YOUNG PERSONS
544. Sasha Gulati: SURGICAL RESECTION OF HIGH-GRADE GLIOMAS
545. John Chr. Fløvig: FREQUENCY AND EFFECT OF SUBSTANCES AND PSYCHOACTIVE MEDICATIONS THE WEEK BEFORE ADMISSION TO AN ACUTE PSYCHIATRIC DEPARTMENT
546. Kristin Moksnes Husby: OPTIMIZING OPIOID TREATMENT FOR CANCER PAIN – CLINICAL AND PHARMACOLOGICAL ASPECTS
547. Audun Hanssen-Bauer: X-RAY REPAIR CROSS-COMPLEMENTING PROTEIN 1 ASSOCIATED MULTIPROTEIN COMPLEXES IN BASE EXCISION REPAIR
548. Marit Saunes: ECZEMA IN CHILDREN AND ADOLESCENTS – EPIDEMIOLOGY, COURSE AND IMPACT. THE PREVENTION OF ALLERGY AMONG CHILDREN IN TRONDHEIM (PACT) STUDY, YOUNG-HUNT 1995-97
549. Guri Kaurstad: CARDIOMYOCYTE FUNCTION AND CALCIUM HANDLING IN ANIMAL MODELS OF INBORN AND ACQUIRED MAXIMAL OXYGEN UPTAKE
550. Kristian Svendsen: METHODOLOGICAL CHALLENGES IN PHARMACOEPIDEMIOLOGICAL STUDIES OF OPIOID CONSUMPTION
551. Signe Nilssen Stafne: EXERCISE DURING PREGNANCY
552. Marius Widerøe: MAGNETIC RESONANCE IMAGING OF HYPOXIC-ISCHEMIC BRAIN INJURY DEVELOPMENT IN THE NEWBORN RAT – MANGANESE AND DIFFUSION CONTRASTS
553. Andreas Radtke: MOLECULAR METHODS FOR TYPING *STREPTOCOCCUS AGALACTIAE* WITH SPECIAL EMPHASIS ON THE DEVELOPMENT AND VALIDATION OF A MULTI-LOCUS VARIABLE NUMBER OF TANDEM REPEATS ASSAY (MLVA)
554. Thor Wilhelm Bjelland: PHARMACOLOGICAL ASPECTS OF THERAPEUTIC HYPOTHERMIA
555. Caroline Hild Hakvåg Pettersen: THE EFFECT OF OMEGA-3 POLYUNSATURATED FATTY ACIDS ON HUMAN CANCER CELLS – MOLECULAR MECHANISMS INVOLVED
556. Inga Thorsen Vengen: INFLAMMATION AND ATHEROSCLEROSIS – RISK ASSOCIATIONS IN THE HUNT SURVEYS
557. Elisabeth Balstad Magnussen: PREECLAMPSIA, PRETERM BIRTH AND MATERNAL CARDIOVASCULAR RISK FACTORS
558. Monica Unsgaard-Tøndel: MOTOR CONTROL EXERCISES FOR PATIENTS WITH LOW BACK PAIN
559. Lars Erik Sande Laugsand: INSOMNIA AND RISK FOR CARDIOVASCULAR DISEASE
560. Kjersti Grønning: PATIENT EDUCATION AND CHRONIC INFLAMMATORY POLYARTHRITIS – COPING AND EFFECT
561. Hanne Gro Wenzel: PRE AND POST-INJURY HEALTH IN PERSONS WITH WHIPLASH: THE HUNT STUDY. EXPLORATION OF THE FUNCTIONAL SOMATIC MODEL FOR CHRONIC WHIPLASH
562. Øystein Grimstad: TOLL-LIKE RECEPTOR-MEDIATED INFLAMMATORY RESPONSES IN KERATINOCYTES
563. Håkon Olav Leira: DEVELOPMENT OF AN IMAGE GUIDANCE RESEARCH SYSTEM FOR BRONCHOSCOPY
564. Michael A. Lang: DIVING IN EXTREME ENVIRONMENTS: THE SCIENTIFIC DIVING EXPERIENCE

565. Helena Bertilsson: PROSTATE CANCER-TRANSLATIONAL RESEARCH. OPTIMIZING TISSUE SAMPLING SUITABLE FOR HISTOPATHOLOGIC, TRANSCRIPTOMIC AND METABOLIC PROFILING
566. Kirsten M. Selnæs: MR IMAGING AND SPECTROSCOPY IN PROSTATE AND COLON CANCER DIAGNOSTICS
567. Gunvor Steine Fosnes: CONSTIPATION AND DIARRHOEA. EFFECTIVENESS AND ADVERSE EFFECTS OF DRUGS
568. Areej Elkamil: SPASTIC CEREBRAL PALSY: RISK FACTORS, BOTULINUM TOXIN USE AND PREVENTION OF HIP DISLOCATION
569. Ruth Derdikman Eiron: SYMPTOMS OF ANXIETY AND DEPRESSION AND PSYCHOSOCIAL FUNCTION IN MALES AND FEMALES FROM ADOLESCENCE TO ADULTHOOD: LONGITUDINAL FINDINGS FROM THE NORD-TRØNDELAG HEALTH STUDY
570. Constantin Sergiu Jianu: PROTON PUMP INHIBITORS AND GASTRIC NEOPLASIA IN MAN
571. Øystein Finset Sørdal: THE ROLE OF GASTRIN AND THE ECL CELL IN GASTRIC CARCINOGENESIS
572. Lisbeth Østgaard Rygg: GROUP EDUCATION FOR PATIENTS WITH TYPE 2 DIABETES – NEEDS, EXPERIENCES AND EFFECTS
573. Viola Lobert: IDENTIFICATION OF NOVEL REGULATORS OF EPITHELIAL POLARITY AND CELL MIGRATION
574. Maria Tunset Grinde: CHARACTERIZATION OF BREAST CANCER USING MR METABOLOMICS AND GENE EXPRESSION ANALYSIS
575. Grete Kjelvik: HUMAN ODOR IDENTIFICATION STUDIES IN HEALTHY INDIVIDUALS, MILD COGNITIVE IMPAIRMENT AND ALZHEIMER'S DISEASE
576. Tor Eivind Bernstein: RECTAL CANCER SURGERY. PROGNOSTIC FACTORS RELATED TO TREATMENT
577. Kari Sand: INFORMED CONSENT DOCUMENTS FOR CANCER RESEARCH: TEXTUAL AND CONTEXTUAL FACTORS OF RELEVANCE FOR UNDERSTANDING
578. Laurent Francois Thomas: EFFECTS OF SINGLE-NUCLEOTIDE POLYMORPHISMS ON microRNA-BASED GENE REGULATION AND THEIR ASSOCIATION WITH DISEASE
579. Øystein Sandanger: THE INNATE IMMUNE SYSTEM: A PARADOXICAL MEDIATOR OF HOST DEFENSE, TISSUE REPAIR AND COLLATERAL DAMAGE
580. Line Knutsen Lund: MENTAL HEALTH IN LOW BIRTH WEIGHT INDIVIDUALS APPROACHING ADULTHOOD
581. Nils Kristian Skjærvold: AUTOMATED BLOOD GLUCOSE CONTROL – DEVELOPMENT AND TESTING OF AN ARTIFICIAL ENDOCRINE PANCREAS USING AV NOVEL INTRAVASCULAR GLUCOSE MONITOR AND A NEW APPROACH TO INSULIN PHARMACOLOGY
582. Håvard Kallestad: SLEEP DISTURBANCE: CLINICAL SIGNIFICANCE IN MENTAL HEALTH CARE AND COGNITIVE FACTORS
583. Anders Wallenius: URACIL-DNA GLYCOSYLASE, ACTIVATION-INDUCED DEAMINASE AND REGULATION OF ADAPTIVE IMMUNE RESPONSES
584. Gry Børmark Hoftun: CHRONIC NON-SPECIFIC PAIN IN ADOLESCENCE PREVALENCE, DISABILITY, AND ASSOCIATED FACTORS – YOUNG-HUNT AND HUNT 3, 2006-2008
585. Elisabeth Hansen: THE SIGNIFICANCE OF RESISTANCE TRAINING AND PSYCHOBIOLOGY IN PRIMARY PREVENTION OF TYPE 2 DIABETES AMONG PEOPLE WITH IMPAIRED GLUCOSE TOLERANCE
586. Ragnhild Omli: URINARY INCONTINENCE AND URINARY TRACT INFECTIONS IN THE ELDERLY: RISK FACTORS AND CONSEQUENCES
587. Christina Sæten Fjeldbo: GASTRIN-MEDIATED REGULATION OF GENE EXPRESSION; A SYSTEMS BIOLOGY APPROACH
588. Yunita Widyastuti: RISK FACTORS FOR COMMON COMPLICATIONS FOLLOWING ADULT HEART SURGERY
589. Anders Thorstensen: 2D AND 3D ECHOCARDIOGRAPHY DURING INOTROPIC ALTERATIONS AND AFTER RECENT MYOCARDIAL INFARCTION
590. Torstein Schrøder-Aasen: EFFECTS OF PURPLE CONEFLOWER (ECHINACEA PURPUREA) ON CYP3A4 METABOLISM AND P-GLYCOPROTEIN MEDIATED TRANSPORT *IN VITRO*

591. Saeed Mehdizadeh: ADAPTIVE BEAMFORMERS FOR ULTRASOUND IMAGING OF ACOUSTICALLY HARD TISSUES
592. Reidar Brekken: ULTRASOUND-BASED ESTIMATION OF STRAIN IN ABDOMINAL AORTIC ANEURYSM